Far-Infrared-Radio Relations in Clusters and Groups at Intermediate Redshift

By

Solohery Mampionona Randriamampandry

A Thesis Submitted in Partial Fulfillment of the Requirements
for the Degree of
Doctor Philosophiae

in the Department of

Physics & Astrophysics Group

University *of the* Western Cape

UNIVERSITY *of the*
WESTERN CAPE

May 2014

Supervisor: Dr. Steven Crawford

Co-supervisor: Prof. Catherine Cress

© Copyright 2014

by

Solohery Mampionona Randriamampandry

Far-Infrared-Radio Relations in Clusters and Groups at Intermediate Redshift

Solohery Mampionona Randriamampandry

KEYWORDS

Galaxy clusters

Spectroscopy

Star-forming galaxies

Radio continuum

Radio luminosity

Photometry

Infrared emission

Intracluster medium
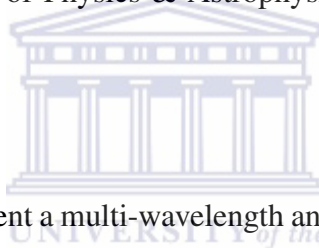
Cosmic rays

Magnetic fields

Abstract

**Far-Infrared-Radio Relations in Clusters and Groups at Intermediate
Redshift**

S. M. Randriamampandry

PhD Thesis, Department of Physics & Astrophysics Group, University of the Western
Cape.

In this thesis, we present a multi-wavelength analysis of star-forming galaxies to shed
new light on the evolution of the far-IR-radio relations in intermediate redshift ($0.3 < z
< 0.6$) galaxy clusters and galaxy groups. The far-infrared (far-IR) emission from galaxies is dominated by thermal dust emission. The radio emission at 1.4 GHz is predominantly produced by non-thermal synchrotron radiation. The underlying mechanisms,
which drive the far-IR-radio correlation, are believed to arise from massive star formation.

A number of studies have investigated the relationship as a function of redshift in
the field and have found no evolution out to at least $z \sim 2$, however few works have
been done in galaxy clusters. In nearby clusters, the median logarithmic ratio of the
far-IR to radio luminosity is $q_{\mathrm{FIR}} = 2.07\pm0.74$, which is lower than the value found in
the field, and there is an indication of an enhancement of radio emission relative to the
far-IR emission. Understanding the properties of the far-IR-radio correlation in a sample
of distant and massive cluster and groups plays an important role in understanding the

physical processes in these systems.

We have derived total infrared luminosities for a sample of cluster, group, and field galaxies through an empirical relation based on *Spitzer* MIPS 24 μm photometry. The radio flux densities were measured from deep Very Large Array 1.4 GHz radio continuum observations. We have studied the properties of the far-IR-radio correlation of galaxies at intermediate redshift clusters by comparing the relationship of these galaxies to that of low redshift clusters. We have also examined the properties of the galaxies showing radio excess to determine the extent that galaxy type or environment may explain the radio excess in galaxy clusters.

We find that the ratio of far-IR to radio luminosity for galaxies in an intermediate redshift cluster to be $q_{FIR} = 1.72 \pm 0.63$. This value is comparable to that measured in low redshift clusters. A higher fraction of galaxies in clusters show an excess in their radio fluxes when compared to low redshift clusters, and corroborates previous evidence of a cluster enhancement of radio excess sources at this earlier epoch as well. We have also investigated the properties of the far-IR-radio correlation for a sample of galaxy groups in the COSMOS field. We find a lower percentage of radio-excess sources in groups as compared to clusters. This provides preliminary evidence that the number of radio-excess sources may depend on galaxy environment. We also find that a larger fraction of radio-excess sources in clusters are red sequence galaxies.
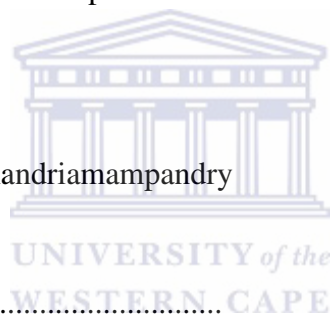
May 2014

Declaration

I declare that *Far-Infrared-Radio Relations in Clusters and Groups at Intermediate Red-shift* is my own work, that it has not been submitted for any degree or examination in any other university, and that all the sources I have used or quoted have been indicated and acknowledged by means of complete references.

Solohery Mampionona Randriamampandry   May 2014

Signed:...

Acknowledgements

I thank my parents, Louis Randriamampandry and Virginie E. Ravelojaona, my brother Toky H. Randriamampandry and his wife Raivonjazanosainina M. R. Randriamampandry in believing in me and for their continuous support. At last but not least, this thesis is dedicated to my wife Vololonirina R. Randriamampandry and my son Mahery A. Randriamampandry for always giving me love, support, and encouragement.

UNIVERSITY *of the*
WESTERN CAPE

Publications

Refereed Journal

Journal Article   MNRAS, **Accepted with minor revisions 2014**

S. M. Randriamampandry, S. M. Crawford, C. M. Cress, K. M. Hess, M. Vaccari,
E. M. Wilcots, M. A. Bershady and G. D. Wirth
Title: The Far-Infrared-Radio Correlation in MS0451-03

Conference Proceedings

IAU Symposium 292   **Cambridge University Press   2013**

Randriamampandry, S. M.; Crawford, S. M.; Cress, C. M.; Hess, K. M.; Giovannoli,
E.; Vaccari, M., 2013. Multi-wavelength Studies of Cluster Star Forming Galaxies at
z~0.54. Molecular gas, dust, and star formation in galaxies, IAU Symp. 292, p. 337,
eds. T. Wong and J. Ott.

Conference Presentations

Tribes of the Deep Sky   Parys, Free State, SA   February 2014
Multiwavelength Astronomy   **Oral Presentation**
Title: The Far-Infrared-Radio Correlation in MS0451-03

The Metrewavelength Sky   NCRA & TIFR, Pune, India   December 2013
Radio Astronomy   **Poster Presentation**

Title: Multi-wavelength Studies of Cluster Star Forming Galaxies: The Far-Infrared-Radio correlation in MS0451-03

CHPC National Meeting   ICC Durban, South Africa   December 2012
Astronomy Session   **Oral Presentation**
Title: Multi-wavelength Studies of Cluster Star Forming Galaxies

IAU XXVIII General Assembly   ICC Beijing, China   August 2012
IAUS292 and SpS2   **Poster Presentation**
Title: Multi-wavelength Studies of Cluster Star Forming Galaxies at z~0.54

19th Young Scientists' Meeting   Taras Shevchenko U. of Kyiv, Ukraine April 2012
Astronomy and Space Physics   **Oral Presentation**
Title: Multi-wavelength Studies of Cluster Star Forming Galaxies

SKA SA Postgraduate Meeting   Stellenbosch IAS, South Africa   2011 - 2013
Annual Conferences   **Oral Presentation**
Title: Multi-wavelength Studies of Cluster Star Forming Populations

Contents

UNIVERSITY *of the*
WESTERN CAPE

List of Figures

List of Tables

Chapter 1

Introduction

1.1 Overview

Galaxy clusters are the largest gravitational bound structures in the Universe. Clusters contain from a few hundred to thousands of galaxies within a radius of the order of ~ 2 Mpc (Abell 1958; Abell et al. 1989) although much of the baryonic material is contained in a hot, X-Ray emitting gas (e.g. Briel et al. 1992; White and Fabian 1995). Clusters are massive with a total mass typically ranging from $\sim 10^{14}$ $M_\odot$ to $\geq 10^{15}$ $M_\odot$. The fraction of the total mass of a galaxy cluster consists of $\sim 5\%$ stars, $\sim 15\%$ hot intracluster gas, and roughly $\sim 80\%$ dark matter. Clusters provide evidence of dark matter and they are unique laboratories to study the evolution of large scale structures in the Universe as well as the evolution of galaxies in high density regions. Understanding the properties of galaxies in clusters plays an important role in understanding galaxy evolution.

In this work, we study the correlation between the far-IR and radio luminosities from galaxies in clusters and groups using a multi-wavelength observations. The multi-wavelength data sets include optical spectroscopic, infrared, and radio observations. Despite the ability to observe across the entire electromagnetic spectrum, multi-wavelength studies have opened up new views of galaxies that could lead to a complete picture of

their evolution. Here the critical importance of a multi-wavelength approach for disentangling the observed far-IR and radio relationship for galaxies at intermediate redshift clusters and groups and its implications are further pursued.

This Chapter covers a general overview of cluster galaxies and multi-wavelength analysis that are needed for this work. In Section 1.2, we provide a short review of galaxy classification. In Section 1.3, we briefly outline the properties of local cluster galaxies, the relationship between galaxy types and environment, and the postulated physical processes that drive galaxy evolution in clusters. In Section 1.4, we introduce the need for multi-wavelength studies and summarise the dominant mechanisms that produce infrared and radio emission in galaxies. We briefly review radio source populations that include radio galaxies and active galactic nuclei (AGN) as well as star-bursting galaxies in Section 1.5. We outline the structure of this thesis in Section 1.6.

1.2   Galaxy Classification

Galaxies are divided into classes based on their shape or morphology. The Hubble classification scheme divides galaxies into four classes: Ellipticals (E), Lenticulars (S0), Spirals (S), and Irregulars (Irr). The Hubble classification scheme (Hubble 1926, 1936) known as the Hubble tuning fork diagram is shown in Figure 1. The images shown in the montage were taken from Faulkes Telescope North and are displayed for a visual illustration. Galaxies that appear to have spiral structures are called spiral galaxies. Elliptical galaxies tend to be smoother and elliptically shaped. Lenticular galaxies (S0) are disk galaxies with no spiral arms, while Irregular galaxies (Irr) are galaxies that have other shapes which do not fit into these three major classes.

The Hubble morphological classification of galaxies has two basic galaxy types: early-type (E and S0) dominated by ellipticals and late-type (S, SB and Irr) dominated by spirals. Elliptical galaxies are composed of old stars moving in random orbits and have very little gas. Ellipticals can be divided into subclasses depending on their ellipticity which is the ratio between the major and minor axis. Spiral galaxies are composed of a
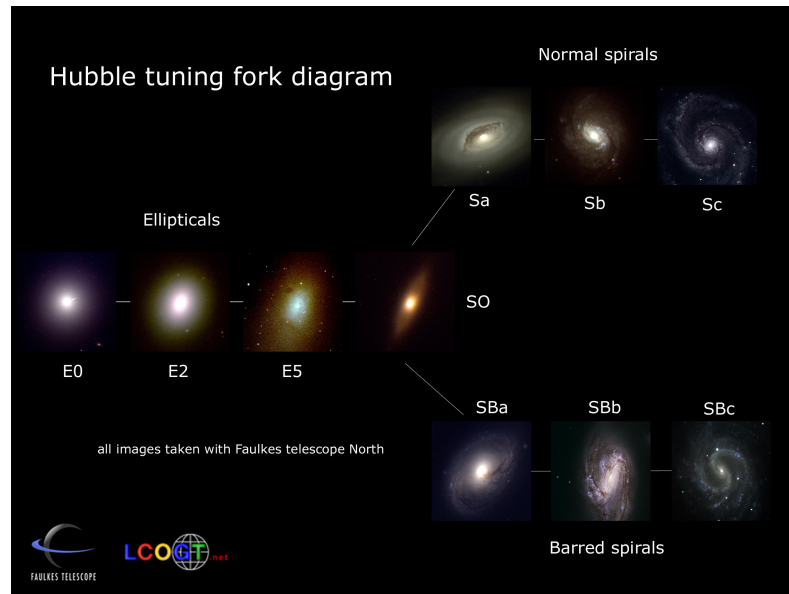
Figure 1: The Hubble tuning fork diagram of galaxy classification. The classification shown here consists of three types of galaxies which include ellipticals, S0, normal and barred spirals. The division of the S0 class into barred and unbarred, and irregular galaxies are not shown. (Credit: Las Cumbres Observatory Global Telescope Network).

flat rotating disk with a central bulge. The disk component contains young stellar population, gas, and dust, while the bulge component is populated by old stars. Spirals can be divided into normal spirals and barred spirals if they have bars in the central regions. Normal and barred spirals can still be divided into subclasses depending on the looseness of their spiral structures (see, Choudhuri 2010, Chapter 9, for a review).

1.3 Evolution of Galaxies in Clusters

1.3.1 Observed Relationships in Clusters

1.3.1.1 Colour-Magnitude Relationship

It has been established that local galaxies have a bimodal distribution in color space (Strateva et al. 2001; Baldry et al. 2004; Balogh et al. 2004) that allows the separation

of the red sequence (early-type) galaxies with low SFRs from the blue cloud (late-type) galaxies with high SFRs. These findings were further constrained for high-redshift galaxies in the colour-magnitude diagram of galaxies out to at least z $\sim$ 1 (Bell et al. 2004). The bimodality of galaxy properties is also observed in their colour-magnitude diagram, luminosity function, and stellar mass (Faber et al. 2007; Drory et al. 2009). This implies that the morphology of galaxies correlates with their intrinsic properties such as colour, mass, and age.

1.3.1.2 Morphology-Density Relationship

The "Morphology-Density Relationship" (MDR) is a correlation between morphology and galaxy environment and was discovered by Dressler (1980). The MDR reveals that early-type galaxies preferentially reside in the cores of local massive clusters, whereas star forming disk galaxies reside mostly on the outskirts of clusters or in the field. This relationship between the galaxy morphology and the galaxy density or environment has also been found to hold for galaxy groups (Postman and Geller 1984).

The giant elliptical galaxies in massive clusters have been found to be in place at earlier epochs around redshift of at least z $\sim$ 0.6 (Ellis et al. 1997) or even at z $\sim$ 1 (Lubin et al. 1998). The MDR seen in the local clusters is perhaps the result of the build-up of the red sequence which is known to start at some point in the past. The red sequence is populated by early-type galaxies. In particular, S0 galaxies are rare in distant (z $\sim$ 0.5) clusters (Dressler et al. 1997), indicating they are relatively recent arrivals in the cluster environment. Transformations between galaxy morphological types include conversion of spirals into S0 galaxies via environmental mechanisms (Fasano et al. 2000; Smith et al. 2005; Postman et al. 2005).

1.3.1.3 Butcher & Oemler Effect

It is now well established that elliptical galaxies are found to reside in local cluster cores, while spiral galaxies tend to dwell in the cluster outskirts (MDR). In contrast, at higher

redshift, it is also found that the fraction of blue, star-forming galaxies in cluster cores increases with redshift. Butcher and Oemler (1978) found, for the first time, that the cores of galaxy clusters at z ∼ 0.4 contain a large number of blue galaxies with an increasing level of star-formation activity.

The build-up of the fraction of blue galaxies within the core of clusters as a function of redshift is known as the "Butcher-Oemler effect" (Butcher and Oemler 1978, 1984). This increase of the fraction of blue galaxies as a function of redshift has been found to be even stronger in the sample of galaxies studied by Rakos and Schombert (1995) where at z ∼ 0.4 the blue fraction was 20% and at z ∼ 0.9 the blue fraction was 80%. Figure 2 shows the original "Butcher-Oemler effect" or "BO effect" along with some more recent works for a comparison.

These distant blue galaxies have been observed to transform into passive galaxies over cosmic time and eventually build-up the red-sequence population (e.g. Smail et al. 1997). Therefore, it is likely that a large population of cluster blue galaxies evolve into (red) local ellipticals which fulfill the existence of MDR.

It has been suggested that a variety of processes across different environments of the cluster transform spiral galaxies into S0 population in clusters (Moran et al. 2007). The frequently proposed physical processes that are predicted to be responsible for these transformations include ram-pressure stripping, mergers, galaxy harassment, strangulation, and starvation. We provide a brief review for these physical mechanisms in the next section.

1.3.2 Transformation Mechanisms in Clusters

A number of physical mechanisms have been proposed to explain the observed morphological and SFR evolutions of cluster galaxies. In this Section, we attempt to provide a list of the most important physical mechanisms that are likely driving morphological transformations in cluster galaxies. These proposed transformational mechanisms have long been invoked to explain the trend seen on both the MDR and BO effect. We summarise
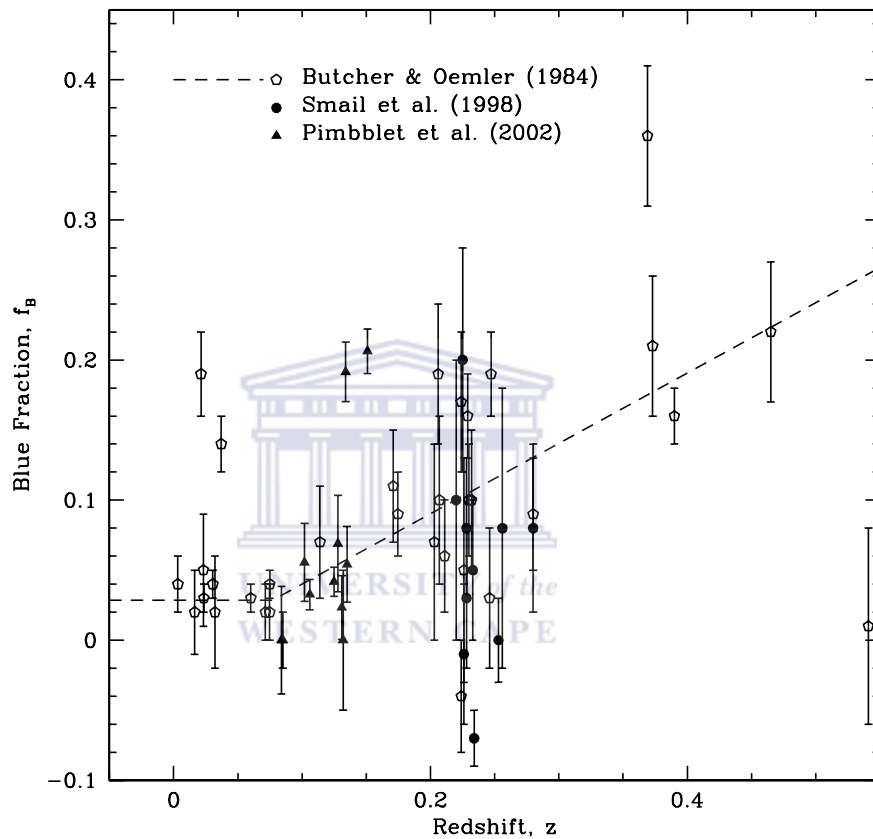
Figure 2: The Butcher-Oemler effect. This figure shows a comparison of the fraction of blue galaxies within clusters at different redshifts. The original data of Butcher and Oemler (1984) (empty circles), data from Smail et al. (1998) (filled circles), and data from Pimbblet et al. (2002) (filled triangles). The Butcher-Oemler evolutionary trend is shown as the dashed line. (Figure adopted from Pimbblet 2003).

the most relevant ones as follows.

"Ram-pressure stripping" is among the mechanisms that removes a galaxy's gas via interactions between a galaxy and the intracluster medium (ICM) (Gunn and Gott 1972). The galaxy's gas is stripped by the pressure due to the passage of the galaxy through the ICM. Simulations have shown that galaxy's gas could be stripped from the disk (Abadi et al. 1999; Quilis et al. 2000) and/or from the halo (Larson et al. 1980; Bekki et al. 2002). Ram-pressure stripping is likely to be efficient within the central region of clusters, where there is a large amount of hot ICM gas (Haynes and Giovanelli 1986; Bureau and Carignan 2002; Vollmer 2003). It is also predicted to be more effective in rich clusters because the relative velocity of a galaxy is larger in these systems (Bahcall 1977; Fujita and Nagashima 1999; Fujita 2001).

"Galaxy-galaxy mergers" are predicted to occur via interactions between equal-mass (major merger) galaxies which could create an elliptical galaxy (Toomre and Toomre 1972; Naab and Burkert 2003). It can also occur when unequal mass (minor merger) spiral galaxies are interacting (interactions could cause the B-O effect, e.g. Lavery and Henry 1988) which could form an S0 galaxy (Icke 1985; Bekki 1998). Galaxy mergers seem to rarely happen in cluster cores due to large relative velocity of galaxies (Mamon 1992; Makino and Hut 1997), which would prevent the formation of gravitationally bound pairs during close encounters. On the other hand, mergers are likely to occur in a relatively low galaxy density at the cluster outskirts (Mihos 2003).

"Galaxy-galaxy harassment" is predicted to occur when two unequal mass galaxies moving at high velocity come to close encounters (Moore et al. 1996). The tidal forces due to high-speed encounters would disturb the gas in the galaxies which could trigger star formation. Galaxy harassment would be important for lower mass galaxies and could affect morphology and star formation rate of cluster galaxies (Moore et al. 1998, 1999).

Galaxy and the cluster gravitational potential is predicted to tidally interact via either "starvation" or "strangulation" (Larson et al. 1980; Balogh et al. 2000; Bekki et al. 2001) mechanism that can strip off galaxy's halo gas due to the cluster environment which can trigger or truncate star formation. Alternatively, the interactions between a galaxy and the

cluster gravitational potential can tidally compress the galactic gas which would increase the star formation rate of a galaxy (Byrd and Valtonen 1990; Valluri 1993; Henriksen and Byrd 1996; Fujita 1998).

"Strangulation" is predicted to occur via tidal interactions between the galaxy and the cluster potential well where a galaxy's envelope of hot gas is being stripped off. This envelope of hot gas is no longer available to cool and accrete gas onto a galaxy to sustain star formation (Larson et al. 1980; Diaferio et al. 2001). This mechanism would truncate a galaxy's star formation but the quenching process would occur over longer timescales ($>$ 1 Gyr) (Poggianti 2004). "Starvation" is predicted to occur via tidal interactions between a galaxy and cluster dark matter halo where galaxy's hot gas halo is being stripped off (Bekki et al. 2002), halting the accretion of cold halo gas onto the galaxy disk to fuel star formation. Due to the cluster potential forces, starvation would tidally truncate galaxy's star formation with slower quenching time at about few Gyr.

To illustrate which mechanism is expected to be more important in what regions of the cluster environment, a diagram that indicates the effectiveness of each proposed mechanisms for two massive intermediate redshift (z$\sim$0.5) clusters (MS0451-03 cluster is part of our cluster sample) are shown in Figure 3. In this graph it is noted that tidal processes in this diagram refer to interactions with the cluster potential, while tidal forces during galaxy-galaxy interactions are a component of the harassment mechanism (Moran et al. 2007). As can be seen, tidal stripping is more effective in cluster cores, while ram pressure stripping, starvation, and harassment play an important role towards larger radii. Galaxy-galaxy mergers dominating at the cluster outskirts. Moran et al. (2007) studies suggested that spiral (infalling) galaxies are being slowly converted into S0s via a heterogeneous process that nevertheless proceeds robustly across a variety of different environments. It is likely that ICM-related processes globally affect star formation rate (quenching), while tidal-driven processes (e.g. harassment) is likely to be effective in morphological transformation. Nonetheless, the magnitude of the importance of each mechanism is still controversial.

Although these proposed mechanisms have provided us some important clues for
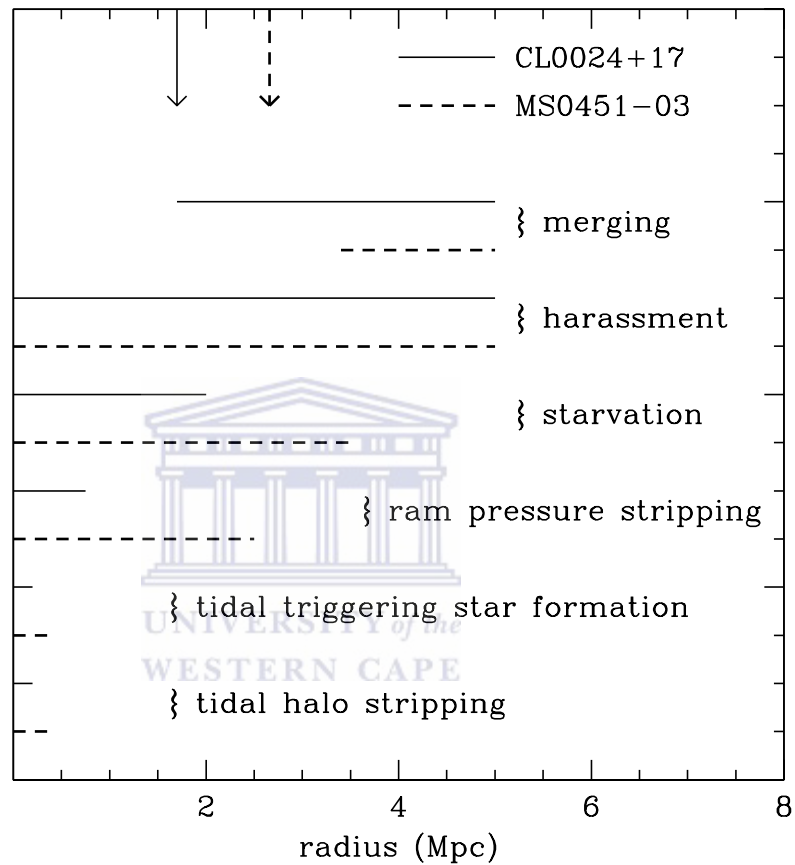
Figure 3: This schematic diagram shows the clustercentric radius and an example of performances of the listed physical mechanisms. It indicates the effectiveness of each of the proposed physical mechanisms that may be fully halting star formation or transforming the visual morphology of a radially infalling galaxy. The physical mechanisms acting in two clusters are being compared that consists of CL0024+17 (solid line) and MS0451-03 (dashed line). The arrows indicate the virial radius of each cluster. (Figure from Moran et al. 2007).

galaxy evolution, no substantial observational evidence has been gathered to demonstrate which processes are the dominant mechanisms driving the evolution of galaxies. To date, the details of the mechanisms that quench and or trigger star formation which transform blue (spiral), actively star-forming galaxies into red (elliptical), passive galaxies are still a subject of debate. In the next Section, we introduce a multi-wavelength analysis that aims to shed new light on our understanding the evolution of these galaxies.

1.4 Multi-wavelength Astrophysics

The ideal approach to studying the details of a cluster's populations is to have large sample drawn from a very deep and large survey. There have been extensive work in aiming to achieve this although there are still various limitations such as a survey's depths. An alternative approach to address these issues is to carry out a multi-wavelength analysis. Multi-wavelength approach aims to study galaxy's properties in different part of the electromagnetic spectrum and combine them in order to yield a much more complete view of the galaxy's features.

In Figure 4, we show a picture of radio galaxy Centaurus A in a panchromatic view to illustrate the different features that can be viewed at different wavelengths. As can be seen, an analysis from one waveband does reveal unique features which the other wavelengths do not. Therefore, studies of galaxies using multiple observations at different wavelengths (i.e. taken at different wavelengths that include γ-ray, x-ray, ultraviolet (UV), visible, infrared (IR), and radio waveband) consolidate these features to enable us to study the evolution of galaxies in greater details. For instance, unlike the visible light, in the IR one sees galaxies obscured by dust, while in the X-ray and radio wavelengths galaxies' large scale structures are readily observed.

Understanding the morphological transformation and evolution of star formation rate are among the important goals in astrophysics. Multi-wavelength analysis of star forming galaxies in clusters is one of the most promising approaches to investigate them and the
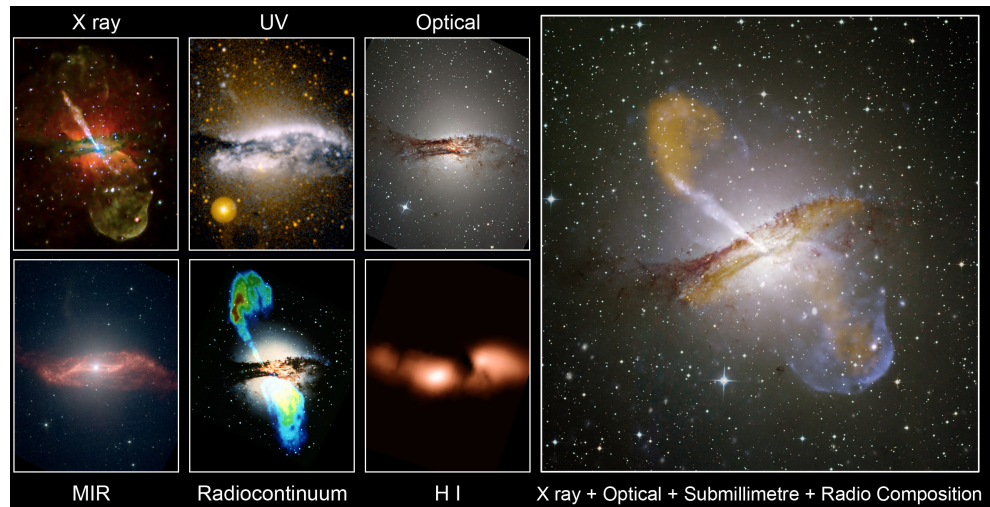
Figure 4: The Centaurus A galaxy or NGC 5128 observed at various wavelengths. Montage of galaxy imagery to illustrate the different features that can be viewed at different frequencies. (Credit: Ángel R. López-Sánchez).

evolution of galaxies via the link between star formation, cluster environment, and galaxy properties. In order to fully understand the processes driving these evolutions in clusters a multi-wavelength approach is needed.

1.4.1   Infrared Emission

IR emission is emitted by any astronomical object that radiates heat. In galaxies, most far-IR emission is produced by starlight re-processed by dust (Beichman 1987; Soifer et al. 1987), IR dust thermal emission. IR galaxies are galaxies that emit more radiation in the wavelength range about (0.7–350 μm) than all other wavelengths. IR emission from galaxies can be split into three spectral regions that consists of near-IR (NIR; 0.7–5 μm), mid-IR (MIR; 5–25 μm), and far-IR (FIR; 25–350 μm). NIR observations are useful tools to study the stellar mass of galaxies. The MIR can be used to probe various properties of dusty obscured star formation activity. The FIR are excellent tracers of very cold gas where intense star formation is triggered.

The capability of the ground based observations is limited by the atmospheric seeing

since IR emissions (also γ-ray, X-ray, and UV light) are either absorbed or scattered by the Earth's atmosphere. Space observatories which detect IR light include the *Infrared Astronomical Satellite* (*IRAS*, Neugebauer et al. 1984), *Infrared Space Observatory* (*ISO*, Kessler et al. 1996), *Spitzer* Space Telescope (*Spitzer*, Werner et al. 2004), and the *Herschel Space Observatory* (*Herschel*, Pilbratt et al. 2010). Each of these satellites has revolutionised, at some level, our IR view of galaxies both at low and high redshift.

1.4.2 Radio Emission

Radio continuum emission arises from both thermal and non-thermal processes. The non-thermal emission includes "synchrotron emission", while the thermal emission includes "free-free emission". Different type of galaxies produce radio emission in various mechanisms where one production mechanism can be more dominant when compared to others.

1.4.2.1 Non-Thermal Radio Emission

The non-thermal radio emission known as synchrotron emission is produced by electrons moving at relativistic velocities that gyrate along a magnetic field. In Figure 5, a schematic to illustrate the production of synchrotron radiation is shown. The energies of the emitted photons significantly depend on the energy of the electrons and on the magnetic field strength. For an electron, the power law distribution is used to approximate its energy spectrum which is given by:

$$\mathrm{P}(\omega) \sim \omega^{-\alpha} \tag{1}$$

where α is the spectral index, ω is the frequency of the gyration. Likewise, for the sum of the energy spectrum of individual electrons, the spectrum of synchrotron radiation can also be characterized by a power law spectrum.

$$P_{\text{tot}}(\omega) \sim \omega^{-(p-1)/2} \tag{2}$$

where $\alpha = \frac{(p-1)}{2}$ is the spectral index, p is the particle distribution index. The radio synchrotron spectrum is often written in the form $S_\nu \sim \nu^{-\alpha}$ where S_ν is the radio flux density at frequency ν, and α is the spectral index. For a complete derivation of the above equations, we refer the readers to Chapter 6 of the text-book by Rybicki and Lightman (1979).
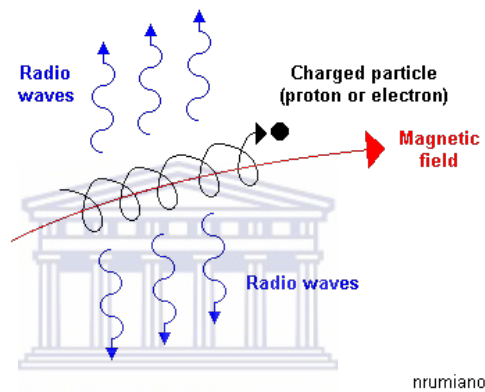
Figure 5: Synchrotron radiation is produced when relativistic cosmic-rays electrons spiral around magnetic field. (Credit: http://nrumiano.free.fr).

The value of the spectral index depends on the properties of the astronomical sources. For AGN, it generally lies between (-1 $< \alpha <$ +1), while $\alpha \sim 0.8$ is typical for normal star-forming galaxies (Condon 1992). As shown in Figure 6, the spectrum of synchrotron emission steepens at higher frequencies. The common sources that produce synchrotron emission include supernova remnants, radio galaxies, and AGN. The synchrotron radiation can be polarized (up to 75%) in a regular magnetic field.

1.4.2.2 Thermal Radio Emission

The thermal emission or bremsstrahlung also known as free-free emission is due to decelerating electrons interacting with an ionized gas. This form of radiation occurs when an

electron passes close to a positive ion and is decelerated by Coulomb forces. In thermal equilibrium, velocities of the electrons will obey the Maxwell-Boltzmann distribution. The velocity and the energy (E) of the electron are determined by their temperature T. The intensity of the bremsstrahlung radiation at energy E is given by

$$I(E,T) \; = \; AG(E,T)Z^2 n_e n_i (kT)^{1/2} e^{-E/kT} \tag{3}$$

where G(E,T) is the Gaunt factor, n_e and n_i are the electron and ion densities, respectively. A is a constant, k is Boltzmann's constant, and Z is atomic number.

The common sources that produce free-free emission include HII regions, gas heated by X-rays from massive stars, star-forming galaxies, and the ICM. The thermal radio emission is not intrinsically polarized, but rather a random process.

1.4.2.3 Synchrotron versus Free-Free Emission

In Figure 6, we display the observed radio spectrum of spiral galaxy M82 that includes both synchrotron and free-free emissions. The far-IR spectrum of this bright nearby starburst galaxy is also shown. The synchrotron emission is shown in the dot-dashed line, while free-free emission is indicated in the dashed line, and dust emission is drawn using a dotted line. The solid line is the sum of the three components.

As we can see in Figure 6, HII regions in M82 become opaque below $v \sim 1$ GHz due to free-free absorption, while the free-free component is largest at an observed frequency > 30 GHz. The dust emission (T $\sim$ 45 K) with opacity proportional to $v^{1.5}$ (Condon 1992) dominates the emission at higher frequencies. Thermal emission or "free-free emission" (dashed line) is from HII regions ionized by massive (M > 15 M$_\odot$) and shorter-lived stars. The free-free component particularly dominates the poorly observed frequency range which is between 30 and 200 GHz.
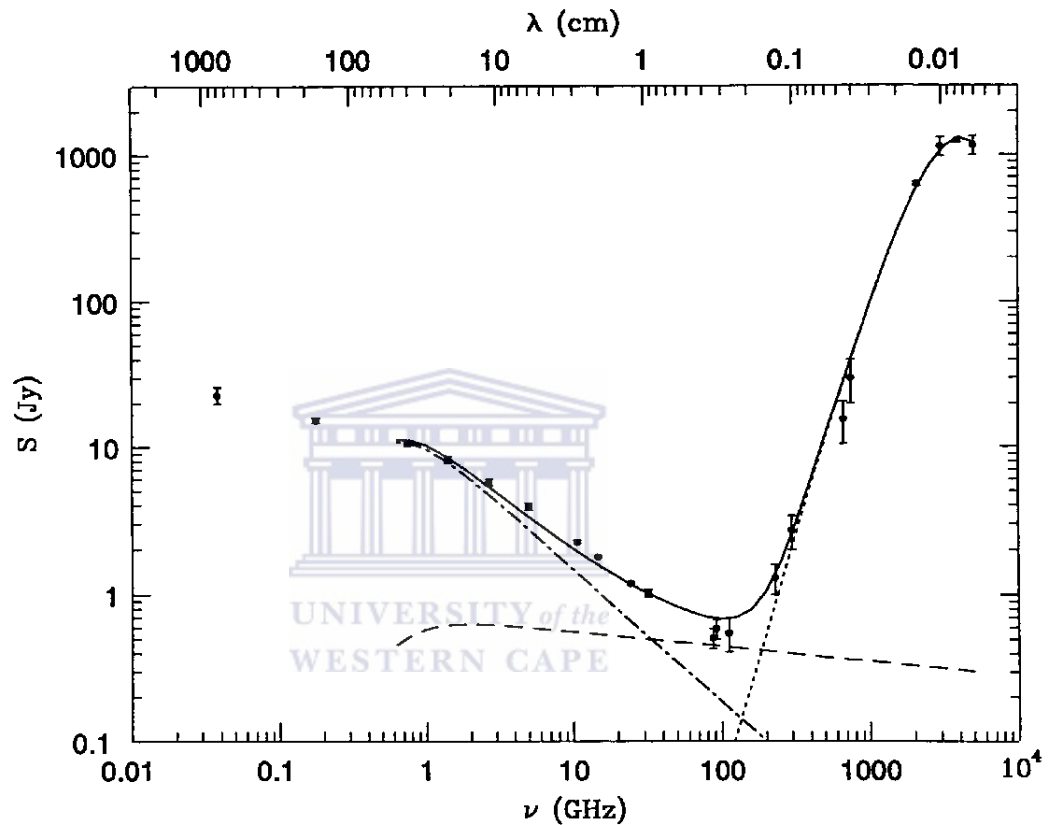
Figure 6: A graph showing the flux density (Jy) as function of frequency (GHz) and wavelength (cm). The synchrotron emission is shown in the dot-dashed line, while free-free emission is indicated in the dashed line, and dust emission is drawn in dotted line. The solid line is the sum of the three components. Synchrotron radiation (dot-dashed line) from cosmic-ray electrons accelerated by the supernova remnants of massive (M > 8 $M_\odot$) and short-lived (t < 3×10^7 yr) stars governs the radio continuum emission of M82 at frequencies 30 GHz. (Figure adopted from Condon 1992).

1.5 Radio Source Population

The population of extragalactic radio sources can be broadly divided into two categories: (1) star-forming galaxies which consists of galaxies where its radio emission is predominantly fuelled via (ongoing) star formation related-processes; (2) AGN which consists of galaxies where its radio emission is predominantly fuelled via an active nucleus; powered by an accretion activity on to a super massive black-hole.

In particular, star-forming galaxies and active galactic nuclei (AGN) are two main populations of radio sources in deep radio surveys at 1.4 GHz (20 cm) (Condon 1984; Windhorst et al. 1985). At this frequency the radio emission is dominated by synchrotron emission powered either by cosmic-ray electrons accelerated in supernova remnants or by accretion onto the central supermassive black hole (e.g. Condon 1992). It is also known that the radio properties of star-forming galaxies and AGN (e.g. Seyferts, LINERs) are comparable, at least, in the local Universe (Sadler et al. 1999), thus additional observations at other wavelengths are often needed to disentangle AGN and star-forming galaxies in the radio regime. We provide a brief description of these radio sources as follows.

1.5.1 Radio Galaxies

The majority of radio galaxies often have steep spectrum with $\alpha \sim 0.5 - 1$. The optical counterparts of radio galaxies are usually elliptical and show continuum emission and/or broad and narrow emission lines.

The main features that distinguish AGN from "normal" star-forming galaxies include high nuclear luminosity, broad-band (non-thermal) continuum emission, presence of strong high ionisation lines in their optical spectra, rapid variability of lines and continuum, and jets. Furthermore, AGN show strong features in the radio and emit jets of plasma that feed energy and particles to the radio lobes (Begelman et al. 1984).

1.5.2 Active Galactic Nuclei

The term active galactic nuclei (AGN) refers to the existence of a very energetic central region of a galaxy which shows substantial radiation over a portion or across the electromagnetic spectrum. The excess emission has been observed through γ-ray to radio wavelengths. It is known that most, or perhaps all, massive galaxies host a supermassive black hole at their centre (Kormendy and Richstone 1995). It is believed that the radiation from AGN is powered by accretion of material into a supermassive black hole in the central region of a galaxy and is not connected to stellar activity. AGN are known to be significant sources of energy in the Universe. Radio AGN release a substantial energy at radio wavelengths.

AGN can be broadly classified, via radio luminosities, into radio-quiet ($L_{1.4 \text{ GHz}} \leq 10^{22}$ W Hz^{-1} sr^{-1}) and radio-loud ($L_{1.4 \text{ GHz}} > 10^{22}$ W Hz^{-1} sr^{-1}) (Jarvis and Rawlings 2004). (1) Radio-quiet AGN, which consists of $\sim$ 90% of the overall AGN population, are divided into two subclasses: (a) high optical luminosity radio quiet AGN or quasars, Seyfert galaxies; (b) low luminosity AGN, Low Ionisation Nuclear Emission lines Regions (LINERS). (2) Radio-loud AGN, which are characterised by strong radio emission, typically consists of quasars and blazars.

The current unified model of AGN postulates the presence of black-hole surrounded by an accretion disk where the primary emission comes from (Antonucci 1993). The accretion disk is the result of materials such as interstellar gas that orbit the black-hole which powers up the AGN. The rapidly rotating matter is heated and ejected at a relativistic speed which produce the jets emitted at different wavelengths from radio to γ-rays. There are also the presence of two gas clouds regions with different radii and velocity dispersions that eventually constitute the broad line region (BLR) and the narrow line region (NLR) (see, Urry and Padovani 1995). Finally, a torus which consists of a thick dust particles and molecular gas, and is one of the basis component in the model.

1.5.3 Star-Forming / Starburst Galaxies

Starburst galaxies are undergoing an episode of tremendous star formation. The stellar populations of starburst galaxies are dominated by massive OB stars (e.g. Aitken et al. 1982; Conti 1991) and evolved red supergiants stars (Oliva et al. 1995). Their high IR bolometric luminosities are known to be dominated by young hot giant stars formed from recent or ongoing intense star formation activity (e.g. Moorwood 1996), and nebular emission lines (including those of the Balmer series) are observed in their optical spectra. In starburst galaxies, by definition, the rate at which stars are forming is higher (Scoville and Young 1983) hence gas depletion is faster, and therefore the duration of the starburst episode is short ($\sim 10^9$ yr).

There are two main emissions from star-forming galaxies which consists of line emission and continuum emission. Line emission results from atomic processes that only have a very specific quantized energies. While continuum emission is processed through non-quantized exchange of energy where the radio photons emitted have a continuous energy distribution. We provide further detail of the continuum emission with particular relevance to this work as follows.

There are two main types of continuum emission: the thermal radiation and the non-thermal radiation. In the case of thermal radiation, emission depends solely on the temperature of the emitter such as free-free radiation (see other e.g. blackbody radiation at short wavelengths). The non-thermal radiation does not depend on the temperature of the emitters but requires magnetic field and an example of such emissions is the synchrotron radiation (see other e.g. maser radiation). The dominant mechanism for radio emission in star-forming galaxies are free-free emission (for cooler sources with temperature about < 10 K) and synchrotron emission.

1.6 Outline of this Thesis

Understanding the evolution of galaxies remains one of the most important goals in astrophysics. In this thesis, we present a multi-wavelength data analysis of galaxies in clusters and groups at intermediate redshift in an attempt to shed new light on the evolution of these galaxies. In particular we look at the still unrevealed nature of the far-IR-radio relationship in massive and distant galaxy clusters as well as in groups where the relationship is relatively unexplored.

Chapter 1 covers a general overview of the evolution of cluster galaxies and multi-wavelength techniques and analyses that are needed for this work.

Chapter 2 provides a literature review of the far-IR-radio relations. In particular it covers an overview of the early work, theoretical models, prediction and observations for the relation for field galaxies. It also provides a thorough overview of far-IR-radio correlation for low redshift galaxy clusters.

Chapter 3 gives the details of the spectroscopic redshifts for each cluster and describes our selection of the cluster and galaxy samples.

Chapter 4 introduces the specifications of the VLA continuum observations, data reductions, and data analysis.

Chapter 5 summarizes the IR data followed by the details of the photometry and data analysis as well as the method for measuring IR luminosities of galaxies.

Chapter 6 presents and discusses our findings on the far-IR-radio relationship for a sample of distant galaxy clusters.

Chapter 7 presents and discusses our findings on the radio and infrared properties of galaxy groups in the COSMOS field.

Chapter 8 provides a summary and conclusions of our findings followed by the future work.

Chapter 2

The Infrared and Radio Properties of Galaxies

2.1 Overview

Multi-wavelength analysis using IR and radio observations play an important role for a better determination of the properties of galaxies, especially those suffering from obscuration due to dust at optical wavelengths. Observations by the Very Large Array (VLA, Hjellming and Bignell 1982) and the *Spitzer* Space Telescope (*Spitzer*, Werner et al. 2004) have rapidly increased the number of multi-wavelength studies of star-forming galaxies. The study of the correlation between the far-IR and radio continuum emissions for normal star-forming galaxies, the so-called "far-IR-radio correlation", is among the most interesting results of multi-wavelength studies in astrophysics. Like other cutting-edge topics in extragalactic astronomy, the far-IR-radio correlation also has a long history which is given as per outlined as follows.

This Chapter is dedicated to provide a thorough literature review on the far-IR-radio correlation. Section 2.2 introduces the early works on the IR-radio correlation. Section 2.3, Section 2.4, and Section 2.5 present various aspects behind the relationship that include theoretical modelling, spatially resolved studies within galaxies, and simulation.

Section 2.6 presents the universality of the relation for field galaxies, then reviews the observed relation for star forming galaxies as a function of redshift, and also focuses especially on the state-of-the-art for cluster galaxies at low redshift. Section 2.7 presents the far-IR-radio relationship for AGN. In Section 2.8, we provide the main motivation for this thesis work.

2.2 The IR-radio Relationship: Earlier Works

The history of the IR-radio correlation began four decades ago when van der Kruit (1971) discovered a relation between mid-IR luminosity at 10 μm and the radio luminosity at 1415 MHz. The paper of van der Kruit (1971) first showed the existence of the observed relation for the nuclei of Seyfert galaxies. The two emissions were believed to be originating within the core of Seyfert galaxies. The existence of the relation between these emissions for Seyfert galaxies was further confirmed by Rieke and Low (1972). A subsequent analysis by van der Kruit (1973) reported that the relation might also persist for the nuclei of normal spiral galaxies.

Radio emission originating from the nuclei of spiral galaxies was found to be associated with either starbursts or active nuclei (Condon et al. 1982). Furthermore, Condon et al. (1982) found that the IR and radio fluxes from these nuclei were linearly correlated. The non-thermal radio emission is believed to be produced by relativistic electrons accelerated in supernova remnants (Harwit and Pacini 1975), while the IR emission is postulated to be thermal emission coming from starlight of young massive stars re-radiated by dusty HII regions (Harwit and Pacini 1975; Rickard and Harvey 1984).

The initial works on the IR-radio relation use IR data at 10 μm, although many subsequent works have benefited from the availability of observations from the *Infrared Astronomical Satellite* (IRAS, Neugebauer et al. 1984) at 12 μm, 60 μm, and 100 μm. Helou et al. (1985) were among the earliest to use IRAS to explore the far-IR-radio correlation in the disks of galaxies. Helou et al. (1985) were the first to define the well-known parameter, q, which is the logarithmic ratio of the far-IR-radio luminosities that has been

used to measure the tightness of the far-IR-radio correlation. The relation between the IRAS far-IR (FIR, $40 - 120\mu m$) luminosities and the 20 cm radio continuum luminosities were found to be universal. Figure 7 shows the behaviour of the FIR-radio correlation for nearby cluster and field galaxies observed by Helou et al. (1985).

The relation has been found to hold for various galaxy morphological types including spiral galaxies in Virgo (Helou et al. 1985), a sample of mixed galaxies including spiral and irregular galaxies (Wunderlich et al. 1987), barred spiral galaxies (Hummel et al. 1988), lenticular and various other stages of spiral galaxies (Dressel 1988), and FIR bright elliptical galaxies (Wrobel and Heeschen 1991). The relation between the radio and far-IR emission seems to universally hold even for these different morphological types of normal star-forming galaxies although both the IR and radio emissions are known to be produced through different mechanisms of (ongoing) massive star formation (Harwit and Pacini 1975; Wunderlich and Klein 1988).

Nevertheless, some early observational work had already claimed that the magnetic field seemed to affect the observed relation. For example, by using "minimum energy conditions" as an assumption to estimate the strength of the magnetic field, Hummel (1986) noticed that the frequency distribution of the deviations of the far-IR-radio relation varies with the frequency distribution of the magnetic field strengths for Sbc galaxies. The deviations in the relation was the first evidence that the scatter in the far-IR-radio correlation is due to a magnetic field (Hummel 1986).

2.3   The IR-radio Relationship: Theoretical Models

A number of theoretical models have been developed to explain the observed tight correlation between the far-IR and radio luminosities. Among the models that have been proposed to explain the observed global far-IR-radio correlation are presented as follows:

(i) The "calorimeter" theory was proposed by Voelk (1989) which assumes that all of the ultraviolet (UV) radiation from massive stars are absorbed by interstellar
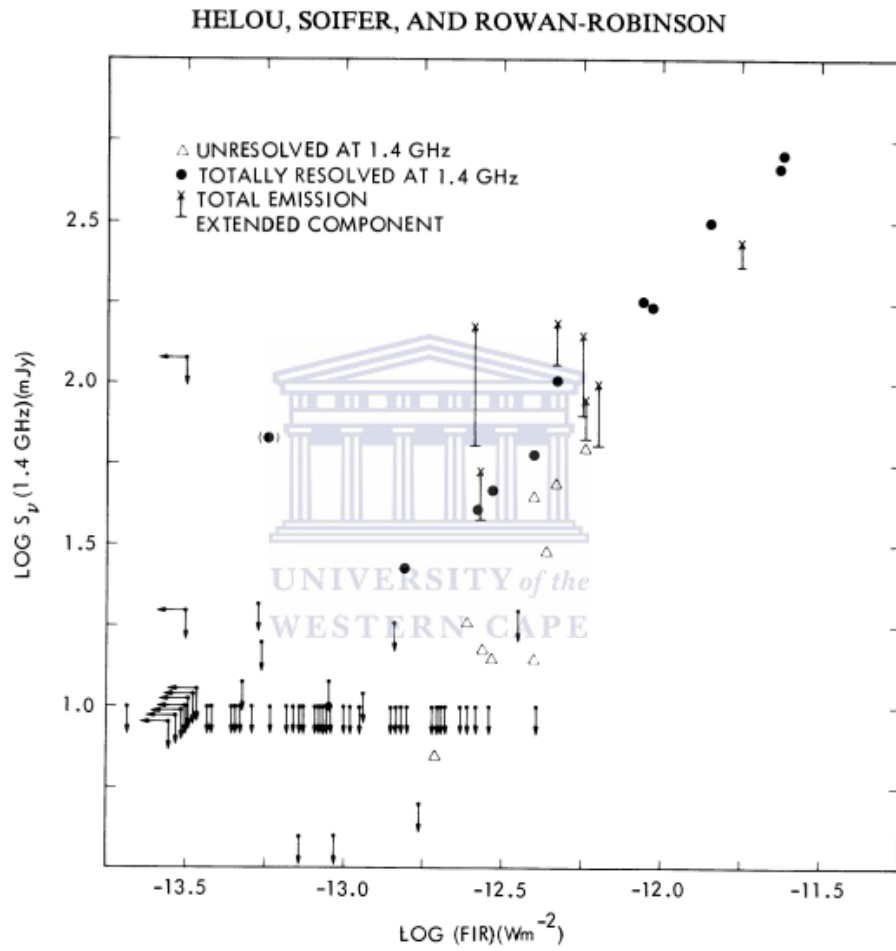
Figure 7: The 20 cm radio continuum luminosity ($L_{1.4GHz}$) against the far-IR luminosity (L_{FIR}) for Virgo cluster and field galaxies. (Figure adopted from Helou et al. 1985).

dust that re-radiates this energy in the far-IR and all of the cosmic-ray electrons are trapped in and dissipated by radio synchrotron emission within the galaxy (optically thick model). The proportionality between far-IR and radio emission shall then be achieved if both UV light from massive stars and cosmic-ray electrons from supernova remnants are correlated with the supernova rate (Voelk 1989). This model also assumed that the energy density of the magnetic field and the interstellar radiation field are proportional which maintains a constant ratio of synchrotron to inverse Compton losses. The subsequent "calorimeter" model by Lisenfeld et al. (1996) offers a variable optical depth for the stellar UV radiation and finite escape probabilities for the cosmic-ray electrons.

(ii) Chi and Wolfendale (1990) proposed a model to explain the non-linearity of the far-IR-radio relation which postulated that the strong suppression of the non-thermal emission (Klein et al. 1984; Price and Duric 1992) from low-luminosity galaxies is due to increasing escape probability of the cosmic-ray electrons. As these galaxies are small in size and have lower magnetic field strengths leading to a decreased electrons confinement. Thus the cosmic rays are more likely to escape from the galaxy which leads to a faster decrease in synchrotron luminosity than in FIR luminosity (Klein et al. 1984; Chi and Wolfendale 1990).

(iii) The "non-calorimetric" model considered by Helou and Bicay (1993) allows most of the UV radiations and cosmic-ray electrons to escape the galaxy disc and assume that the disc scale-height and escape scale-length for CR electrons is correlated (optically thin model). The large dependence of the synchrotron emission on the magnetic field is compensated by coupling the magnetic field strength (important for the synchrotron emissivity) and gas density (important for UV absorption) locally. This was a plausible explanation to ensure that the tight far-IR-radio correlation is maintained (i.e. by maintaining equal escape rates for photons and CR electrons).

(iv) Alternative "non-calorimetric" models have also been proposed to explain the observed far-IR-radio correlation. Niklas and Beck (1997) proposed that observations

favor a combination of the correlations between the volume density of the cold gas, star formation rate, and the magnetic field strength, and that between the star formation rate and the far-IR luminosity. Their model assumes an equipartition between the magnetic field strength and cosmic ray electrons energy. This model seems to explain the observed far-IR-radio relation on both a global and also local scales (i.e. spatially resolved studies on kpc scale– see §2.4) within the discs of individual galaxies.

The validity of these suggested models is still under intense scrutiny.

2.4   IR-radio Relationship: Spatially Resolved Studies

The correlation holds not only on galactic scales but is also found to hold for regions within star-forming galaxies (Beck and Golla 1988; Bicay and Helou 1990; Paladino et al. 2006). In particular, Beck and Golla (1988) showed that the far-IR-radio correlation also holds within M31 and M33 spiral galaxies down to scales on the order of a few 100 pc. Further investigations of the observed local correlation within star-forming galaxies have been carried out (Hoernes et al. 1998; Hughes et al. 2006; Murphy et al. 2006; Tabatabaei et al. 2007a) in aiming to shed new light on the detail of the origin of the far-IR-radio correlation and its driving mechanisms.

Strong constraints on the calorimetry model (Voelk 1989) and non-calorimetric model (Helou and Bicay 1993; Niklas and Beck 1997) may be further achieved, for example, when the spatial scales on which the far-IR-radio correlation breaks down is well-determined. These spatially resolved studies show that while both IR and radio emissions peak at nearly similar spatial scales (Hoernes et al. 1998), radio images appear to be smeared versions of the IR images (Murphy et al. 2006) reflecting the diffusion of the cosmic ray electrons in the ISM (Bicay and Helou 1990).

The local galaxies are a good place to spatially resolve galaxies at parsec scales due to their proximity. As a result, much work has also been focused on the details of the nature

of the far-IR radio correlation whether the relation is linear or not, which is defined as $L_{Radio} \sim L_{IR}^{\gamma}$ where γ is the slope of the relationship. In the next Subsections, we briefly present a combination of the different components of the IR and radio emission that have been studied as among the interests of some early works.

2.4.1 Radio Emission Components

Radio emission of local galaxies have been decomposed into thermal and the non-thermal components (Price and Duric 1992; Hughes et al. 2006) at various spatial scales. For example, Price and Duric (1992) found that the total far-IR emission remains correlated with both the thermal bremsstrahlung ($\gamma \sim 1$) and the non-thermal synchrotron emissions ($\gamma \sim 1.13$) which holds over 5 orders of magnitude in luminosity though the synchrotron slope is slightly higher. For further details on decomposing the radio emission as well as a technique for measuring the distribution of the non-thermal spectral index see e.g. Tabatabaei et al. (2007b) on their analysis of M33.

2.4.2 IR Emission Components

IR emission of local galaxies have been decomposed into two components that consist of warm dust emission from young massive stars (traced by shorter IR waveband) and cold dust emission from lower mass old stars (traced by longer IR waveband) and analysed separately (e.g. Pierini et al. 2003). It is found that the total radio emission remains correlated with both the warm far-IR emission ($\gamma \sim 1$) and the cold far-IR emission ($\gamma \sim 1.13$) and the correlation can still be tight but not linear.

2.4.3 Radio Components versus far-IR Components

Berkhuijsen et al. (2000) have decomposed the radio emission into thermal and non-thermal emissions, and the far-IR emission into warm and cold dust emissions for a local galaxy (M31). The cold far-IR emission versus either thermal or non-thermal emission

was found to have a higher slope ($\gamma \geq 1$), while the warm far-IR emission against either thermal or non-thermal emission was found to correlate much stronger. It turns out that γ is greater than unity for some cases which was defined as the non-linearity in the relationship. The non-linearity between the synchrotron component and cold far-IR component is among the challenges. In the next subsection, we present some works that focus on non-linear aspects of the relationship.

2.4.4 The IR-radio Relationship: Non-linearity

The observed far-IR-radio correlation shows a non-linearity that is evident in the observed luminosities. The observed non-linearity may be due to an increase of the local far-IR-radio luminosity ratio which has been found to increase as a function of the galaxy surface brightness (Marsh and Helou 1995; Hoernes et al. 1998; Hippelein et al. 2003). On the other hand, the observed non-linearity may be due to the decreasing of the global far-IR-radio luminosity ratio which has been found to decrease as the radio power of galaxies increases faster than the infrared luminosity (Fitt et al. 1988; Cox et al. 1988; Devereux and Eales 1989; Condon et al. 1991). Furthermore, Cox et al. (1988) analyzed a sample of luminous galaxies at 151 MHz and found that their radio luminosities are higher with respect to those predicted in the far-IR.

The non-linearity in the local / global far-IR-radio correlation may imply that the far-IR or radio luminosity is not directly tracing the star formation activity. The non-linearity found in the global far-IR-radio correlation has been linearized in various ways as follows.

(a) Fitt et al. (1988) and Devereux and Eales (1989) subtracted the far-IR emission contributions that come from old stellar populations of each galaxy and found a linear far-IR-radio correlation. Devereux and Eales (1989) specifically subtracted a fixed fraction of the blue luminosity from the far-IR luminosity of each galaxy and assumed that the intensity of the radiation field heating the cirrus component is proportional to the blue luminosity.

(b) Condon et al. (1991) linearized the far-IR-radio correlation using optical blue to radio luminosities ratio and found that non-linearity is due to heating of dust by old stellar populations.

These plausible methods for linearization seem to be in agreement with the proposed two-components model of Helou (1986); Lonsdale Persson and Helou (1987). Their model splits the far-IR emission into two components: (1) warm "active" component and (2) "cirrus" component. The first one comes from dusty molecular clouds heated by the massive young stars (5 – 20 $M_\odot$) (Xu 1990) while the second one is being heated by old stars and the general interstellar radiation field. To obtain a linear far-IR-radio correlation, it seems that the contribution of the second component to the L_{FIR} needs to be subtracted assuming that the cirrus is heated by the older and radio-quiet stellar population. Furthermore, the empirical correction of Condon et al. (1991) is consistent with the two-component model of Helou (1986) and Lonsdale Persson and Helou (1987) if the population of young ($<$ Gyr) massive ($M \geq 8\ M_\odot$) stars heat the HII regions (warm dust component) and also contribute to the heating of the cirrus component (cool dust component).

2.5   The IR-radio Relationship: Simulation

A number of studies have recently investigated the physics of the far-IR-radio relationship by numerical simulation. For example, Bressan et al. (2002) considered a comprehensive model of the far-IR-radio correlation that includes stellar population synthesis, dust radiative transfer, and a simplified model of radio emission from cosmic rays generated by supernova (SN). It was shown that the correlation in starburst galaxies may not be surprising if the synchrotron mechanism dominates the inverse Compton scattering and the decay of the SN rate is longer than the cooling time of electrons (Bressan et al. 2002). However, for post-starburst galaxies with high IR, a radio excess (a factor of 5 or so) is expected due to the fact that the timescale for radio emission is longer with respect to the timescale for IR emission (Bressan et al. 2002). They argued that the significantly lower

q-values for post-starburst galaxies is not due to radio emission enhancement rather than evolutionary effect of galaxies (i.e. morphological effect and SFR changes). This effect leads to a scatter in q that has been found to match well the observed scatter in ULIRGs.

Many different models which include a few or many of the physical processes thought to influence the behaviour of the Far-IR-radio correlation (e.g. dust opacity) have been proposed to address the observed scatter in q_{FIR} without success (Bicay and Helou 1990; Murphy et al. 2006). By re-visiting the calorimetric model, Lacki et al. (2010) predict the linearity of the correlation to be the result of a complex combination of the bremsstrahlung, inverse Compton cooling, ionisation, and the relative fraction of cosmic ray electrons and observing frequency. It is argued that deviations from linearity of the IR and radio luminosity ratio is unavoidable and the linearity of the global relationship may be due to a conspiracy of various factors (Lacki et al. 2010).

2.6   The Observed far-IR-radio Relationships

The current availability of various space telescopes with a wide range of IR filters allows for the easy estimation of IR luminosities. There are several definitions of the IR luminosities used in the literature based on these observations. We provide these various definitions as follows. On the one hand, the monochromatic IR fluxes often include the *IRAS* 12, 60 μm, and the *Spitzer* 24, 70, 160 μm as well as the *Herschel* 250, 360, 500 μm; (these define q_{12}, q_{60}, etc.). On the other hand, the integrated IR luminosity usually includes the far-IR luminosity L(FIR, $40 - 120$μm), total IR luminosities L(TIR, $8 - 1000$μm), and L(TIR, $3 - 1100$μm). The monochromatic q is defined as the logarithmic ratio of the monochromatic IR flux and radio flux. The integrated q is defined as the logarithmic ratio of the integrated IR luminosity and radio luminosity. In the next Subsection, we note that the total IR luminosity used throughout this work is mostly defined as L(TIR, $8 - 1000$μm), and in other cases we always use subscript to distinguish them.

2.6.1 Far-IR-radio Relationship in Nearby Universe

Apart form Helou et al. (1985) which is already discussed in §2.2, Yun et al. (2001) also further studied the correlation between the IRAS far-IR flux and the radio flux of a sample of 1809 local field galaxies. They were the first to define the radio- or IR-excess objects as those sources with radio or IR emission exceeding the far-IR-radio correlation prediction by a factor of 5. This is the measured 5σ scatter around the nominal q_{FIR} = 2.34 ± 0.01 i.e. over roughly five orders of magnitude in luminosity. Yun et al. (2001) strikingly also found a tight linear correlation between the far-IR and radio luminosity with small fraction of radio-excess sources ($< 1\%$; 10 galaxies in the sample).

Bell (2003) demonstrated that either the radio or FIR luminosity is not directly proportional to star formation. They showed that the IR luminosity traces most of the star formation in luminous galaxies and only a small fraction of the star formation in faint galaxies, suggesting a revision for SFR calibrations. Bell (2003) used IRAS data to compute q_{TIR} using L(TIR, $8 - 1000\mu$m) and q_{FIR} L(FIR, $40 - 120\mu$m) and found that the far-IR-radio correlation is almost linear. They argued that this linearity is observed not because the IR and radio emission reflect the SFRs correctly but because in low-luminosity galaxies they are both underestimated by similar factors. In other words, the observed linear correlation is rather just the competition of the lower dust content and suppressed synchrotron emission that balance each other.

2.6.2 Far-IR-radio Relationship as a function of Redshift

Here we present a chronological non-exhaustive list of all studies that have investigated the far-IR-radio relationship as a function of redshift in field galaxies.

The far-IR-radio relationship was, for the first time, extended by Garrett (2002) to cover high redshift galaxies. Garrett (2002) used data taken from the Infrared Space Observatory (ISO) at 15μm and extrapolated using the SED templates of local galaxies. They found that the far-IR-radio correlation holds up to at least z $\sim$ 1.3. Gruppioni et al. (2003) later used European Large-Area ISO Survey mid-infrared data at 15 μm

to compute q_{15}. They showed that the mid-IR-radio correlation also holds well and is almost as tight as the far-IR-radio relationship out to at least z $\sim$ 0.6.

Appleton et al. (2004) were among the first to use *Spitzer* observations at 24 μm, and the 70 μm First Look Survey (FLS) to probe the mid-IR- and far-IR-radio correlation of field galaxies as a function of redshift. They used q_{24} of 508 sources and q_{70} of 227 sources to study the mid-IR- and far-IR-radio correlation, respectively. Appleton et al. (2004) results demonstrated that both mid-IR- and far-IR-radio correlation consistently hold out to at least z $\sim$ 1.

For sub-millimeter galaxies, the correlation between the submm and radio emission at 450 μm (q_{450}) has been found to hold up to at least z $\sim$ 2 (Chapman et al. 2005). Frayer et al. (2006) used *Spitzer* observations at 70 μm to probe the evolution of the far-IR-radio correlation in the extragalactic First Look Survey (xFLS) region. They found that the observed q_{70} holds out to z $\sim$ 1. Studies of the far-IR-radio correlation using q_{350} also confirmed the relation holds out to z $\sim$ 3 for sub-millimeter galaxies (Kovács et al. 2006).

Murphy et al. (2006) carried out a detailed analysis of the far-IR-radio correlation within nearby field galaxies where they used *Spitzer* observations at 24 μm and 70 μm to compute q_{24}, q_{70}, and q_{FIR}. They showed that the local far-IR-radio relationship within a galaxy at $\sim$ 0.1-1 kpc scales holds as well as the global far-IR-radio relationship. Furthermore, Murphy et al. (2006) also used an image-smearing model to approximate a galaxy radio map as a smoother version of its IR image due to the diffusion of CR electrons and found that the far-IR-radio relationship for these nearby spiral galaxies improved by a factor of 2.

Boyle et al. (2007) applied a stacking technique to the Australia Telescope Compact Array radio data at the positions of *Spitzer* Wide Field Survey sources at 24 μm to reach an RMS down to 1 μJy. Boyle et al. (2007) found that the mid-IR-radio relationship using q_{24} holds and extends well to faint sources down to few μJy radio flux densities. Beswick et al. (2008) applied a similar technique down to an order of magnitude deeper than the works of Boyle et al. (2007). They found a small deviation from mid-IR-radio

correlation at the faintest infrared flux densities.

Ibar et al. (2008) found that the mid-IR-radio relationship using q_{24} holds out to z $\sim$ 3.5. Sajina et al. (2008) used *Spitzer* observations at 70 μm and 160 μm to study the far-IR-radio relationship for a sample of higher redshift field galaxies. They found a lower q_{FIR} values from z $\sim$ 1.5 out to z $\sim$ 3. Garn et al. (2009) used *Spitzer* observations at 24μm, 70μm and GMRT observations at 610 MHz to determine q_{24}. They found a good linear correlation between the IR and the radio luminosities out to z $\sim$ 2.

Murphy et al. (2009a) used *Spitzer* observations at 24 μm with IR luminosity L(TIR, 8 – 1000μm) derived by SED fitting of the observed 24 μm data to compute q_{TIR}. They found that the relationship shows no evidence for evolution over z $\sim$ 0.6 – 2.6. Seymour et al. (2009) used *Spitzer* observations at 70 μm and reported a decrease in observed q_{70} with redshift for their sources detected either in the imaging or stacked images. They argued that the decrease in q_{70} towards z $\sim$ 3 implies a change in the ULIRG SED at high redshift. Younger et al. (2009) used *Spitzer* MIPS observations to test the far-IR-radio correlation in ULIRGs. They also found that the far-IR-radio correlation at higher redshift out to $\sim$ 3 is consistent with the local relation.

Ivison et al. (2010a) used observations from the Balloon-borne Large Aperture Submillimetre Telescope (BLAST) at 250 μm and found no evidence of q_{250} redshift dependence out to z $\sim$ 3. They stacked radio data at the position of *Spitzer* observations at 24 μm and computed q_{TIR} defined as IR luminosity L(TIR, 8 – 1000μm). They found a steady decrease of q_{TIR} as a function of redshift (where $q_{TIR} \sim (1 + z)^{-0.15\pm0.03}$) from z $\sim$ 1. The tentative decline was speculated to be due to an increase of radio background activity. Ivison et al. (2010b) subsequent studies used *Hershel* observations in the GOODS-North field to study the far-IR-radio correlation for a IR-selected galaxy sample. They found no evolution of the q_{TIR} defined under L(TIR, 8 – 1000μm) out to z $\sim$ 2, when discarding 18 galaxies at z < 0.5 which had the least reliable data.

Jarvis et al. (2010) used data from the *Hershel*-ATLAS to study the evolution of q_{TIR} defined as L(TIR, 8 – 1000μm) and found no evidence for evolution of the far-IR-radio correlation in the redshift between 0 < z < 0.5. They showed that claims for deviation

of the correlation in the literature may partially be a result of resolving out extended emission from the high spatial resolution radio data.

Sargent et al. (2010a) used *Spitzer* MIPS observations at 24 and 70 μm to investigate the evolution of the IR-radio correlation in the COSMOS field. They computed both q_{24}, q_{70} and q_{TIR} defined as L(TIR, 8 − 1000μm) for a jointly IR- and radio-selected sample. They confirmed that the q_{TIR} relation does not change out to at least z ∼ 1.4, and with local relationship q_{24}, q_{70} likely to still hold across the redshift range 2.5 < z < 5. We note their jointly IR- and radio-selected sample contains relatively similar abundances of star-forming galaxies and AGN at < 1.4, which may imply that IR-selected sample would naturally pick up more dusty starburst galaxies or obscured AGN, while radio-selected sample would favor more active radio galaxies (radio-AGNs). Sargent et al. (2010b) subsequently used *Spitzer* MIPS observations at 24 and 70 μm for a sample of galaxies in the COSMOS field. They further confirmed that the q_{TIR} defined as L(TIR, 8 − 1000μm) for ULIRGs remains unchanged out to z∼2

Bourne et al. (2011) used *Spitzer* MIPS observations at 24, 70, 160 μm to study the far-IR-radio relationship at higher redshift using stacking technique. They computed q_{24}, and q_{TIR} for a stellar mass selected galaxies in the Extended Chandra Deep Field South. They found that q_{TIR} does not show significant evolution between the redshift range out to z ∼ 2. While they also found a tentative decline beyond z ∼ 1 when q_{TIR} is based on 70 μm flux.

Mao et al. (2011) used *Spitzer* observations at 70 μm to investigate the evolution of the far-IR-radio correlation at higher redshift using both survival and stacking technique. They computed q_{70} and q_{TIR} for a star-forming galaxies in the Extended Chandra Deep Field South. They found that the q_{TIR} does not change in the redshift range 0 < z < 2. Furthermore, no evolution in the relationship was found out to z ∼ 2 when using MIPS 70 μm .

Overall, the behaviour of the far-IR-radio correlation for field galaxies is remarkably similar out to at least a redshift of z ∼ 2. In these field studies, the relationship has been found to hold for various galaxy types out to z ∼ 3 as well. In summary, these works in

the field galaxies have found and confirmed that there is no firm evidence for evolution of the far-IR and radio luminosity ratio as a function of redshift particularly from the nearby Universe out to at least z∼2 (e.g. Appleton et al. 2004; Ibar et al. 2008; Sargent et al. 2010a,b; Bourne et al. 2011; Mao et al. 2011).

2.6.3 Far-IR-radio Relationship in Galaxy Clusters

In this section, we present a chronological list of all studies which investigate the behaviour of the far-IR-radio relationship in low redshift clusters. It is well known that the star formation rates of galaxies in high density environments are often different from that of field galaxies. It stands to reason that the far-IR-radio correlation may behave differently in clusters as well.

Andersen and Owen (1995) used IRAS observations to compute q_{FIR}. Andersen and Owen (1995) was among the first to look at the effect of the cluster environments on both the IR and radio luminosities in the nearby cluster galaxies. They found that spiral galaxies in rich clusters have enhanced radio emission. It was postulated that the excess radio emissions in rich clusters may be due to the galaxy's interstellar medium (ISM) being compressed via ram pressure when the galaxy moves through the ICM. In poor clusters galaxy-galaxy tidal interaction may be the responsible of the excess radio emissions.

Rengarajan et al. (1997) used IRAS observations and radio continuum data at 1.4 GHz to study the effect of cluster environment on the IR and radio properties of nearby cluster galaxies. They found that the radio luminosity of cluster galaxies showed a strong connection with cluster radial distance such that it increases towards the cluster core. On the other hand, no correlation was found between the far-IR luminosity and the cluster radius. They also found that the correlation tends to depend on galaxy type with Sc galaxies having a stronger correlation when compared to early-type galaxies. The observed changes in SFR within the cluster environment were not found to be responsible for the radio emission enhancement. Rengarajan et al. (1997) proposed that the radio

emission enhancement may be due to the result of the interplay between the increased magnetic field and the increased diffusion of cosmic ray electrons in the galaxys disc as well as the SN rate.

Miller and Owen (2001) used IRAS observations to compute q_{FIR} to study the effect of cluster environment on the far-IR-radio correlation in nearby Abell cluster galaxies. Miller and Owen (2001) found that the far-IR-radio correlation for star-forming galaxies in clusters show an excess of radio emission relative to their IR emission. They found that the radio emission of star-forming galaxies is enhanced within the cluster core by a factor of 2 or 3. The enhancement of radio emission was argued as not due to the AGN component but rather to cluster environmental effect. They postulated that thermal pressure from the ICM is most likely the source of magnetic field compression rather than the ram pressure; resulting in lower q_{FIR} values for galaxies in rich clusters.

Reddy and Yun (2004) used IRAS observations to compute q_{FIR}. Reddy and Yun (2004) studied the effect of the cluster environment on the star formation and AGN activity in 7 nearby galaxy clusters by focusing on a sample of 114 cluster galaxies. They also find evidence of an excess of radio emission for cluster galaxies, especially for early-type galaxies (70%, and all may host AGN) which was more pronounced towards the cluster core. They found that the far-IR luminosity does not change with cluster projected radius, though the collisional heat of dust in the cluster core may affect this observed far-IR luminosity. They supported the proposed model such that the thermal compression of the galaxy's ISM due to the ICM may increase the magnetic field giving rise to synchrotron emission from the disk of a galaxy within the cluster core.

Murphy et al. (2009b) used *Spitzer* MIPS observations observations to compute q_{FIR}. Murphy et al. (2009b) investigated the far-IR-radio relationship of Virgo cluster galaxies by focusing on the effects of the ICM on the ISM of the cluster galaxies. By smoothing MIPS images, they created mock radio maps for a sample of 10 Virgo cluster galaxies. They have compared these mock radio maps to VLA observations and found that there is a deficient of radio emission in the outer part of the galaxy which was interpreted as the galaxy's edges being affected by the ICM. The observed radio-deficit regions found in

these galaxies were interpreted to be a signature that galaxies encountering an ICM wind sweeping the CR-electrons away at the edges.

In the nearby clusters, an enhancement of radio sources have noticeably been found towards the cluster cores (Ledlow and Owen 1995), and the excess of radio emission with respect to the far-IR emission from these galaxies is believed to be the main driver of the deviation observed in the far-IR-radio correlation between field and cluster galaxies. This is indicated in the observed differences between the nominal q_{FIR} values of 2.34 ± 0.01 (Yun et al. 2001) for field galaxies and the q_{FIR} values of 2.07 ± 0.74 (Reddy and Yun 2004) for cluster galaxies.

Clearly, for cluster galaxies the far-IR and radio emissions are still found to be correlated but many local galaxies studies have found that the relation is relatively offset compared to the field. In fact, the far-IR-radio relationship in the cluster galaxies has more scatter than those found for field galaxies, and it is due to an excess of radio emission for cluster galaxies (Reddy and Yun 2004). In Table 1, we attempt to summarise various definition of IR-luminosity and q-values in the literature.

Table 1: This table attempts to summarize various range of the IR and radio luminosity ratios mean values found in the literature. A non-exhaustive list of paper is presented as per the following: reference, redshift, environment, value q_{24} or q_{FIR} and value of q_{TIR}.

Reference	Redshift	Env.	Mean q_{24}	Mean q_{FIR}	Mean q_{TIR}
This work	~0.54	Cluster	1.74±0.64	1.92±0.61; λ(42–122)	2.22±0.61; λ(8–1000)
Reddy and Yun (2004)	0.0120<z<0.025	Cluster	—	2.07±0.74; λ(42–122)	—
Yun et al. (2001)	≤0.16	Field	—	2.34±0.01; λ(42–122)	—
Murphy et al. (2009b)	~0.0036	Cluster	—	2.10±0.25; λ(42–122)	—
Rieke et al. (2009)	≤0.088	Field	1.22±0.02	2.42±0.23; λ(42–122)	—
Miller and Owen (2001)	0.016<z<0.033	Cluster	—	2.30±0.20; λ(42–122)	—
Andersen and Owen (1995)	<<0.2	Cluster	—	2.27±0.20; λ(42–122)	—
Younger et al. (2009)	1.5<z<3.0	Field	—	2.23±0.04; λ(40–120)	—
Sajina et al. (2008)	0.5<z<3.0	Field	—	2.07±0.01; λ(40–120)	—
Kovács et al. (2006)	1<z<3	Field	—	2.07±0.09; λ(42–122)	—
Garrett (2002)	≤1.4	Field	—	2.00; λ(40–120)	—
Helou et al. (1985)	~0.0036	Field	—	2.14±0.14; λ(42–122)	—
Bourne et al. (2011)	0<z<2	Field	1.47±0.03	—	2.66±0.12; λ(8–1000)
Sargent et al. (2010a)	0<z<5	Field	1.26±0.13	—	2.57±0.13; λ(8–1000)
Sargent et al. (2010b)	0<z<2	Field	—	—	2.585±0.245; λ(8–1000)
Ivison et al. (2010a)	0<z<3	Field	—	—	2.41±0.20; λ(8–1000)

Continued. This table attempts to summarize various range of the IR and radio luminosity ratios mean values found in the literature. A non-exhaustive list of paper is presented as per the following: reference, redshift, environment, value q_{24} or q_{FIR} and value of q_{TIR}.

Reference	Redshift	Env.	Mean q_{24}	Mean q_{FIR}	Mean q_{TIR}
Ivison et al. (2010b)	0<z<2	Field	—	—	2.40±0.24; λ(8–1000)
Jarvis et al. (2010)	0<z<0.5	Field	—	—	2.40±0.12; λ(8–1000)
Murphy et al. (2009a)	0.6≤z≤2.6	Field	—	—	2.41±0.30; λ(8–1000)
Bell (2003)	local	Field	—	2.36±0.02; λ(42–122)	2.64±0.02; λ(8–1000)
Garn et al. (2009)	0<z<2	Field	0.92±0.10	—	—
Beswick et al. (2008)	0<z<1.2	Field	0.52±0.20	—	—
Ibar et al. (2008)	≤3.5	Field	0.71±0.47	—	—
Boyle et al. (2007)	≤2.15	Field	1.39±0.02	—	—
Murphy et al. (2006)	≤0.002	Field	0.92±0.35	2.33±0.14; λ(42–122)	—
Appleton et al. (2004)	≤2	Field	0.94±0.23	—	—
Seymour et al. (2009)	≤3	Field	q_{70} = 2.13±0.24	—	—
Frayer et al. (2006)	≤1	Field	q_{70} = 2.10±0.16	—	—

2.7 Far-IR-radio Relationship for AGN

Although the far-IR-radio correlation is known to be driven primarily by star formation activity, it has been noticed that the far-IR and radio fluxes for cluster AGN are also correlated (Miller and Owen 2001). However, Miller and Owen (2001) found larger scatters in the observed far-IR-radio relationship for AGN when compared with star-forming galaxies, as a result of an excess of radio emission for these sources. This has been found in a number of studies which showed that the strong departure from the observed relationship is an indication of AGN activity (e.g. Sopp and Alexander 1991; Reddy and Yun 2004; Norris et al. 2006).

2.8 Thesis Motivation

The far-IR-radio relationship is relatively unexplored at higher redshifts clusters where we do observe an increase in radio sources and star-forming galaxies (Butcher and Oemler 1984), transitional galaxies like E+A (Barger et al. 1996), and AGN (Martini et al. 2009) in galaxy clusters. It is established that the relationship is known to be scattered in the nearby clusters resulting in lower values of q_{FIR} (Reddy and Yun 2004).

We build upon the works of Yun et al. (2001) and Reddy and Yun (2004) in studying the far-IR-radio relation of cluster galaxies at intermediate redshift. This thesis is motivated by the lack of study to look for potential deviations of the far-IR-radio relationship at intermediate redshift galaxies in clusters as well as in groups. This work uses multi-wavelength observations of a sample of clusters of galaxies and aims to shed some light on the unraveled behaviour of the far-IR-radio relationship in clusters and groups of galaxies at intermediate redshifts.

At these redshifts, galaxy clusters are also expected to offer an unique opportunity to study galaxy properties as a function of the cluster high density environment. For cluster galaxies, studies of the relationship would be as an extended examination on the effects of the cluster environment. Furthermore, the far-IR-radio connection is of great interest,

as it can constrain the relative importance of SF and comic ray electrons in establishing the observed properties of cluster star-forming galaxies.

Chapter 3

Cluster Sample & Spectroscopic Redshift

3.1 Overview

In this Chapter, we present the cluster and galaxy samples used in this work. The Chapter is structured as follows. In Section 3.2, we briefly describe the procedure for selecting our cluster sample. In Section 3.3, we present the multi-wavelength data being analyzed in this thesis. We then present the available spectroscopic redshift in the literature hence the size of galaxy sample for each cluster. In Section 3.4, we provide short notes on individual galaxy clusters that include a brief history and the basic properties of the cluster.

3.2 Cluster Sample

The cluster sample analyzed in this work consists of six clusters of galaxies in the redshift range between 0.3 and 0.6. The choice of the redshift interval was based on our objective which is to measure the far-IR-radio correlation in a sample of massive clusters (velocity dispersion: $\sigma > 500$ km s^{-1}) at intermediate redshift range. This sample serves as an intermediate redshift baseline which we will compare to the low redshift clusters works.

The sample selection criteria ensured that we study the far-IR-radio correlation of cluster galaxies in the unexplored parameter space in mass and redshift.

The selected cluster sample was limited to the availability of archival VLA radio continuum observations at 1.4 GHz and *Spitzer* super mosaic MIPS observations at 24 μm. The details of the selection of these clusters can be described as follows. We first searched clusters and then inspected their public multi-wavelength data for the following cluster catalogues which are given in a particular order in the following. The WIYN Long Term Variability (WLTV) cluster list, MAssive Cluster Survey (MACS) catalogue, Crawford et al. (2011) cluster list, Sloan Digital Sky Survey (SDSS), Abell, European Southern Observatory Distant Clusters Survey (EDisCS), and Cluster Lensing And Supernova survey with Hubble (CLASH).

Since we aim to study rich clusters at intermediates redshift as defined above and with larger virial radius $R_{200} \geq 2$ Mpc where possible. Cluster sample was then limited by the availability of the multi-wavelength observations, while galaxy sample was limited by the availability of the spectroscopic redshifts of galaxies in the clusters. These are the main criteria that were used to search the available catalogues of clusters and catalogue of galaxies and led to the sample presented in Table 2.

In Table 2, we provide a central position and mean redshift along with the total spectroscopic redshift of galaxies available for each selected cluster. Spectroscopic redshifts for the cluster and field galaxies in MS0451 and Cl0016 clusters were obtained from Crawford et al. (2011). The spectroscopic redshifts for galaxies in the remaining clusters in the sample were obtained from the literature. We retrieved any available spectroscopic redshifts in the range $0 < z < 1$ for our sample galaxies from the NASA/IPAC Extragalactic Database (NED) for the sources in these clusters. The size of galaxy sample for each cluster was limited to the availability of the spectroscopic redshift. In Table 2, we organize these clusters depending upon the usefulness of the available archival data from the literature.

Table 2: Recapitulation of clusters of galaxies studied in this work. This list is organised based on the available infrared (IR) super mosaic images MIPS at 24 μm, radio continuum data at 1.4 GHz, and the number of sources with spectroscopic redshift (Spec-z)
.

Cluster Full Name	Cluster Name Tag	Redshift (z)	RA (h:m:s)	DEC (d:m:s)	Spec-z
MS 0451.6-0305	MS0451	0.540	04:54:10.90	-03:01:06.90	350-1107
Cl 0016+16	Cl0016	0.550	00:18:33.80	16:26:17.00	577
Abell 0370	A370	0.370	02:39:50.50	-01:35:08.00	180
MS 1512.4+3647	MS1512	0.372	15:14:25.10	36:36:30.00	370
NSCS J121119+391250	J121119	0.340	12:11:16.10	39:11:41.00	35
1RXS J032649.5-004341	J032649	0.448	03:26:49.50	-00:43:41.00	43

3.3 Multi-wavelength Data

The multi-wavelength observations consist of deep VLA (VLA; Hjellming and Bignell 1982) continuum observations at 1.4 GHz and the *Spitzer* Infrared Array Camera (IRAC; Fazio et al. 2004) and the Multiband Imaging Photometer for *Spitzer* (MIPS; Rieke et al. 2004) data along with optical spectroscopic data from the literature. The spectroscopic redshifts are key in measuring the far-IR-radio relationship as they ensure that we only select confirmed cluster members and field galaxies. The multi-wavelength data therefore allow us to investigate the still unrevealed nature of the far-IR-radio relationship of spectroscopically confirmed galaxies in massive and distant galaxy clusters.

We retrieved observations of the cluster sample that include the VLA observations using the National Radio Astronomy Observatory (NRAO) science data archive[1] advanced tool, whilst all of the *Spitzer* super mosaic imaging available at the *Spitzer* Enhanced Imaging Products using SEIP science data archive[2]. In Figure 8, we show a montage of optical images of the clusters for visual check purposes for all clusters.

The cluster sources and field galaxies in MS0451 and Cl0016 have been classified as star-forming galaxies via emission lines diagnostics that include measurement of the

---

[1]https://archive.nrao.edu/archive/advquery.jsp
[2]http://irsa.ipac.caltech.edu/data/SPITZER/Enhanced/Imaging/
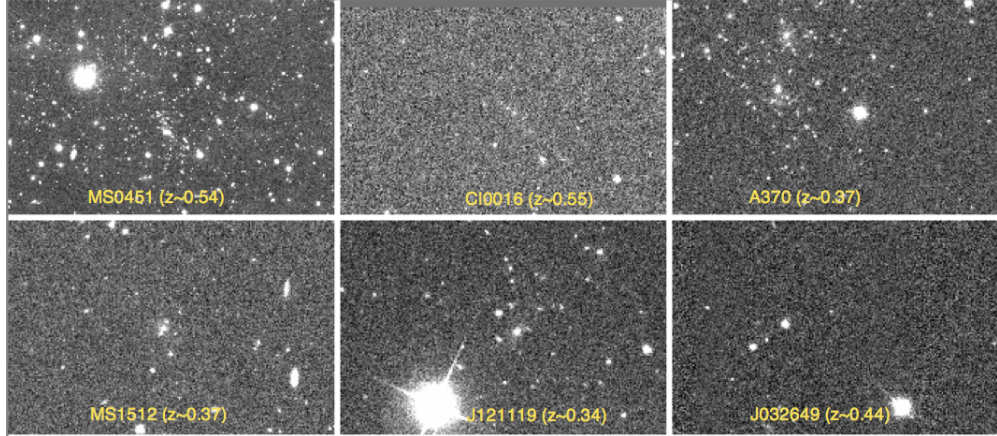
Figure 8: Montage of images of the cluster sample presented in Table 2. WIYN deep R-band (9.6'×9.6') optical image for MS0451 cluster and SDSS r-band (5'×5') for other clusters are shown. (Credit: DSS-SAO: SkyView accessed via DS9).

width of the [OII]3727, Hα, Hβ and [OIII]5007 emission lines. Cluster members were identified in the clusters through a "shifting-gapper" analysis (see Crawford et al. 2014) similar to Fadda et al. (1996) which determined membership through analysis of the radius-velocity diagram.

In Table 3, we summarise the velocity dispersion (σ) and virial radius (R$_{200}$) for the well-studied clusters in our sample.

Table 3: Basic properties of the well-studied clusters that include velocity dispersion (σ) and virial radius (R$_{200}$).

Cluster	σ (km s^{-1})	R$_{200}$ (Mpc)	Reference
MS0451	1354	2.5	Crawford et al. (2009)
Cl0016	1230	2.25	Crawford et al. (2009)
MS1512	575	2.0	Lotz et al. (2003)
A370	1263	2.57	Lah et al. (2009)

3.4   Notes on Individual Clusters

We provide a short note on individual galaxy clusters that include a brief history and the basic properties of each cluster as follows.

3.4.1   MS 0451.6-0305

The galaxy cluster MS0451 was identified from the Einstein Medium Sensitivity Survey (EMSS) (Gioia et al. 1990; Stocke et al. 1991). The cluster redshift was confirmed by Gioia and Luppino (1994) and further refined by the Canadian Network for Observational Cosmology (CNOC) observations (Yee et al. 1996). It is a distant, rich (in cluster galaxy members) and X-ray luminous cluster which is also found to have a high X-ray temperature (Donahue 1996). The basic properties of the cluster that include velocity dispersion and virial radius are presented in Crawford et al. (2009) Table 1.

3.4.2   Cl 0016+16

The galaxy cluster Cl0016 was in the Einstein Extended Medium Sensitivity Survey (EMSS) (Stocke et al. 1991) and it is one of the distant cluster under the Clark Lake Radio Observatory (Cl) catalogue. Cl0016 is a rich and X-ray luminous cluster and has long been studied in the optical including cluster galaxy population studies using both photometric data (Koo 1981) and spectroscopic observations (Dressler et al. 1999; Crawford et al. 2011). This cluster has also been used to determine the Hubble constant value via its X-ray properties and SZ effect (see, Hughes and Birkinshaw 1998). The basic properties of the cluster that include velocity dispersion and virial radius can be found in Table 1 of Crawford et al. (2009).

3.4.3 Abell 0370

The galaxy cluster A370 was part of Abell rich galaxy cluster sample in the Palomar Observatory Sky Survey (Abell 1958). This cluster is one of the distant and rich clusters included in the revised Abell clusters catalogue (Abell et al. 1989, ACO). Studies of the evolution of galaxy population in A370 cluster have long been carried out (e.g. Couch et al. 1994) and the redshifts for the ACO have been compiled by Struble and Rood (1999). The basic properties of the cluster that include velocity dispersion and virial radius can be found in Lah et al. (2009).

3.4.4 MS 1512.4+3647

The galaxy cluster MS1512 was in the X-ray sources included in the Einstein Extended Medium Sensitivity Survey (EMSS) then identified in the optical (Gioia et al. 1990; Stocke et al. 1991). MS1512 is a rich cluster and was part of Canadian Network for Observational Cosmology Cluster Redshift Survey (CNOC1) sample (Abraham et al. 1998). The basic properties of the cluster that include virial mass and radius are presented in Molikawa et al. (1999); Lotz et al. (2003).

3.4.5 NSCS J121119+391250

The galaxy cluster J121119 was in the Einstein Extended Medium Sensitivity Survey (EMSS) X-ray sources then identified in the optical (Stocke et al. 1991). J121119 was detected in the intermediate redshift galaxy cluster catalogue of the Northern Sky Optical Cluster Survey (Lopes et al. 2004). The cluster observational properties in the literature include cluster spectroscopic redshift (Mullis et al. 2003), spectroscopic data follow-up (Horner et al. 2008), and other cluster properties such as X-ray and Sunyaev Zel'dovich (SZ) (Piffaretti et al. 2011).

3.4.6   1RXS J032649.5-004341
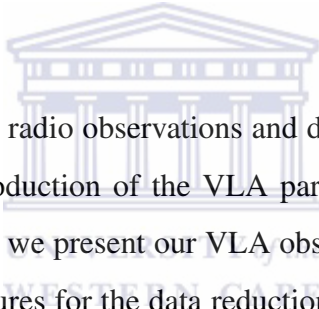
The galaxy cluster J032649 was in the extragalactic X-ray sources included in the ROSAT 1RXS catalogue (Voges et al. 1996) and discovered as part of the cluster in the ROSAT All Sky Survey Bright Source Catalogue (RASS-BSC) (Voges et al. 1999). The basic X-ray properties of the cluster is presented in Gilmour et al. (2009) who studied the distribution of AGN in galaxy clusters at z > 0.1.

Chapter 4

VLA Data Reduction and Analysis

4.1   Overview

This Chapter presents the radio observations and data analysis for this work. In Section 4.2, we give a brief introduction of the VLA parameters that are needed for the data reduction. In Section 4.3, we present our VLA observations. In Section 4.4, we provide a summary of the procedures for the data reduction. In Section 4.5, we present the data analysis that include source extraction and cataloguing. In Section 4.6, we provide the formulation for deriving the rest frame radio luminosity for our sample galaxies.

4.2   Introduction

The primary beam (PB) of the each VLA antenna is given by PB = $\frac{\lambda}{D}$ where λ is the wavelength and D is the diameter of the reflecting surface of the telescope. The diameter of each dish in the VLA telescope is 25 meters. To work out the PB value for each antenna, we used the small angle approximation to convert linear distance into angular size in arcsec (i.e. 206 265 arcsec in a radian). For the case of L-band observations i.e. at 1.4 GHz or 20 cm, the VLA PB is as follows:

$$\text{PB} \quad = \quad \frac{20}{2500} \times \frac{206265}{60} \sim 30'$$

The VLA angular resolution (θ) is given by $\theta = \frac{\lambda}{B}$ where λ is the observing wavelength and B is the baseline which depends on the array configurations of the telescope. The VLA antennas configurations are summarised in Table 4. The angular resolution in arcsec for all four different array configurations given in Table 4 are provided as follows. For an A-array configuration (36.4 km), it is then given by:

$$\theta \quad = \quad \frac{20}{3640000} \times 206265 \sim 1.2"$$

For B (11.1 km), C (3.4 km), and D (1.03 km) array configurations, VLA angular resolutions are about 4", 12", 40", respectively.

Table 4: The VLA telescopes array configurations.

Array Configuration	Max. Antennas Separation (km)
A	36.4
B	11.1
C	3.4
D	1.03

4.3   VLA Observations

Very Large Array (VLA) archival observations at 1.4 GHz were retrieved from the National Radio Astronomy Observatory (NRAO) data archive. VLA continuum observations were selected based on the target total on-source integration time (TOS). The TOS included in the sample were set by the availability of the *Spitzer* observations counterparts. The maximum TOS of raw uv data set were taken for each cluster when its *Spitzer* observations at 24 µm were available.

Table 5: The VLA radio continuum observations obtained at 1.4 GHz. The indicated observing time is the total time on-source (TOS) in each intermediate frequencies (IFs) for the target excluding calibrators integration time.

Cluster Name	Project ID	Array Conf.	BW MHz	Res. (arcsec)	Sensitivity (mJy beam^{-1})	Time (hrs)
MS0451	AN109/AB1199	BnA/A	25	3.9/1.4	0.052/0.04	20.6
Cl0016	AF304	D	50	44	0.015	2.55
A370	BK127	D	50	44	0.015	3.81
MS1512	AP245/AH491	A/C	50/12.5	1.4/12.5	0.041/0.051	2.21
J121119	AP219/AP245	BnA/A	50	3.9/1.4	0.064/0.04	1.48
J032649	AE147	B	50	3.9	0.025	0.82

The continuum observations (and pseudo-continuum data i.e. in spectral line mode for observations at bandwidths of 25 MHz or narrower; for the case of MS0451) were obtained in two IFs i.e. VLA standard L-band continuum frequencies of 1364.9 MHz and at 1435.1 MHz, with dual polarization in both left and right circular polarization. In Table 5, we summarise the details of the observing parameters that include cluster name, project ID, array configurations, bandwidths, resolutions, sensitivities, and TOS for each cluster.

4.4 VLA Data Reductions

The radio data reduction and analysis were entirely conducted using the NRAO Astronomical Image Processing System (AIPS, Greisen 2003) package. The reductions followed the standard calibration procedure that includes data inspection, exploring source visibilities, flagging corrupted data, phase and flux calibrations. We summarise the main steps of the reduction process as follows.

In the data inspection process, for the case of Project ID AB1199, data quality issues were reported in the NRAO data achieve. We first fixed the log files warnings posted in the NRAO VLA data archive that include Doppler Tracking error and Mozaicing error. These issues come from the fact that observations were acquired during the upgrade of the

VLA in which a mix of EVLA with VLA antennas has been set over the observing period. As instructed, a workaround that fixed this problem was to discard the EVLA antennas and all the associated baselines. Therefore, we excluded all three EVLA antennas that were present in the array during the observing run.

The data visibilities were explored with AIPS task UVPLT. Over the reduction process, any corrupted data were visually identified and flagged. Polarization was kept as default (Stokes I) since we are mainly interested in the total flux of the sources in the field. For each cluster, amplitude and phase were tracked using a nearby "secondary" calibrator, while absolute flux and bandpass were set via a well-known "primary" calibrator or a model where appropriate. Finally, the amplitude and phase solutions found were interpolated onto the target data.

In the case that the cluster observations were made in two sets of days, we independently reduced them and treated each array configuration as a single epoch. We then combined the two fully calibrated uv data sets in the uv-plane using AIPS task DBCON. No re-weighting was considered as the removal of corrupted data and calibration were performed in a similar fashion for each dataset. No self-calibration was applied since we are essentially interested in detecting point-like sources. The final calibration solutions were applied to the averaged IF at 1.4 GHz. The mapping parameters are based on the higher resolution data i.e. on the larger array configuration.

In the imaging process, we used a wide field imaging technique to image a larger field of view which is well beyond the primary beam. Using AIPS SETFC routine, we aimed to cover facets on all bright sources within one square degree of the pointing centre to properly account for flux and also the diminishing caused by sidelobe contamination. Facets were auto-generated for our targeted field coverage, resulting of the number of facets given in Table 6. Each facet was set to the same pixel scaling and image size in pixels, and these are also summarised in Table 6. The imaging processes were performed using AIPS task IMAGR. For all field, during the cleaning process, regions cleaned were limited to each bright source by putting clean box around it.

In the end, we examined our images background noise and found it to be comparable

Table 6: Number of facets, pixel scaling, and images size.

Cluster	Number of facets	Field covered (°)	Pixel scaling (")	Facet Image (IMAGR)
MS0451	61	1.03×1.03	0.3	4096"×4096"
Cl0016	19	1.17×1.17	10	256"×256"
MS1215	721	1.02×1.02	0.3	1024"×1024"
A370	19	1.17×1.17	10	256"×256"
J121119	55	1.06×1.06	0.3	4096"×4096"
J032649	73	1.06×1.06	1	1024"×1024"

to previously reduced data in the literature. Besides, no convolutional artifacts were particularly inspected around point sources.

The details of the final cleaned and flattened maps which include convolved beam size (HPBW), position angle (PA), image RMS noise, imaged FOV coverage are summarized in Table 7. As an example, for MS0451 cluster we obtained images with a 1σ RMS noise level of 12 µJy, with a 1.99"×1.8" synthesised beam (HPBW) at a position angle 0.56°.

Table 7: Summary of the specifications for the final cleaned and flattened maps that include convolved beam size (HPBW) and RMS noise of the images in µJy beam^{-1}.

Cluster	Conv. Beam Size (")	RMS Noise	P. Angle	Image (FLATN) (")	FOV (°)
MS0451	1.99×1.63	12	0.56	8192×8192	0.7×0.7
Cl0016	56.21×45.07	110	69.65	512×512	1.4×1.4
MS1215	1.39×1.29	52	-70.63	2048×2048	0.2×0.2
A370	55.79×44.51	55	-47.06	512×512	1.4×1.4
J121119	1.58×1.40	53	74.33	8192×8192	0.68×0.68
J032649	5.42×4.43	46	-27.07	2048×2048	0.57×0.57

4.5 Radio Data Analysis

4.5.1 Source Extraction and Cataloguing

We conducted an automated source detection and extraction in all images using a built-in function in the AIPS package. We used AIPS "Search And Destroy" (SAD) routine to detect sources and estimate flux densities of the sources in our maps.

SAD routine automatically searches for potential sources in a radio map, estimates their flux densities, generates and outputs source catalogue based on Gaussian fitting procedures. The routine is designed to find sources that have integrated and peak flux densities greater or equal than a given detection threshold. To run SAD, a RMS noise map for each cluster image is required.

(i) Firstly, AIPS task RMSD was used to produce a RMS noise map for each cluster image. The calculation of the noise map was preceeded by fitting a Gaussian function to the histogram of the pixels values. The noise maps were all calculated within a 30" in diameter correspond to 100 neighbor pixels, i.e. IMSIZE=100,-1, OPTYPE='HIST', by following the method of Morrison et al. (2010); Wold et al. (2012).

(ii) Secondly, we ran SAD routine in signal-to-noise mode where S/N$\geq$3 cut off was applied to both integrated and peak flux densities. SAD considers that each group of pixels above the given S/N is a potential source (island). SAD fits one or more Gaussian components to these islands and then estimates the size of the source.

(iii) Finally, a list of potential radio sources is then generated and output along with the associated best fit parameters. The AIPS task SAD has been used to generate initial radio source catalogues for large radio continuum surveys such as in the Deep Swire Field of Owen and Morrison (2008); VLA-COSMOS of Schinnerer et al. (2010); and GOODS-North Field of Morrison et al. (2010).

4.5.2 Unresolved & Marginally Resolved Sources

Source classification and flux density were assigned based on the method adopted by Owen and Morrison (2008) that uses the best-fit major axis value. Following Owen and Morrison (2008) method, we used our 1.4 GHz photometry catalogue resulted from AIPS task SAD to assign the flux density of the sources. For marginally resolved sources i.e. sources that have lower-limit best-fit major axis greater than zero, the integrated flux densities are directly assigned to the sources. While the peak flux densities are equal to integrated flux density for the unresolved sources (Low MAJ-AXIS = 0).

Radio sources in our moderate redshift clusters are mostly point-like sources and thus were classified as unresolved and marginally resolved. Therefore, we entirely made use of the flux densities computed through AIPS SAD routine. The uncertainty in the integrated flux densities for both unresolved and marginally resolved sources were computed through AIPS SAD routine over the source detection and extraction processes.

4.6 Radio Luminosity ($L_{1.4GHz}$)

We determined the rest-frame radio luminosities ($L_{1.4GHz}$) of the sources by converting the integrated radio flux densities ($S_{1.4GHz}$) using the following equation (Sargent et al. 2010b).

$$L_{1.4GHz}(\text{W Hz}^{-1}) = \left(\frac{4\pi \, [D_L(z)]^2}{(1+z)^{1-\alpha}} \right) \times S_{1.4GHz} \tag{4}$$

where $S_{1.4GHz}$ is the integrated flux density at 1.4 GHz in Jy, and $D_L(z)$ is the luminosity distance at the redshift of the source in metre. The *K*-correction $1/(1+z)^{(1-\alpha)}$ consists of $1/(1+z)^{-\alpha}$ terms which is the "colour" correction and $1/(1+z)$ terms which is "bandwidth" correction (Morrison et al. 2003). The radio spectral index α is the power law slope of the synchrotron radiation, and is defined as $S_\nu \sim \nu^{-\alpha}$. We assumed $\alpha \sim 0.8$ for normal star-forming galaxies of Condon (1992).

Since the uncertainty in the integrated radio flux density measured from AIPS is only
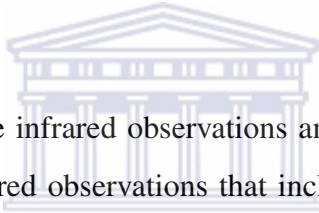
a tentative estimates of the uncertainty, therefore, we worked out the representative error bars in $L_{1.4\text{GHz}}$ to be as either the standard deviation of the means which is given by $\sqrt{\frac{\sum(x-\bar{x})^2}{n(n-1)}}$ or rather solely by the standard deviation.

Chapter 5

Infrared Observations and Analysis

5.1 Overview

This Chapter presents the infrared observations and analysis for this work. In Section 5.2, we present our infrared observations that include the specifications of the *Spitzer* post basic calibrated data and the sensitivities of the super mosaic imaging. In Section 5.3, we describe the data analysis that includes photometry and the IR source catalogue. In Section 5.4, we provide the details for matching radio sources counterparts from IR source catalogue. In Section 5.5, we present our methods for estimating IR luminosities of galaxies. In Section 5.6, we describe our attempt to use IR longer wavelengths data for MS0451 cluster.

5.2 *Spitzer* Observations

The *Spitzer* Space Telescope (*Spitzer*, Werner et al. 2004) features three science instruments which consists of the Infrared Array Camera (IRAC, Fazio et al. 2004), the Infrared Spectrograph (IRS, Houck et al. 2004), and the Multiband Imaging Photometer for *Spitzer* (MIPS, Rieke et al. 2004). MIPS has three detector arrays at 24 µm, 70 µm, 160 µm. IRAC operates simultaneously at four wavelengths of 3.6 µm, 4.5 µm, 5.8

μm and 8 μm. In this work, we retrieved and analysed *Spitzer* MIPS archival observations at 24 μm along with IRAC data where available for a sample of galaxy clusters at intermediate redshift.

There are two high level products that we accessed through the *Spitzer* data archive centre. It consists of post basic calibrated data (PBCD) products and the *Spitzer* enhanced imaging products (SEIP) or super mosaic images. These mosaic products were all produced from a pipeline-processed basic calibrated data (BCD) through the *Spitzer* MOPEX (Makovoz and Marleau 2005) software package. The differences between the two products can be described as follows:

(a) The PBCD products were retrieved through the *Spitzer* heritage archive (SHA[1]). Each single bandpass of the IRAC and MIPS data has multiple pointings and thus several mosaic images. The PBCD product consists of one particular program or one specific observing run. Each program is associated with a specific list of astronomical observation request (AOR) or a list of observing parameters.

(b) The super mosaic images were retrieved through the *Spitzer* enhanced imaging products archive (SEIP[2]). The super mosaic images were produced from a combination of multiple programs. Thus, MIPS imaging at 24μm as well as each single bandpass of IRAC where available is made of a combination of several mosaic images from multiple pointing. As a result, super mosaic images are much deeper and have wider field of view (FOV) than the PBCD images. The super mosaic images of the MIPS at 24μm for each cluster consist of a single large mosaic-ed imaging ranging from 0.25 to 0.6 square degrees in size.

We initially attempted to use the PBCD products for our analysis by choosing the most suitable dataset available for the cluster MS0451. However, our sample was limited by the insufficient data coverage and depth for both the IRAC and MIPS 24μm images (e.g. 93.6 sec integration time per pixel for the IRAC bands and 30.93 sec for the MIPS at 24μm). Therefore, in this work we make use of the large and deep super mosaic images.

---

[1]http://sha.ipac.caltech.edu/applications/Spitzer/SHA
[2]http://irsa.ipac.caltech.edu/data/SPITZER/Enhanced/Imaging/

5.2.1 Super Mosaic Imaging

Spitzer MIPS 24 μm imaging mosaics along with the coverage maps and the uncertainty maps for the cluster sample were retrieved from the *Spitzer* SEIP data archive. This high level product consists of a combination of multiple programs and has a field of view of $\sim 0.3° \times 0.3°$. The MIPS 24 μm data has a median pixel scaling of 2.45" and a mean FWHM of 5.9".

Additionally, *Spitzer* IRAC super mosaics at 3.6 μm, 4.5 μm, 5.8 μm, 8.0 μm were also retrieved although images are only available for few clusters. The IRAC images have a median pixel scaling of ~ 1.2" and the image mean FWHM is 1.66", 1.72", 1.88", and 1.98", respectively.

5.2.2 Image Sensitivity

We summarise the image sensitivities which is the mean integration time for each cluster in Table 8. The mean integration time of the MIPS 24μm super mosaic imaging are given in seconds per pixel.

Table 8: The *Spitzer* super mosaic MIPS 24μm mean exposure time in seconds per pixel.

Cluster	Exp. time (sec pix.$^{-1}$)
MS0451	1637
Cl 0016	764
A370	2646
MS1512	566
J032649	45
J121119	438

5.3   *Spitzer* **Data Analysis**

We used the most recent version of APEX 18.5.6, *Spitzer* MOPEX, software to perform
aperture photometry via the APEX User List Single Frame pipeline. The *Spitzer* IRAC
and MIPS images are in units of surface brightness i.e. in Mega Jansky per Steradian
(MJy Sr^{-1}). The *Spitzer* APEX is specifically designed to handle images in these units
and flux density is output in µJy (Makovoz and Marleau 2005).

5.3.1   **Aperture Photometry**

5.3.1.1   **Aperture Sizes**

There are five default aperture sizes in APEX which consists of 4", 6", 8", 10" and 20"
in radius for the IRAC pipeline, while four default aperture sizes that consists of 1.22",
2.45", 5.31" and 7" for the MIPS 24µm imaging. The optimal aperture sizes for the
measurements were selected based on sizes that are likely to produce the minimum flux
density error. The default aperture sizes in APEX turns out to fall within the ideal range
for error estimates as within a radius of about 3 pixels scaling of the image and also
consistent with the point sources assumption of about 9".

For the *Spitzer* super mosaic IRAC images (where 1 pixel = 1.2"), we worked out that
flux density errors estimated within 3.6" should represent well the uncertainties for the
measurements in the IRAC images. Likewise, for MIPS (1 pixel = 2.45") errors should
be estimated within 7.35". The aperture size for our measurements for both the MIPS
24µm and IRAC 3.6, 4.5, 5.8 and 8 µm data were selected based on these criteria and the
optimal size suggested for point sources based on the pixel sampling of the MIPS 24 µm
PSF[3]. The MIPS 24µm aperture size of 5.31" in radius and the IRAC aperture size of 4"
in radius were used.

------

[3]irsa.ipac.caltech.edu/data/SPITZER/docs/

5.3.1.2 Photometry

Optical coordinates were used to perform aperture photometry on the *Spitzer* observations. Aperture photometry was done using APEX (Makovoz and Marleau 2005, *Spitzer* MOPEX). The aperture size was set to a radius of 5.31" in the MIPS 24 μm imaging. The RMS noise of each image are given in Table 10.

Our cluster sources are expected to be essentially unresolved at this redshift in the MIPS 24 μm data. Thus, we note that we did not perform an aperture correction for our flux density measurements, because this only applies to resolved sources. If our sources were resolved additional corrections may be needed to compensate for any missing flux.

5.3.1.3 Flux Density Upper / Lower limits

Photometry was performed on the MIPS 24 μm image for all spectroscopic sources in our sample appearing in those images. Sources outside of the MIPS 24 μm image were removed from our sample along with sources with flux densities below the RMS noise. In a few cases, we defined a lower limit on MIPS flux density at 24μm resulting from cases in which sources have poor detection due to high background noise in the images (e.g. at the edges), where a value of $\geq 2\sigma$ of the RMS noise level was substituted for these sources, except for MS0451 which is at $\geq 1.5\sigma$.

5.3.1.4 Photometric Catalogue

We summarise the number of sources with secure spectroscopic redshifts that were successfully detected in the IR photometry for the full cluster sample in Table 9. For example, the final catalogue of MS0451 sources with secure spectroscopic redshifts and IR photometry consists of 157 cluster galaxies and 483 field galaxies.

5.4 Matching of Radio Sources Counterparts

We searched for radio source counterparts in the 1.4 GHz photometry catalogue using the optical positions. We determined the optimum value for our search radius by conducting a series of searches that include four matching radius of 1.3", 1.63", 1.99" and 3.24". We selected these search radii trial values to be within the FWHM of the imaging with a search radius of $< (\frac{\text{FWHM}}{3})$, where a matching radius of 2" was used. Furthermore, any unambiguous identification were also discarded from the final catalogue.

We summarise the number of sources in both the IR and radio catalogue and the number of matched sources in Table 9. Due to the limited number of the IR-radio matched sources, we note that we have additionally included sources at $\geq 1.5\sigma$ either in IR or in radio into the analysis. For example, we matched IR-radio sources 18 out of 156 cluster member galaxies and 45 out of 483 field galaxies in MS0451.

Table 9: Summary of the number of sources in the IR and radio catalogue. The radio counterparts were matched within the matching radius of FWHM/3 or 2" (or FWHM of the larger PSF of the two bands involved in the match). Confirmed cluster members are indicated in (CG) and field galaxies are denoted in (FG).

Cluster	IR photometry	SAD radio catalogue (S/N$\geq$3)	IR-radio catalogue
MS0451	157 (CG)	9545	18 (CG)
MS0451	483 (FG)	—	45 (FG)
Cl0016	412	170	10
MS1512	94	724	3
A370	115	253	5
J032649	8	996	2
J121119	5	10130	2

We show an example of multi-wavelength cut-out from the optical, IR, and radio images for selected cluster galaxies in Figure 9. Our full sample of matched sources is presented in Table 10 for cluster galaxies and field galaxies. Table 10 provides the details of all stages in the analysis that include cluster name, spectroscopic redshift, IR photometry, RMS noise of the MIPS 24 μm image in μJy, IR lower limit, 1.4 GHz photometry, matching radius, and IR-radio matched catalogue. In the next Section (§5.5),

we derive the IR luminosities along with other intrinsic properties for the resulting IR-radio galaxy sample.
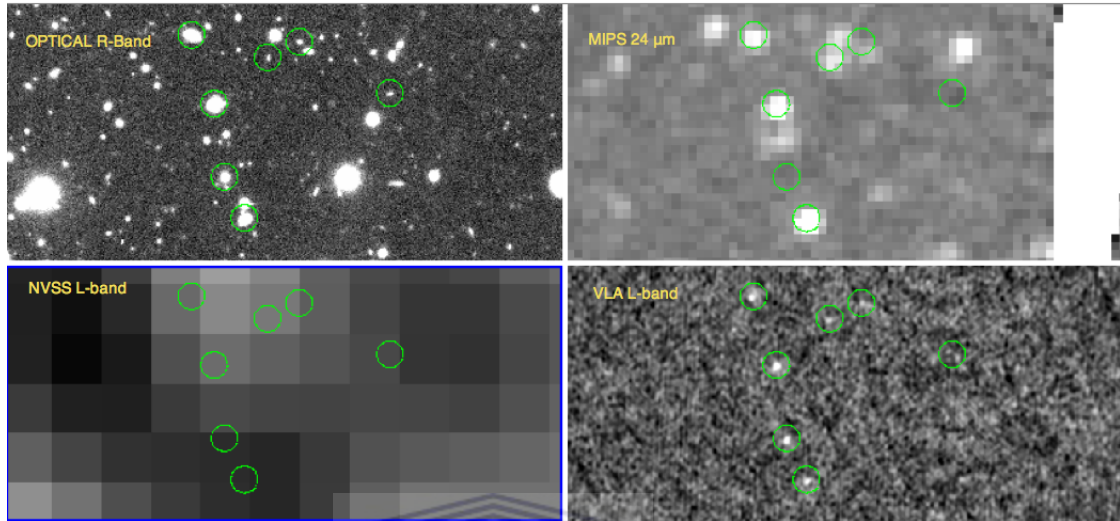
Figure 9: Montage of multi-wavelength observations for MS0451 cluster that consists of optical R-band, MIPS 24μm, VLA 1.4 GHz, NVSS 1.4 GHz images. As can be seen, our VLA data are much better than NVSS. A DS9 regions of detected cluster galaxies in MS0451 shown in green circles that include (in top-down order) source ID 1178, 1081, 1143, 940, 1093, 1158, and 1118 are shown.

Table 10: Summary of the different stages in the analysis that include cluster name, spectroscopic redshift, IR photometry, RMS noise of the MIPS 24 μm image, IR lower limit, 1.4 GHz photometry, matching radius (FWHM/3 of the larger PSF of the two bands involved in the match), and the number of sources matched in both catalogues.

Cluster	Spec-z	IR-phot	RMS noise (μJy)	IR lower limit	1.4GHz-phot	Match radius	IR-Radio catalogue
MS0451	350 (CG)	157	26	39	9545	2"	18
MS0451	1107 (FG)	483	26	39	9545	2"	45
Cl0016	577	412	32	64	170	18"	10
MS1512	370	94	28	—	724	2"	3
A370	180	115	30	90	253	18"	5
J032649	43	8	120	—	996	3"	2
J121119	35	5	29	87	10130	2.5"	2

5.5 IR Luminosities of Galaxies

The total IR luminosities of our sample galaxies were derived from empirical relations that use the MIPS data at 24μm which were adopted from Rieke et al. (2009). It is based on the formulation of Sanders et al. (2003) and defined as (TIR, 8–1000μm). The details of the formulations are given as follows.

5.5.1 The IR Luminosity at 24μm ($L_{24\mu m}$)

We determined $L_{24\mu m}$ based on the best-fit SFR calibration which uses the 24μm flux density as formulated in Rieke et al. (2009). The SFR can be estimated using Equation 5; (see also Rieke et al. 2009, Equation 14):

$$\log(\text{SFR}) = A(z) + B(z)\,(\log(4\pi D_L^2\, f_{24,\text{obs}}) - 53) \tag{5}$$

where the SFR is in $M_\odot\ \text{yr}^{-1}$, D_L is the luminosity distance in cm, and $f_{24,\text{obs}}$ is the observed flux density at 24μm in Jy. The coefficients A(z) and B(z) are redshift-dependent and can be obtained by interpolating the values in Table 1 of Rieke et al. (2009). The 24μm luminosity, $L_{24\mu m}$, was calculated using Equation 6 and 7. Hence, we now have the K-corrected monochromatic or spectral luminosity ($L_{24\mu m}$) estimated at $\nu = 24$μm.

$$\text{SFR}\ [M_\odot\ \text{yr}^{-1}] = 7.8 \times 10^{-10} L(24\mu m, L_\odot)$$

$$L(24\mu m, L_\odot) = \frac{\text{SFR}\ [M_\odot\ \text{yr}^{-1}]}{7.8 \times 10^{-10}};\ \text{for}\ (6 \times 10^{8} L_\odot \le L_{24\mu m} \le 1.3 \times 10^{10} L_\odot) \tag{6}$$

$$\text{SFR}\ [M_\odot\ \text{yr}^{-1}] = 7.8 \times 10^{-10} L(24\mu m, L_\odot) \times (7.76 \times 10^{-11} L(24\mu m, L_\odot))^{0.048}$$

$$L(24\mu m, L_\odot) = \left(\frac{SFR \; [M_\odot \; yr^{-1}]}{7.8 \times 10^{-10} \times (7.76 \times 10^{-11})^{0.048}} \right)^{0.954} ; \text{if} \; (L_{24\mu m} > 1.3 \times 10^{10} L_\odot)$$

(7)

In addition to $L_{24\mu m}$, we also computed the IR luminosities, L_{TIR}, $L_{60\mu m}$, and L_{FIR} to allow a comparison of our measurements to other works. We adopt the definition from Rieke et al. (2009) that L_{TIR} is the luminosity between L(TIR; 8–1000 μm) and we adopt the definition of L_{FIR} from Helou et al. (1985) as L(FIR; 42–122 μm). We provide the details of these transformations in the proceeding sections.

5.5.2 Estimating Total IR Luminosity (L_{TIR})

We estimated the total IR luminosity L_{TIR} from the rest-frame IR luminosity $L_{24\mu m}$. Rieke et al. (2009) compute L_{TIR}, L(TIR; 8–1000 μm), as described in Sanders et al. (2003); Sanders and Mirabel (1996). The L_{TIR} luminosity estimator of Sanders and Mirabel (1996) is defined at $\lambda = 8-1000 \, \mu m$, and is fully defined as L(TIR; 8–1000 μm):

$$L_{TIR} \; [L_\odot] \sim 4.93 \times 10^{-22}(13.48L_\nu(12\mu m) + 5.16L_\nu(25\mu m) + 2.58L_\nu(60\mu m) + L_\nu(100\mu m))$$

where L_ν [erg s^{-1}Hz^{-1}] is defined as the luminosity per unit frequency at a frequency $\nu = c/\lambda$ where c is the speed of light.

The L_{TIR} was computed based on the 24μm luminosity ($L_{24\mu m}$) using the empirical relation of Rieke et al. (2009); (see, Equation (A6) in Rieke et al. 2009), which is given by Equation 8.

$$\log L_{TIR} = (1.445 \pm 0.155) + (0.945 \pm 0.016) \log L_{24\mu m} \tag{8}$$

Furthermore, in order to be consistent for all our calculations and comparisons, we also used other formulations of Rieke et al. (2009) to estimate the $L_{60\mu m}$ which is presented as per below.

5.5.3 Inferring IR Luminosity ($L_{60\mu m}$)

We inferred the $L_{60\mu m}$ using the following relation taken from Rieke et al. (2009) as well; (see, Equation (A7) in Rieke et al. 2009), that is given by Equation 9.

$$\log(L_{TIR}) = (1.183 \pm 0.101) + (0.920 \pm 0.010) \log(L_{60\mu m})$$

$$\text{Hence, } \log(L_{60\mu m}) = \frac{\log(L_{TIR}) - 1.183}{0.920} \tag{9}$$

5.5.4 Inferring Far-IR Luminosity (L_{FIR})

It is also common to study the relationship between the IR and radio luminosity using the classical far-IR luminosity as defined by Helou et al. (1988) at $\lambda = 42\text{–}122\,\mu m$. The far-IR luminosity L(FIR; 42–122 μm) estimator is given by:

$$L_{FIR}\ [L_\odot] \sim 3.29 \times 10^{-22} \times (2.58 L_\nu(60\mu m) + L_\nu(100\mu m))$$

where L_ν [erg s^{-1}Hz^{-1}] is defined as the luminosity per unit frequency at a frequency $\nu = c/\lambda$ where c is the speed of light.

We inferred the L_{FIR} based on the assumption that the global ratio of L_{TIR}, L(TIR; 8–1000 μm), and L_{FIR} L(FIR; 42–122 μm) luminosity is approximately 2 (see e.g. Bell 2003), and also in L_{TIR} defined as L(TIR; 3–1100 μm), (see Dale et al. 2001; Dale and Helou 2002). We adopted the relation presented in Equation 10.

$$L_{TIR}/L_{FIR} \sim 2; \text{ or } L_{FIR} \sim 0.5 \times L_{TIR} \tag{10}$$

5.6   *Herschel* **Data & Analysis**

We examined data from the recently available *Herschel* observations in the field of MS0451 cluster which consists of both PACS/PACS Evolutionary Probe (PEP) (Lutz et al. 2011; Magnelli et al. 2013) and the SPIRE/*Herschel* Multi-tiered Extragalactic Survey (HerMES) (Oliver et al. 2012; Smith et al. 2012).

The PACS data do not fully cover our field of view and we were only able to detect two sources in the SPIRE observations of MS0451 cluster. As the *Herschel* data are not expected to significantly modify our results (due to inferior quality of the available data) and due to the small number of sources with data, we did not attempt any further analysis using this data. Furthermore, we did not pursue either data collection search and hence analysis for the rest of the clusters in our sample.

Chapter 6

The far-IR-radio Correlation in Cluster Galaxies at Intermediate Redshift

6.1 Overview

In the previous Chapters, we have presented our multi-wavelength observations, cluster sample, galaxy sample, data reduction, and data analysis. Furthermore, we have measured the radio and IR luminosities for our sample of cluster galaxies at intermediate redshifts. In this Chapter, we aim to measure the far-IR-radio relationship of these galaxies to test how this relationship changes between lower and intermediate redshift cluster galaxies as well as field galaxies.

This Chapter is organised as follows. In Section 6.2, we cover a brief background introduction for this work. In Section 6.3, we provide a formulation for computing the IR and 1.4 GHz luminosity ratio q_{FIR}. In Section 6.4, we present our results for the cluster and field galaxy samples. In Section 6.5, we describe potential caveats that may affect this study. In Section 6.6, we discuss the properties of the far-IR-radio correlation for both our cluster and field galaxy samples. Finally, in Section 6.7, we draw conclusions from our findings.

6.2 Introduction

Radio continuum emission from normal star-forming galaxies can be a powerful tracer of recent star formation activity (Condon 1992). The radio luminosities at 1.4 GHz are tightly correlated with the far-IR luminosities for various galaxy types (e.g. van der Kruit 1971; Helou et al. 1985; Condon et al. 1991), in a broad range of star-forming systems (see Helou 1991; Condon 1992; Yun et al. 2001), and over a wide range of redshift (e.g. Garrett 2002; Appleton et al. 2004; Sargent et al. 2010a,b; Ivison et al. 2010a,b; Bourne et al. 2011)

The correlation is believed to be driven by the internal star formation rate. Radio emission from these galaxies are predominantly produced from the synchrotron emission of cosmic-ray electrons accelerated in supernova shocks whereas the infrared emission is due to ultraviolet light from young massive stars that is absorbed and re-radiated by dust (Condon 1992, and references therein). However, it is still unclear what maintains this strong correlation seen over such a wide range of galaxies (Murphy 2009).

The far-IR-radio correlation shows lower far-IR to radio luminosity ratios in galaxy clusters than that found in the field (Andersen and Owen 1995; Reddy and Yun 2004) with much of the variation coming from a subset of objects with large deviations from the relationship (Miller and Owen 2001). A number of different processes drive the evolution of galaxies in clusters such as gravitational interactions and ram pressure (see e.g. Boselli and Gavazzi 2006, for a review), and result in transforming blue, star-forming galaxies into the ubiquitous red, quiescent galaxies that dominate cluster populations today. These physical processes have been invoked to explain the differences seen in the far-IR-radio relationship as measured between the cluster and field (Murphy et al. 2009b).

Unfortunately, little work has been done at higher redshifts where we see an increase of star-forming galaxies (Butcher and Oemler 1984), transitional galaxies like E+A (Barger et al. 1996), and AGN (Martini et al. 2009) in galaxy clusters. Despite studies looking at the multi-wavelength properties of galaxies in distant clusters (e.g. Best et al. 2002; Saintonge et al. 2008), no systematic study has been made of the far-IR-radio

relationship in these clusters, and so, the present work is an unique opportunity to explore part of parameter space in *redshift* and *environment* that has not previously been probed.

6.3   The Luminosity Ratio q_{IR}

We characterised the quantitative measure of the far-IR-radio relationship by calculating the median logarithmic ratio of IR and radio luminosity (q_{FIR}), where q_{FIR} is dimensionless. The luminosity ratio was estimated using the commonly used equation of Helou et al. (1985) as follows:

$$q = \log\left(\frac{L}{3.75 \times 10^{12} \text{ W}}\right) - \log\left(\frac{L_{1.4\text{GHz}}}{\text{W Hz}^{-1}}\right) \tag{11}$$

where $L_{1.4\text{GHz}}$ is the rest frame radio luminosity in W Hz^{-1}, and L is the infrared luminosity in W. The 3.75×10^{12} term is the normalizing frequency in Hz at 80 μm (Helou et al. 1985). The subscript of q indicates which infrared luminosity is being used (i.e. q_{TIR} is for L_{TIR}). For calculating q_{24}, the constant used to normalise the infrared luminosity was 1.125×10^{12} W.

6.4   Results

We primarily aim to compare the far-IR-radio relationship in an intermediate redshift clusters to nearby clusters, and to do so, we will compare our results to the lower redshift measurements of Reddy and Yun (2004). As their results are reported in $L_{60\mu\text{m}}$ and q_{FIR} within L(FIR; 42–122 μm), we transform our $L_{24\mu\text{m}}$ results into comparable bands (see Eq. 9 and 11). We report the luminosities for all the cluster sources in Table 13 and field sources in Table 14.
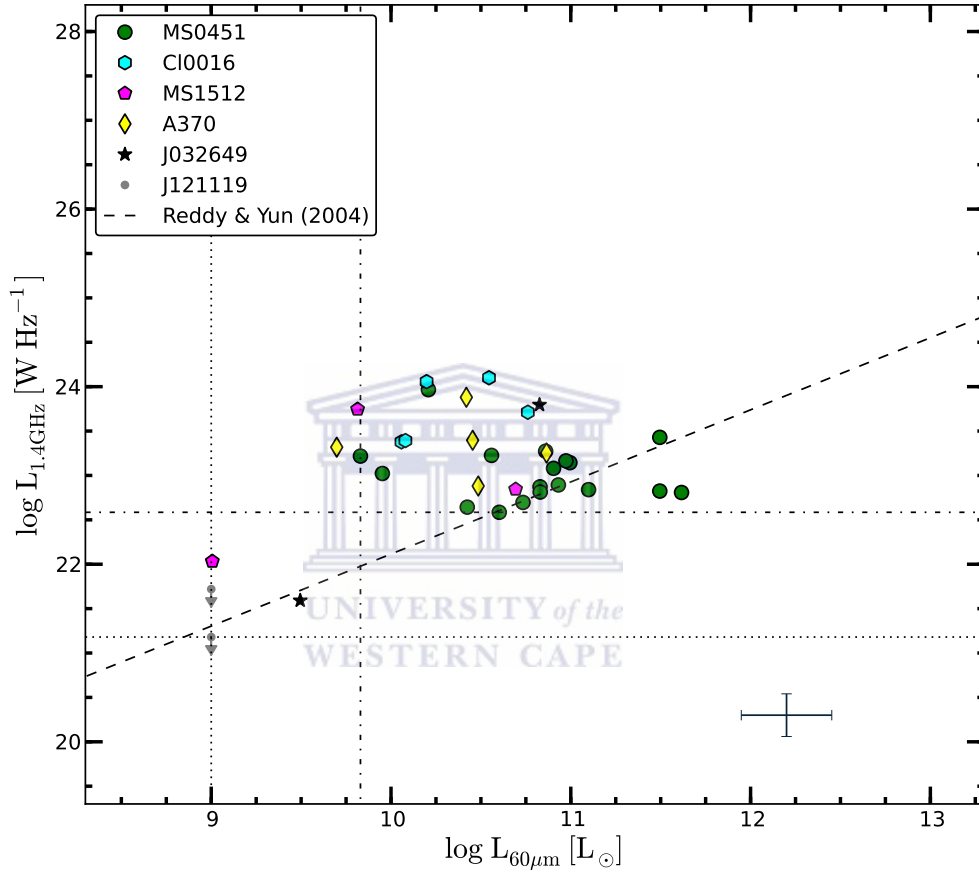
Figure 10: The 20 cm radio continuum luminosity ($L_{1.4GHz}$) against the IR luminosity ($L_{60\mu m}$) for all cluster sources in our sample. The dashed line indicates the formal linear least-square fit (log $L_{60\mu m}$ = 8.92 luminosity cutoff) of the low redshift cluster galaxies from Reddy and Yun (2004). The IR luminosity and radio luminosity lower limits is indicated in dotted lines for all cluster sources (log $L_{60\mu m}$ = 9.0; log $L_{1.4GHz}$ = 21.18), and in dashed dotted lines for MS0451 (log $L_{60\mu m}$ = 9.83; log $L_{1.4GHz}$ = 22.6). The error bars correspond to average 1σ errors.

6.4.1 The IR and Radio Luminosities

In Figure 10, we show the relationship between the rest frame radio luminosity at 1.4 GHz ($L_{1.4GHz}$) against the IR luminosity ($L_{60\mu m}$) for all cluster sources in our sample. The dashed line indicates the formal linear least-square fit of the cluster galaxies of Reddy and Yun (2004). Most of MS0451 cluster sources are consistent with Reddy and Yun (2004) relationship. IR luminosities upper limits were plotted for J121119 sources. The IR luminosity upper limit is indicated in the dashed dotted vertical line. Our IR luminosity and radio luminosity lower limits for MS0451 are log $L_{60\mu m}$ = 9.83 and log $L_{1.4GHz}$ = 22.6, respectively (see dashed dotted lines in Figure 10). For comparison, our lower limits are higher than that of the low redshift cluster galaxies (log $L_{60\mu m}$ = 8.92, log $L_{1.4GHz}$ = 20.47) of Reddy and Yun (2004).

6.4.2 The far-IR Luminosity and q_{FIR}

In Figure 11, we present the far-IR luminosity (L_{FIR}) to radio luminosity ($L_{1.4GHz}$) ratio (q_{FIR}) versus $L_{60\mu m}$. The dashed dotted grey line delineates our sample limiting magnitude. The mean q_{FIR} for these cluster galaxies is q_{FIR} = 1.42±0.70. This value is consistent with Reddy and Yun (2004) value of q_{FIR} = 2.07±0.74 and is also comparable with Andersen and Owen (1995); Miller and Owen (2001); Murphy et al. (2009b) (see Table 1).

In addition, Figure 11 shows no IR-excess sources ($q_{FIR} \geq 3.04$) as defined by Yun et al. (2001), a radio- or IR-excess galaxy is defined to have at least five times greater radio (IR) flux than what is expected from the field galaxy at that redshift for a given far-IR luminosity. We find that the percentage of galaxies that have radio-excess is 51±15% (18 of 35). This number of radio-excess cluster members is higher than the percentage found by Reddy and Yun (2004) (11%) for low redshift clusters. However, our percentage of excess objects is likely an overestimation due to the limiting flux in our radio measurements as discussed below.

The mean q_{FIR} values and the q_{FIR} standard deviation for each cluster are summarised
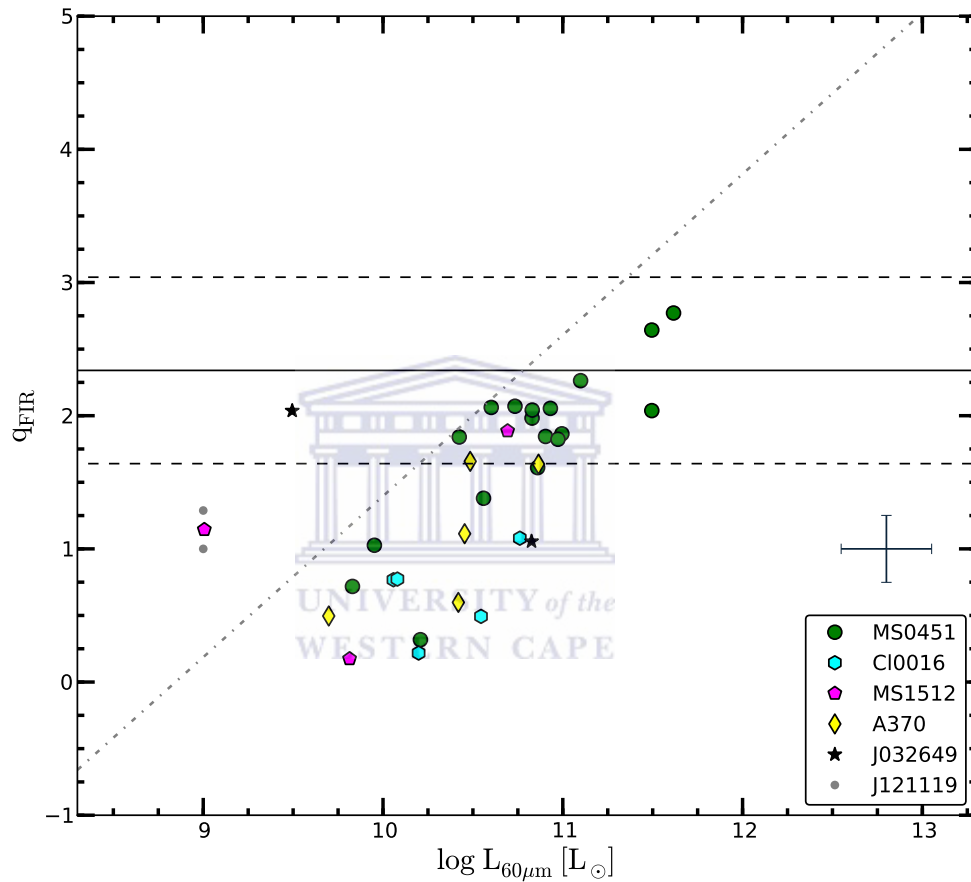
Figure 11: The logarithmic of the far-IR luminosity to 1.4 GHz radio continuum luminosity ratio (q_{FIR}) versus the IR luminosity ($L_{60\mu m}$) for all sources in our sample. The nominal value of q_{FIR} for field galaxies (q_{FIR}=2.34) of Yun et al. (2001) is plotted in the solid black horizontal line. The criteria for both delineating the radio-excess ($q_{\mathrm{FIR}}{\leq}1.64$) and IR-excess ($q_{\mathrm{FIR}}{\geq}3.04$) are shown in the dashed lines. The error bars correspond to average 1σ errors. The dash dotted grey line represents our sample limiting flux.

as follows. The cluster MS0451 sources has a mean q_{FIR} = 1.80±0.61 with a fraction of 28±14% (5 of 18) radio-excess sources. However, due to the radio flux limit, we are preferentially sampling only radio excess sources and likely overestimating our percentage of these sources. For comparison, if we limit our sources at $\log(L_{60\mu m})$ = 10.5 which would be comparable to our radio flux limit for sources at the q_{FIR} value for non-excess sources, then our percentage of excess sources is only 13%. This should be considered to be a lower limit for our percentage of radio-excess sources.

For the remaining clusters, our limiting flux in the radio data prevents us from measuring much, if any, of the population that would lie on the z = 0 far-IR-radio relationship for normal galaxies. As such, we only present our raw measurements for q_{FIR} and excess populations. Sources in Cl0016 have a mean q_{FIR} = 0.67±0.32 with a fraction of 5 of 5 radio-excess sources. Sources in A370 have a mean q_{FIR} = 1.1±0.55 with a fraction of 3 of 5 radio-excess sources. Sources in MS1512 have a mean q_{FIR} = 1.07±0.86 with a fraction of 2 of 3 radio-excess sources. Sources in J032649 have a mean q_{FIR} = 1.55±0.65 with a fraction of 1 of 2 radio-excess sources. Sources in J121119 have a mean q_{FIR} = 1.14±0.20 with a fraction of 2 of 2 radio-excess sources.

For the full sample excluding sources below our flux limits, we find a mean q_{FIR} = 1.43±0.73. The observed lower value of q_{FIR} = 1.43±0.73 has been found in clusters (Reddy and Yun 2004; Murphy et al. 2009b) as well as in the field (Garrett 2002; Kovács et al. 2006; Sajina et al. 2008).

We also compare our other measurements to other works as well. We find mean value of q_{24} = 1.33±0.73 and q_{TIR} = 1.72±0.7 for cluster sources while q_{24} = 1.62±0.64 and q_{TIR} = 1.97±0.63 for our field sources. A comparison of q_{24} and q_{TIR} values in the field indicates that our values are not inconsistent with previously published values of q_{24} (Boyle et al. 2007; Rieke et al. 2009; Sargent et al. 2010a; Bourne et al. 2011) and q_{TIR} (Murphy et al. 2009a; Sargent et al. 2010a; Ivison et al. 2010a; Jarvis et al. 2010; Ivison et al. 2010b). For a full comparison with other works, see Table 1 in Chapter 2. The measured q-values are summarised in Table 11 for each cluster and in Table 12 for the full sample, these will be further discussed in Section 6.6.

Table 11: Summary of our measured q_{FIR}-values.

Cluster	q_{FIR}
MS0451	1.80±0.61
Cl0016	0.67±0.32
A370	1.10±0.55
MS1512	1.07±0.86
J032649	1.55±0.65
J121119	1.14±0.20

Table 12: Summary of all measured q-values.

Sample	q_{24}	q_{FIR}	q_{TIR}
Sources in clusters	1.33±0.73	1.42±0.70	1.72±0.70
Sources in the field	1.62±.64	1.67±0.63	1.97±0.63

6.4.3 The q_{FIR}-values as a function of Galaxy Type

In Figure 12, we show the far-IR luminosity (L_{FIR}) to radio luminosity ($L_{1.4\text{GHz}}$) ratio (q_{FIR}) against $L_{60\mu m}$ particularly for MS0451 and Cl0016 both cluster and field galaxies. We split our sample from these two galaxy clusters into blue cloud (BC) and red sequence (RS) galaxies following the definition in Crawford et al. (2011) for both cluster and field samples. We see that none of the subsamples show any different behaviour. In Figure 12, red and blue colours indicate RS and BC sources and they all have secure photometric measurements from our imaging data. The number of sources that have secure photometric classification is 17 of 23 cluster sources and 23 of 50 field sources, and we focus on these sources with robust photometric information of these two clusters throughout the discussion.

Of these galaxies with known photometric classification, our mean q_{FIR} is 1.72±0.63 for cluster sources with a fraction of 35±17% (6 of 17) radio-excess, and 1.58 ± 0.71 for field galaxies with a fraction of 56±19% (13 of 23) radio-excess. Out of the cluster population, 50±30% (4 of 8) RS galaxies are radio-excess sources. In their sample,
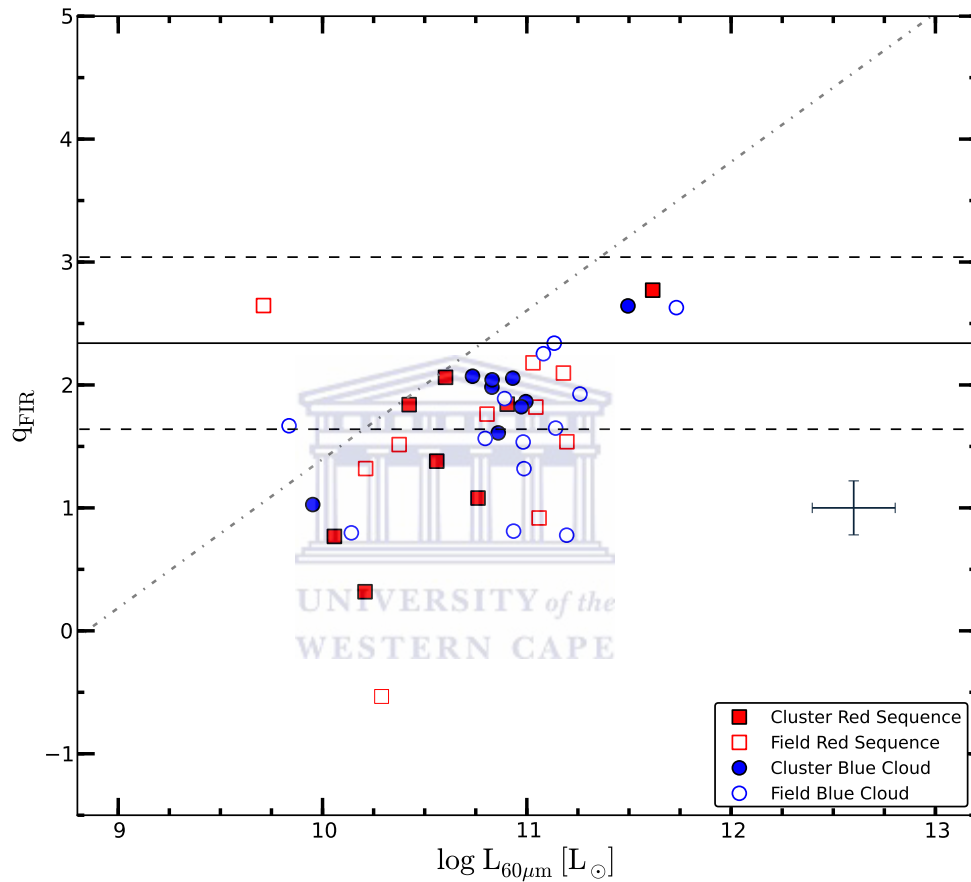
Figure 12: The logarithmic of the far-IR luminosity to 1.4 GHz radio continuum luminosity ratio (q_{FIR}) versus the IR luminosity ($L_{60\mu m}$) for MS0451 and Cl0016 sources. The nominal value of q_{FIR} for field galaxies (q_{FIR}=2.34) is plotted in the solid black horizontal line. The criteria for both delineating the radio-excess ($q_{FIR} \leq 1.64$) and IR-excess ($q_{FIR} \geq 3.04$) are shown in the dashed lines. The error bars correspond to average 1σ errors. The solid grey line represents our sample limiting flux.

Reddy and Yun (2004) find 28% of radio-excess galaxies are early type and that all also display evidence of AGN activity. For the BC cluster galaxies, we find 22±17% (2 of 9) radio-excess sources, which is consistent with the results of Miller and Owen (2001) and Reddy and Yun (2004). In the field, 6 of 13 of the blue galaxies show evidence for an enhanced radio emission, while 5 of 10 of field RS sources show evidence for an enhanced radio emission. The large fraction of field galaxies with enhanced radio emission is possible due to the presence of AGN as well as sampling a significant number of sources that are at higher redshift than our clusters where the scatter in the relationship can become large especially for 24 μm measurements (e.g. Appleton et al. 2004).

6.4.4   The q_{TIR}-values as a function of Redshift

In Figure 13, we plot q_{TIR} as a function of redshift for the COSMOS field (Sargent et al. 2010a) and for all sources in our sample. Our q_{TIR} values are similarly defined as the q_{TIR} of Sargent et al. (2010a) where IR luminosity is L(TIR, $8 - 1000\mu m$) and both follow the method of Helou et al. (1985). Figure 13 shows a number of cluster galaxies with an enhanced radio emission at intermediate redshift, while for a given error bar range we see that the distribution of q_{TIR} values for field galaxies (and some blue cluster galaxies) displays similar trend as those of Sargent et al. (2010a).

6.4.5   The q_{FIR}-values against Galaxy Type and Cluster Radius

In Figure 14, we plot the far-IR and radio luminosity ratio (q_{FIR}) as a function of the galaxy projected radius R [Mpc]. In aiming to use radius as a proxy for local density, similar to Reddy and Yun (2004), we define R_{Core}, R_{Ring} as the projected cluster-centric distance at R ≤ 0.5 Mpc and between [0.5, 1.5] Mpc, respectively. Miller and Owen (2001) and Reddy and Yun (2004) found a higher fraction of core galaxies that have a radio-excess but we see no evidence of this in our sample drawn from two clusters. The bulk of our sources seems to be scattered in the ring region and also lies well below nearby clusters relation as indicated in the solid horizontal line.
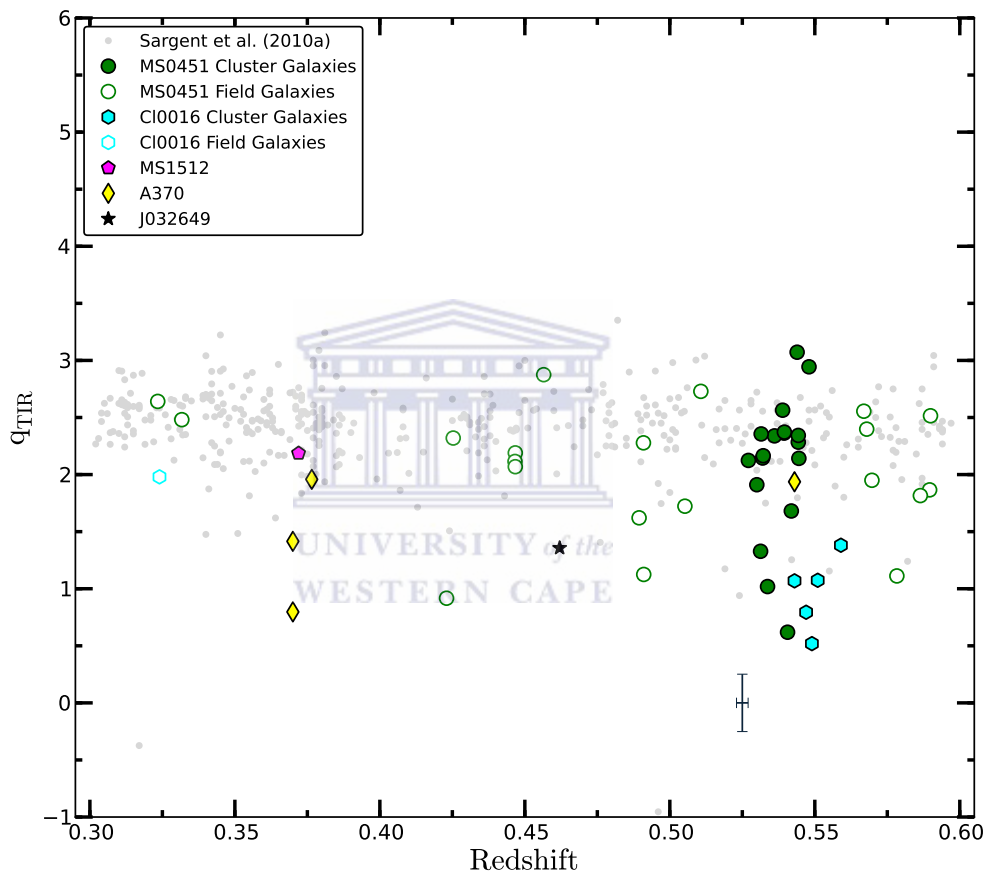
Figure 13: Plot of q_{TIR} values against redshift for both COSMOS field galaxies from Sargent et al. (2010a) in the redshift range between $0.3 < z < 0.6$ and all sources in our sample. The error bars correspond to average 1σ errors.
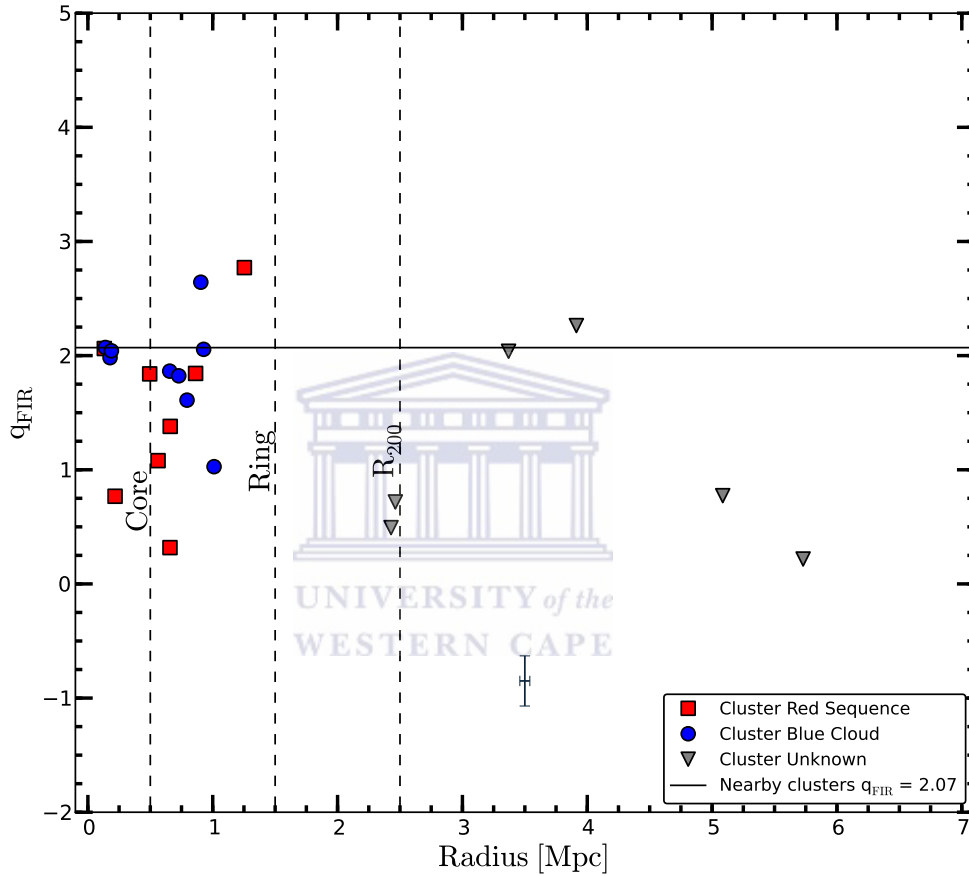
Figure 14: Plot of the galaxy projected radius against the far-IR to radio luminosity ratio q_{FIR} for MS0451 and Cl0016 sources. The mean value of q_{FIR} for low redshift cluster galaxies of Reddy and Yun (2004) is shown in the solid horizontal line (q_{FIR}=2.07). Similar to Reddy and Yun (2004), the vertical dashed lines define the R_{Core}, R_{Ring} as the projected cluster-centric distance at R $\leq$ 0.5 and between [0.5, 1.5] Mpc, respectively. The error bars correspond to average 1σ errors.

Table 13: Properties of cluster galaxies that include the total IR luminosity (L_{TIR}) and rest frame radio luminosity ($L_{1.4\,GHz}$).

ID	RA (Degree)	DEC (Degree)	Redshift	$S_{1.4}$ (μJy)	$S_{1.4}$-err (μJy)	$\log L_{1.4}$ (W Hz^{-1})	S_{24} (μJy)	S_{24}-err (μJy)	$\log(L_{24\mu m})$ ($L_\odot$)	$\log(L_{60\mu m})$ ($L_\odot$)	$\log(L_{FIR})$ ($L_\odot$)	$\log(L_{TIR})$ ($L_\odot$)
940	73.506546	-2.993305	0.531	102.035	31.961	23.022	56.0	27.0	9.412	9.952	10.038	10.339
1081	73.514153	-2.988997	0.531	75.906	24.331	22.893	323.0	27.0	10.364	10.931	10.938	11.239
1093	73.521263	-2.994204	0.527	144.311	21.045	23.164	357.0	27.0	10.405	10.973	10.977	11.278
1118	73.518738	-3.003781	0.532	134.700	25.470	23.144	363.0	27.0	10.427	10.995	10.998	11.299
1143	73.516792	-2.990292	0.532	116.476	24.413	23.080	307.0	27.0	10.339	10.904	10.914	11.215
1158	73.520401	-3.000317	0.542	156.083	24.667	23.226	156.0	27.0	10.002	10.559	10.596	10.897
1178	73.523178	-2.988423	0.530	183.027	54.111	23.273	286.0	27.0	10.295	10.860	10.873	11.174
1489	73.534897	-3.054384	0.548	60.155	20.114	22.824	846.0	27.0	10.914	11.495	11.457	11.758
1726	73.549652	-3.044432	0.541	862.685	98.963	23.966	84.0	27.0	9.661	10.208	10.274	10.575
1811	73.550758	-3.016844	0.539	36.0	12.0	22.585	170.0	23.0	10.045	10.602	10.636	10.937
1968	73.552841	-3.015063	0.544	68.270	31.055	22.872	251.0	23.0	10.265	10.829	10.844	11.146
2143	73.558327	-3.033125	0.544	40.246	14.390	22.643	121.0	26.0	9.871	10.424	10.472	10.774
2707	73.579857	-3.058745	0.544	59.0	26.0	22.808	1079.0	26.0	11.031	11.616	11.568	11.869
7240	73.551170	-3.016482	0.539	46.558	13.505	22.696	216.0	23.0	10.172	10.734	10.757	11.058
7270	73.553276	-3.014704	0.544	59.619	26.992	22.813	252.0	23.0	10.266	10.830	10.845	11.146
8110	73.396484	-3.020605	0.536	255.464	73.437	23.429	897.0	21.0	10.914	11.495	11.457	11.758
8543	73.684250	-3.117824	0.539	64.923	44.906	22.840	425.0	20.0	10.528	11.099	11.093	11.394
8592	73.653625	-3.019160	0.534	158.694	47.826	23.218	45.0	24.0	9.293	9.830	9.926	10.227
220	4.662203	16.452358	0.559	443.637	147.397	23.712	206.479	25.553	10.199	10.761	10.782	11.083
447	4.655342	16.544334	0.547	1141.146	337.459	24.100	148.228	43.068	9.988	10.545	10.583	10.884
184	4.643237	16.431973	0.543	220.000	55.000	23.378	64.000	16.000	9.514	10.058	10.135	10.436
430	4.602367	16.195959	0.549	1023.071	254.139	24.056	79.658	29.067	9.651	10.198	10.264	10.565
422	4.571400	16.233490	0.551	220.000	55.000	23.393	64.000	16.000	9.536	10.080	10.155	10.456

Continued. Properties of cluster galaxies that include the total IR luminosity (L_{TIR}) and rest frame radio luminosity ($L_{1.4GHz}$).

ID	RA (Degree)	DEC (Degree)	Redshift	$S_{1.4}$ (μJy)	$S_{1.4}$-err (μJy)	log $L_{1.4}$ (W Hz^{-1})	S_{24} (μJy)	S_{24}-err (μJy)	log($L_{24μm}$) ($L_{\odot}$)	log($L_{60μm}$) ($L_{\odot}$)	log(L_{FIR}) ($L_{\odot}$)	log(L_{TIR}) ($L_{\odot}$)
79	39.972500	-1.553610	0.370	469.750	60.805	23.318	90.0	30.0	9.164	9.698	9.804	10.105
52	39.982180	-1.572040	0.377	165.0	55.0	22.881	350.463	22.630	9.930	10.485	10.528	10.829
105	40.002080	-1.605830	0.370	562.165	125.402	23.396	346.948	24.614	9.901	10.454	10.500	10.801
3	39.963990	-1.591050	0.543	165.0	55.0	23.253	270.555	25.565	10.301	10.865	10.878	11.179
89	39.993330	-1.609440	0.610	531.438	252.118	23.880	90.0	30.0	9.866	10.419	10.468	10.769
16	228.612770	36.634130	0.162	156.0	52.0	22.033	151.925	16.510	8.491	9.006	9.168	9.469
24	228.562400	36.596300	0.116	16497.963	590.431	23.746	1565.235	18.510	9.277	9.814	9.911	10.212
2	228.593680	36.605850	0.372	156.0	52.0	22.845	524.853	15.309	10.133	10.693	10.720	11.021
18	51.640660	-0.604300	0.022	3714.014	609.087	21.591	27242.236	86.096	8.967	9.495	9.618	9.919
30	51.620710	-0.537570	0.462	843.802	241.674	23.796	383.738	199.920	10.262	10.826	10.842	11.143
31	182.499480	39.196590	0.004	303.842	141.037	21.720	338.263	42.195	5.561	9.0	9.0	9.0
33	182.635740	39.405730	0.003	159.0	53.0	21.180	87.0	29.0	4.686	9.0	9.0	9.0

Table 14: Properties of field galaxies that include the total IR luminosity (L_{TIR}) and rest frame radio luminosity ($L_{1.4GHz}$).

ID	RA (Degree)	DEC (Degree)	Redshift	$S_{1.4}$ (μJy)	$S_{1.4}$-err (μJy)	$\log L_{1.4}$ (W Hz^{-1})	S_{24} (μJy)	S_{24}-err (μJy)	$\log(L_{24\mu m})$ ($L_\odot$)	$\log(L_{60\mu m})$ ($L_\odot$)	$\log(L_{FIR})$ ($L_\odot$)	$\log(L_{TIR})$ ($L_\odot$)
56	73.465767	-3.087744	0.425	94.590	46.975	22.762	412.0	29.0	10.188	10.749	10.771	11.072
821	73.502357	-3.052398	0.568	99.734	37.633	23.080	429.0	32.0	10.606	11.179	11.167	11.468
831	73.503860	-3.053502	0.570	256.420	108.698	23.493	397.0	30.0	10.569	11.141	11.132	11.433
1046	73.513374	-2.989720	0.578	1099.165	125.937	24.141	260.0	27.0	10.368	10.935	10.942	11.243
1299	73.536842	-3.054006	0.128	36.306	21.391	21.180	1023.0	27.0	9.176	9.711	9.816	10.117
1613	73.538635	-2.967907	0.720	125.599	24.770	23.426	42.0	29.0	9.596	10.141	10.212	10.513
1743	73.547653	-3.042384	0.586	64.228	16.439	22.922	91.0	27.0	9.824	10.375	10.427	10.728
1794	73.545914	-3.023800	0.590	137.846	52.492	23.259	191.0	26.0	10.233	10.796	10.814	11.115
1937	73.550400	-3.057221	0.655	1530.335	260.189	24.414	314.0	27.0	10.621	11.195	11.181	11.482
2239	73.561249	-2.985219	0.919	55.846	23.107	23.327	150.0	26.0	10.685	11.260	11.242	11.543
2240	73.562592	-2.971350	0.567	56.635	23.383	22.832	360.0	27.0	10.511	11.081	11.076	11.377
2472	73.570877	-3.027037	0.617	307.426	28.240	23.654	359.0	26.0	10.622	11.196	11.182	11.483
2818	73.587166	-2.987284	0.239	114.590	31.547	22.273	317.0	29.0	9.299	9.836	9.931	10.232
2912	73.586548	-2.998683	0.725	79.373	25.822	23.233	193.0	30.0	10.475	11.044	11.043	11.344
2926	73.589050	-3.101176	0.661	100.350	53.581	23.240	288.0	29.0	10.586	11.159	11.148	11.449
3017	73.591164	-2.990986	0.489	109.072	34.843	22.967	110.0	36.0	9.664	10.211	10.276	10.577
3226	73.603012	-2.980324	0.725	656.767	39.495	24.150	198.0	40.0	10.491	11.060	11.058	11.359
3247	73.601677	-3.100625	0.423	100.204	44.468	22.782	29.0	40.0	8.724	9.245	9.388	9.689
3404	73.607536	-3.016909	0.774	45.292	25.097	23.057	547.0	37.0	11.145	11.732	11.676	11.977
3462	73.610458	-2.947674	0.728	220.184	38.439	23.680	172.0	39.0	10.418	10.986	10.989	11.290
3698	73.629318	-3.025491	0.725	54.540	28.552	23.070	127.0	40.0	10.242	10.805	10.822	11.123
3806	73.626404	-2.999176	0.332	210.369	38.786	22.860	1336.0	34.0	10.461	11.030	11.030	11.331
3957	73.619141	-2.937129	0.323	192.012	58.310	22.795	1741.0	32.0	10.562	11.134	11.125	11.426
5823	73.624580	-2.969661	0.447	153.757	41.791	23.023	472.0	33.0	10.326	10.891	10.902	11.203
6380	73.580307	-2.921304	0.619	245.952	45.472	23.561	453.0	13.0	10.750	11.327	11.302	11.603
6547	73.639511	-2.941837	0.892	135.738	49.572	23.681	43.0	22.0	9.867	10.420	10.468	10.769

Continued. Properties of field galaxies that include the total IR luminosity (L_{TIR}) and rest frame radio luminosity ($L_{1.4GHz}$).

ID	RA (Degree)	DEC (Degree)	Redshift	$S_{1.4}$ (μJy)	$S_{1.4}$-err (μJy)	$\log L_{1.4}$ (W Hz^{-1})	S_{24} (μJy)	S_{24}-err (μJy)	$\log(L_{24\mu m})$ (L$_\odot$)	$\log(L_{60\mu m})$ (L$_\odot$)	$\log(L_{FIR})$ (L$_\odot$)	$\log(L_{TIR})$ (L$_\odot$)
6638	73.648750	-2.975052	0.447	390.0	50.734	23.427	834.0	21.0	10.625	11.199	11.185	11.486
7372	73.573524	-2.971213	0.777	113.395	31.084	23.460	149.0	27.0	10.415	10.982	10.986	11.287
8060	73.394081	-3.050711	0.491	213.045	73.092	23.261	74.0	22.0	9.450	9.992	10.074	10.375
8134	73.402657	-3.035359	0.715	312.974	74.698	23.814	329.0	23.0	10.753	11.330	11.306	11.607
8180	73.454201	-3.085207	0.726	50.879	27.068	23.042	136.0	32.0	10.284	10.848	10.862	11.163
8415	73.586739	-3.150578	0.505	224.847	63.553	23.313	240.0	13.0	10.138	10.699	10.725	11.026
8417	73.570885	-3.115729	0.511	84.175	39.693	22.898	765.0	10.0	10.763	11.340	11.315	11.616
8419	73.588936	-3.143751	0.457	183.087	75.787	23.121	2153.0	16.0	11.155	11.742	11.685	11.986
8506	73.634254	-3.134886	0.884	231.305	62.338	23.904	54.0	22.0	9.993	10.549	10.587	10.888
8575	73.623688	-2.891933	0.900	2337.128	397.688	24.927	454.0	22.0	11.324	11.916	11.845	12.146
8578	73.655594	-2.971230	0.802	247.537	53.255	23.832	864.0	21.0	11.459	12.056	11.973	12.274
8581	73.659332	-2.969704	0.219	115.513	41.055	22.191	1068.0	22.0	9.818	10.370	10.422	10.723
8583	73.648529	-2.962799	0.590	156.628	50.165	23.315	788.0	25.0	10.979	11.562	11.519	11.820
8608	73.670662	-2.991703	0.447	183.367	62.913	23.099	474.0	22.0	10.327	10.893	10.903	11.204
8631	73.664940	-3.052018	0.794	205.325	56.570	23.741	477.0	21.0	11.104	11.691	11.637	11.938
8642	73.693115	-3.053544	0.280	188.581	69.843	22.646	749.0	25.0	9.942	10.497	10.539	10.840
8773	73.578003	-2.830110	0.491	239.729	85.027	23.312	789.0	26.0	10.725	11.301	11.279	11.580
8787	73.340202	-3.070320	0.731	217.975	109.359	23.680	766.0	38.0	11.253	11.843	11.778	12.079
8813	73.656097	-2.904510	0.756	229.033	67.389	23.736	312.0	23.0	10.796	11.374	11.346	11.647
169	4.633176	16.371824	0.650	4694.206	760.862	24.892	64.000	16.000	9.740	10.289	10.348	10.649
149	4.630753	16.345523	1.333	262.815	0.227	24.386	233.088	45.589	12.143	12.757	12.619	12.920
555	4.348325	16.431677	0.656	220.000	55.000	23.572	406.178	40.096	10.762	11.339	11.314	11.615
350	4.744464	16.456812	0.324	220.000	55.000	22.856	508.152	23.642	9.927	10.482	10.525	10.826
573	4.437758	16.470259	0.266	633.750	131.764	23.121	6797.321	27.007	10.987	11.570	11.526	11.827

6.5 Potential Caveats

Before interpreting our findings, there are some caveats related to the derived luminosities which need to be considered.

6.5.1 Far-IR-radio Relation: Presence of AGN

For comparison purposes and conformity to the previous work in the literature (Reddy and Yun 2004), we do not a priori exclude AGN, but analyse both star-forming galaxies and AGN together. It has been established that faint radio populations are mostly found to be composed of star-forming galaxies and radio-quiet AGN (e.g. Jarvis and Rawlings 2004). It is also acknowledged that there is generally a contribution to the net radio flux from an AGN which can affect the observed relationship.

To investigate the contributions from AGN to the sample, we first considered the optical spectra and noted that none of the optical spectra available show broad-line emission indicating the presence of an AGN, although spectra are only available for MS0451. We then followed the method of Stern et al. (2005) to check for AGN contamination using IRAC color-color plots. We particularly adopted the formulation in AB mag system by Messias et al. (2010) as shown in their Figure 4.

In Figure 15, we show the colour [5.8]-[8] (AB) against [3.6]-[4.5] (AB). We have only plotted sources from MS0451 and Cl0016 in this plot due to the availability of IRAC measurements. In the plot, we have differentiated between radio-excess sources and normal sources as well as field and cluster galaxies. From the radio-excess cluster sources, we find no sources show any indication of being an AGN according to the classification as defined by Stern et al. (2005); Messias et al. (2010). For field sources, we find only 1 of 18 sources consistent with AGN activity, although another two radio excess sources also have colors with [3.6]-[4.5] > 0, which may be indicative of AGN activity (Messias et al. 2010).

Additional diagnostics (spectral line ratios, X-ray observations) will be needed to

further confirm the absence of AGN from our sample, but based on a lack of broad lines in the optical spectroscopy and IR colours, it would appear that AGN do not dominate our radio excess sample of galaxies.
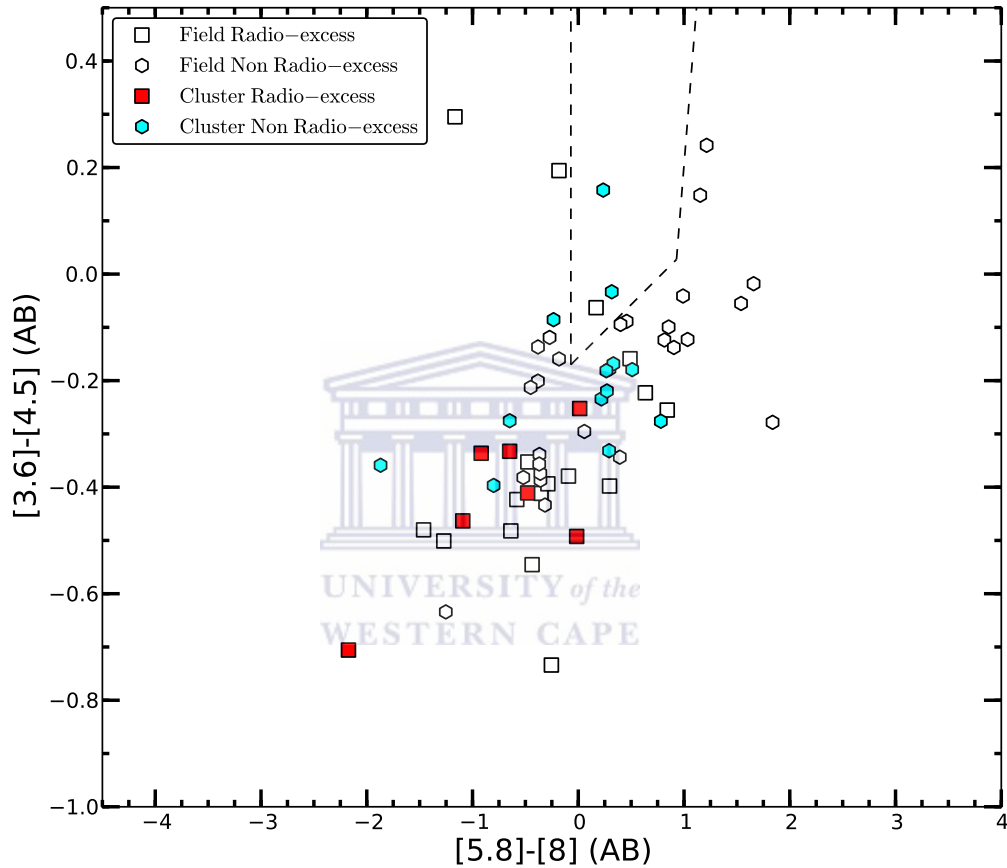
Figure 15: Plot of AGN indices. IRAC color-color diagnostic for AGN.

6.5.2 Far-IR Luminosity derived from 24 μm

Observations at 24 μm may not fully provide an unbiased estimator of the star formation since the peak of the IR SED tracing the cold dust component peaks between 60 μm and 170 μm (Pierini et al. 2003). Furthermore, 24 μm data may be affected by dust

heating from older stellar populations especially for early-type galaxies (Young et al. 2009; Calzetti et al. 2010).

In contrast, Dale et al. (2001) argued that 20-42 μm is essentially a good tracer of the bulk of dust emission and hence can be a robust recent star formation indicator. Recent studies of the relationship in the field have also found consistent results between mid-infrared MIPS 24 μm and MIPS 70 μm results (e.g. Appleton et al. 2004; Beswick et al. 2008). In addition, Murphy et al. (2011) find that 24 μm observations are a sufficient tracer of the total IR luminosity of galaxies for galaxies with $L_{24\mu m} < 10^{12}$ $L_{\odot}$, which includes all of our cluster sample.

Galametz et al. (2013) combined *Spitzer* and *Herschel* data and noted that an inclusion of 24 μm wavelength is essential in order to robustly derive the total IR luminosity for nearby star-forming galaxies. In addition, for luminous galaxies at $z < 1.3$, measurement based on mid-IR is in agreement with those measured directly with *Herschel*, as already shown by Elbaz et al. (2011).

6.5.3   Higher Radio Flux Limit

It is also possible that the abundance or observed radio-excess sources might be due to selection bias. Since our sample is IR-selected and we may only select bright radio sources, resulting the observed enhanced radio emission with respect to the far-IR emission. If true, it might have significantly affected our measurements. For example, by examining the far-IR luminosity cut off at $\log(L_{60\mu m}) > 10.5$ (Figure 12) we would have only observed half of the cluster radio-excess sources. In Table 15, we summarise the limiting radio flux and radio luminosity.

6.5.4   Small Sample Size

Given the fact that we have studied a cluster sample containing only a relatively small number of members, it is important to note that the current results may suffer from small

Table 15: Summary of radio flux upper limit and radio luminosity.

Cluster	Radio flux upper limit (μJy)	Radio luminosity (W Hz^{-1})
MS0451	36	$10^{22.6}$
Cl0016	220	$10^{23.4}$
A370	165	$10^{22.9}$
MS1512	156	$10^{22.1}$
J121119	159	$10^{21.2}$

sample size. In our sample, we did not detect any of the brightest cluster galaxy (which is obscured by a foreground galaxy) while Reddy and Yun (2004) have 4 cDs in their sample.

6.6 Discussion

Among the low redshift cluster studies, the far-IR-radio relationship in rich cluster galaxies is characterised by a lower value of q_{FIR} as compared to the field that is indicative of an excess of radio emission. Cluster environmental effects are believed to drive these observations (Andersen and Owen 1995; Rengarajan et al. 1997). Andersen and Owen (1995) postulated that the ISM of galaxies in rich clusters is being compressed via ram pressure as the galaxies move through the ICM resulting in greater radio emission. More recent work has further examined various models to shed some light on the causes of enhanced radio emission that seems globally present in cluster galaxies (Miller and Owen 2001; Reddy and Yun 2004; Murphy et al. 2009b). The most common scenarios include thermal pressure compression by the ICM and the ram pressure stripping of ISM, which are both likely to augment the galactic magnetic field.

If we compare our results with the study of low redshift clusters by Reddy and Yun 2004, we find the following: (1) the intermediate redshift cluster sample has a lower value of $q_{FIR} = 1.72 \pm 0.63$, but one that is consistent within the errors with the low redshift value of $q_{FIR} = 2.07 \pm 0.74$; (2) the fraction of radio-excess objects in clusters between low

and high redshift is greater (11% vs. 35±17%) where 35% is from the secure photometric sample; (3) a larger fraction of the field population (56±19% vs. 1%) shows excess radio emission at intermediate redshifts. However, we caution that any results from this work may suffer from the small sample size studied here.

Our measurement of q_{TIR} in the field at intermediate redshift is consistent with previous work (Murphy et al. 2009a; Sargent et al. 2010a), and little or no evolution has been reported in the evolution of the q_{TIR} value in the field at these redshifts (e.g. Sargent et al. 2010a,b; Ivison et al. 2010b; Bourne et al. 2011). However, the significant increase in the scatter in the q_{FIR} value is inconsistent with these works as well as the scatter measured by Yun et al. (2001) at low redshift. The high scatter that we are measuring may be due to preferentially selecting radio bright objects especially at higher redshift. For this reason, we will focus on the observed fraction of radio-excess objects seen in the cluster and the behaviour of both red and blue galaxies in the clusters.

In the intermediate redshift cluster, we observe a higher fraction of radio-excess galaxies as compared to lower redshift. The 66±43% (4 of 6) of the sources classified as radio-excess sources are red sequence galaxies. Reddy and Yun (2004) found that 9 of 13 excesses sources at low redshift had AGN signatures and were early-type galaxies. From visual inspection of their spectra, none of our radio-excess galaxies show the telltale IR colours of an AGN, but the large offset of the other galaxies from the relationship may still be indicative of nuclear activity.

As can be seen in Figure 12, most of the blue galaxies appear normal and have a very small scatter in their q_{FIR} values. We find two blue galaxies showing a radio-excess. In Figure 14, we do not see any strong radial trends against the q_{FIR} values. However, we notice that there is a significant scatter within the ring galaxies. Overall, inspection of the median q_{FIR} value indicates that the far-IR-radio relation for cluster blue galaxies at $z \sim 0.5$ is similar to the cluster sample at low redshift.

The quenching mechanisms, such as mergers and ram pressure stripping, at these redshifts must be occurring in such a manner so as not to strongly affect the radio-IR relationship. At low redshift clusters, one interpretation of the presence of radio-excess

within the virial radius can be the results of interstellar medium (ISM) stripped off via ram pressure exerted by infalling galaxies. As we do not see any environmental effects in the blue cluster population at intermediate redshifts, it is possible that the quenching mechanism is different than it is at low redshift although a larger sample would be required to verify this.

However, we note the radio spectral index α depends on frequency and galaxy properties and thus using a single spectral index may also alter the value of q (e.g. Bourne et al. 2011). However, the majority of work of this kind has been using the standard spectral index for normal star-forming galaxies; $\alpha \sim 0.8$ of Condon (1992). Recent results from the local infrared luminous galaxies of Murphy et al. (2013) found that the mid-infrared and radio properties of star-forming galaxies, particularly for those compact starburst galaxies, tend to have a flatter ($\alpha \sim 0.5$) spectral index. This may be a concern for galaxies in clusters as Crawford et al. (2006, 2011) find an increase in compact galaxies in clusters at these redshifts. The recently upgraded VLA correlator now makes it possible to measure the spectral index over a wide bandwidth within a single observation, so it will be a powerful tool for determining the IR-radio relation for large field and cluster samples in the future.

Radio-excess Sources

The radio-excess galaxies can be explained by the dominance of red sequence radio-excess sources in these clusters. It has been found that rich clusters at intermediate redshift (z~0.5) have higher fraction of strong radio emitting sources than in the nearby clusters (e.g. Hill and Lilly 1991). Furthermore, a common characteristic of each cluster could be the presence of post star-bursting phase of galaxies. It has been suggested that the observed radio-excess sources could be a result of the presence of a number of post start-burst galaxies in the core of rich clusters (Bressan et al. 2002). The observed radio-excess sources in these clusters may therefore be due to the enhancement of radio sources towards the cluster cores.

In addition, a number of mechanisms can also specifically affect the observed radio emission. These include ram pressure stripping, thermal compression, and gas compression. We discuss the effectiveness of these mechanisms to our results as follows.

(a) **Ram Pressure Stripping**

Figure 14 shows an indication of the effects of ram pressure stripping where we clearly find that the majority of galaxies are more clustered in the ring region and to a lesser extent into the core region of the clusters. The increased emitted synchrotron power caused by magnetic field enhancement resulting from the ISM being compressed by the ICM has been observed (Scodeggio and Gavazzi 1993; Andersen and Owen 1995; Rengarajan et al. 1997; Gavazzi and Boselli 1999).

In particular, sources in MS0451 show greater extent of the ram pressure stripping process in Figure 14, and this is consistent with previous findings on the physical processes analysis for this cluster (Moran et al. 2007).

(b) **Thermal Compression**

Thermal compression also likely plays an important role within the 1.5 Mpc of the cluster centers (Reddy and Yun 2004) which is apparent in our Figure 14 where we do see cluster sources within this radius appear to have lower q_{FIR} values. The ICM pressure and the hot gas in the ICM itself can also compress the ISM of a galaxy. The simple pressure exerted by the ICM will then enhance the magnetic strength which will eventually increase the emitted synchrotron power (Miller and Owen 2001).

(c) **Galaxy-Galaxy Interactions**

Alternatively, the observed radio emission enhancement may be due to galaxy-galaxy interaction (Moss and Whittle 1993) and galaxy harassment due to the cluster environment (Lake et al. 1998). Galaxy harassment is more effective outside of the cluster

core out to the cluster outskirts which eventually triggers AGN activation however Figure 14 does not seem to support this model.

IR-excess Sources

We do not find any IR-excess sources in our sample. The depression of the observed far-IR emission is postulated to be a collision of the ICM electron with heated dust grains Irwin et al. (2001), resulting a removal of cool dust (cirrus) component via ICM wind which is a major contributor to the total far-IR emission. However, Reddy and Yun (2004) found that collisional dust heating only has a small effect in dust heating rate and therefore has no significant effect on the far-IR emission for most galaxies living in the cluster environment.

6.7 Conclusion

We have studied the far-IR-radio relation in a sample of distant galaxy clusters and investigated, for the first time, how this relationship behaves at lower and intermediate redshift cluster environment as well as the field. We have constructed the far-IR-radio relationship of star-forming galaxies using deep VLA and *Spitzer* archival data. We have measured the rest frame radio luminosity at 1.4 GHz and the total IR luminosity ratios for both sample of confirmed cluster and field galaxies. We based our conclusions upon the results from sources with known photometric classification, and we note that our calculated values might be overestimated due to the limiting flux for the radio luminosity. Our main findings are summarised as follows:

(i) We find that the far-IR-radio relationship for distant cluster populations (q_{FIR} = 1.72$\pm$0.63) is in agreement with those measured in the low redshift clusters (q_{FIR} = 2.07$\pm$0.74), and indicates evidence of a cluster enhancement of radio-excess sources at this earlier epoch as well.

(ii) We find two radio-excess populations among the blue star forming galaxies and the four RS galaxies where the latter are likely to be obscured AGN if they are similar to the low redshift sample.

(iii) We find that cluster galaxies (q_{FIR} = 1.72±0.63) and field galaxies (q_{FIR} = 1.58 ± 0.71) appear to have similar values and scatter of q_{FIR}. However, further analysis (as well as much better data) are required to confirm the observed scatter in q_{FIR} for field galaxies due to higher probability of elevated AGN activities in the field.

(iv) In agreement with other findings in the low redshift cluster galaxies (Miller and Owen 2001; Reddy and Yun 2004), our results suggest that cluster environmental effects can also be equally important at this earlier epoch, implying that the physical mechanism responsible for the far-IR-radio relationship in clusters is related to the ICM – with a limited role played by the galaxy-galaxy interactions and mergers.

Chapter 7

The far-IR-radio Correlation: Environment of Galaxies in Groups from the COSMOS field

7.1 Overview

In Chapter 6, we showed that the far-IR-radio correlation for cluster galaxies show a radio-excess population that do not appear to be associated to AGN. We reported that the cluster galaxies have lower value of q_{FIR} which is also an indication of radio-excess. In this Chapter, we aim to use cross-matched galaxies in groups to study the effect of local environment on the far-IR-radio correlation in groups of galaxies. The local density is based on the number of galaxy members in the group and it is used to explore the far-IR-radio correlation as a function of galaxy type with the main intention of quantifying the behavior of the far-IR-radio correlation in groups as compared to that of cluster galaxies.

The Chapter is structured as follows. In Section 7.2, we give a brief introduction for this work. In Section 7.3, we present our galaxy sample that include the VLA-COSMOS photometry catalogue, S-COSMOS photometry catalogue, and an optical spectroscopic redshift catalogue. In Section 7.4, we present the methods and analysis performed for this

work. In Section 7.5, we present our results. In Section 7.6, we discuss the properties of the far-IR-radio correlation for the group sample along with a comparison to the cluster sample. Finally, in Section 7.7, we draw conclusions from our findings.

7.2 Introduction

Galaxy groups can be considered as being as scaled-down versions of clusters. The definition of a group and cluster is extremely loose but the common rule assigns galaxy groups as systems that consists of a number of galaxies up to 50 members. The term "galaxy group" that is used in this work refers to a collection of galaxies with two or more members living in the same dark matter halo bound by mutual gravitational attraction.

In general, galaxies are preferentially found in groups or clusters where most of physical processes occur. As the transformation mechanisms in group environment can be similar to the cluster that include most notably galaxy harassment and ram-pressure stripping, depending on the group host halo mass, and the dynamics of the group. Therefore, studies of the properties of the IR and radio emission in the group member galaxies and the far-IR-radio relation both group and cluster population may provide important clues to the role of the environmental processes in galaxy evolution.

Studies of galaxies in clusters, groups, and the general field at higher redshift have shown an increased star formation activity in all environments. The basic hypothesis of the far-IR-radio relationship of star-forming galaxies is known to be a result of coupling between star formation activity and supernova rate. The far-IR emission mainly generated through re-processing of starlight by dust, while radio emission is predominantly coming from cosmic rays electrons traveling through magnetic field (Harwit and Pacini 1975; Rickard and Harvey 1984). To the best of our knowledge, in studying of far-IR-radio relationship, there have been no work looked at the relationship in groups as a function of galaxy type.

7.3 Galaxy Sample

The Cosmic Evolution Survey (COSMOS, Scoville et al. 2007) uses multi-wavelength data, which include imaging and spectroscopic observations from X-rays to radio wavelengths, to study galaxy formation and evolution as a function of redshift (out to z $\sim$ 5) and the large scale structure environment, covering a 2 square degree area in the sky. We used two data sets from the COSMOS survey which consists of the VLA-COSMOS sources catalogue and the *Spitzer* S-COSMOS sources catalogue. The catalogues were retrieved through the online tool GATOR from the COSMOS data archive[1]. In addition, we obtained two catalogues of optical spectroscopic redshifts which come from the ESO VLT zCOSMOS catalogue and the Magellan telescope.

7.3.1 VLA-COSMOS Photometry Catalogue

The VLA-COSMOS project (Schinnerer et al. 2004, 2007) has observed the COSMOS field at 1.4 GHz (20 cm) with the VLA in A- and C- array configuration. The images have uniform RMS noise in the central $(1° \times 1°)$ on average RMS of 10.5 µJy and the flux densities were measured with AIPS (Greisen 2003).

We used a "joint" catalogue from the VLA-COSMOS (Schinnerer et al. 2010) which consists of the VLA-COSMOS Deep project merged with the revised catalogue of the VLA-COSMOS Large project (Bondi et al. 2008). The total number of sources obtained from the "joint" catalogue is 2864 detected at S/N $\geq$ 5.

7.3.2 S-COSMOS Photometry Catalogue

The S-COSMOS project (Sanders et al. 2007) has *Spitzer* imaging of the COSMOS field in all IRAC and MIPS filters. The S-COSMOS project FWHM of the point spread function at 24 µm is 5.8 and a 1σ point source detection limit of $\sim$ 0.018 mJy over a large fraction of the imaged area (Le Floc'h et al. 2009). The flux densities in the MIPS

---

[1]http://irsa.ipac.caltech.edu/data/COSMOS/

24 µm were measured with the PSF-fitting algorithm DAOPHOT (Stetson 1987).

We used a catalogue that consists of MIPS at 24 µm from the S-COSMOS GO3 catalogue (Le Floc'h et al. 2009). The total number of sources obtained from the GO3 catalogue is 17713 with total flux density ranging from 0.15 to 126.515 mJy and an uncertainty in the flux density from 0.012 to 9.05 mJy.

7.3.3   Optical Spectroscopic Redshift

In this work, we used spectroscopic redshifts of sources totaling 10126 which consists of 9168 obtained from the VLT zCOSMOS (Lilly et al. 2007, 2009) which are supplemented by 958 source redshifts obtained from the Magellan (Baade) telescope (Trump et al. 2007).

7.4   Method and Analysis

We searched for S-COSMOS counterparts to each VLA-COSMOS source using a matching radius of 2". We then used the matched IR-radio catalogue to search for optical spectroscopic counterparts using a similar matching radius. The resulting sample consists of 573 sources that are successfully matched in the IR-radio and have secure spectroscopic redshifts. We measured the IR and radio luminosities as well as various galaxy's q for this galaxy sample.

The computation of the radio luminosity, far-IR luminosity, and q is carried out following the same step described in previous Chapters i.e. in Chap. 4 §4.6, Chap. 5 §5.5, and Chap. 6 §6.3. The rest frame radio luminosities were measured following the method of Sargent et al. (2010b) (see Equation 4), while the IR luminosities were all estimated via the empirical relations of Rieke et al. (2009) (see Equation 8 and Equation 10). The ratio of the IR luminosity and the radio luminosity were measured using the formulation of Helou et al. (1985) (see Equation 11).

As we aim to study galaxies in groups, we then cross-matched our catalogue with the

20k zCOSMOS galaxy groups catalogue of Knobel et al. (2012). A group of galaxies is defined as a set of galaxies that occupy the same dark matter halo (Knobel et al. 2012). The group members were identified based on two group-finding algorithms (Knobel et al. 2009) which consists of the Friends-of-Friends (FOF) (Eke et al. 2004) and Voronoi–Delaunay method (VDM) (Marinoni et al. 2002; Gerke et al. 2005).

7.5 Results

7.5.1 The q_{TIR}-values as a function of Redshift

In Figure 16, we plot q_{TIR} as a function of redshift for the COSMOS field (Sargent et al. 2010a) and our sample. Our q_{TIR} values are similarly defined as the q_{TIR} of Sargent et al. (2010a) where IR luminosity is L(TIR, 8 − 1000μm) and both follow the method of Helou et al. (1985). Figure 16 clearly shows that the distribution of our q_{TIR} values displays similar trend when compared with those of Sargent et al. (2010a). As expected, both q_{TIR} measurements are consistent with one another.

Our catalogue contains 183 sources in $0.3 < z < 0.6$ where the measured mean value of q_{TIR} is 2.40±0.38. For comparison, Sargent et al. (2010a) sample with redshift cut off $0.3 < z < 0.6$ consists of 423 sources having a mean value of q_{TIR} is 2.41±0.38. We note that in addition to the radio sources with S/N $\geq$ 5 from the "joint" catalogue, Sargent et al. (2010a) subsequently searched for additional radio detections with S/N $>$ 3 in the original observations. This results in the difference between the number of sources in our sample and Sargent et al. (2010a).

7.5.2 The IR and Radio Luminosities

In Figure 17, we present the rest frame radio luminosity at 1.4 GHz ($L_{1.4\mathrm{GHz}}$) against the IR luminosity ($L_{60\mu\mathrm{m}}$). Galaxies in groups are represented by filled hexagon symbols and non-groups are drawn in circles. Figure 17 shows the linear correlation found between
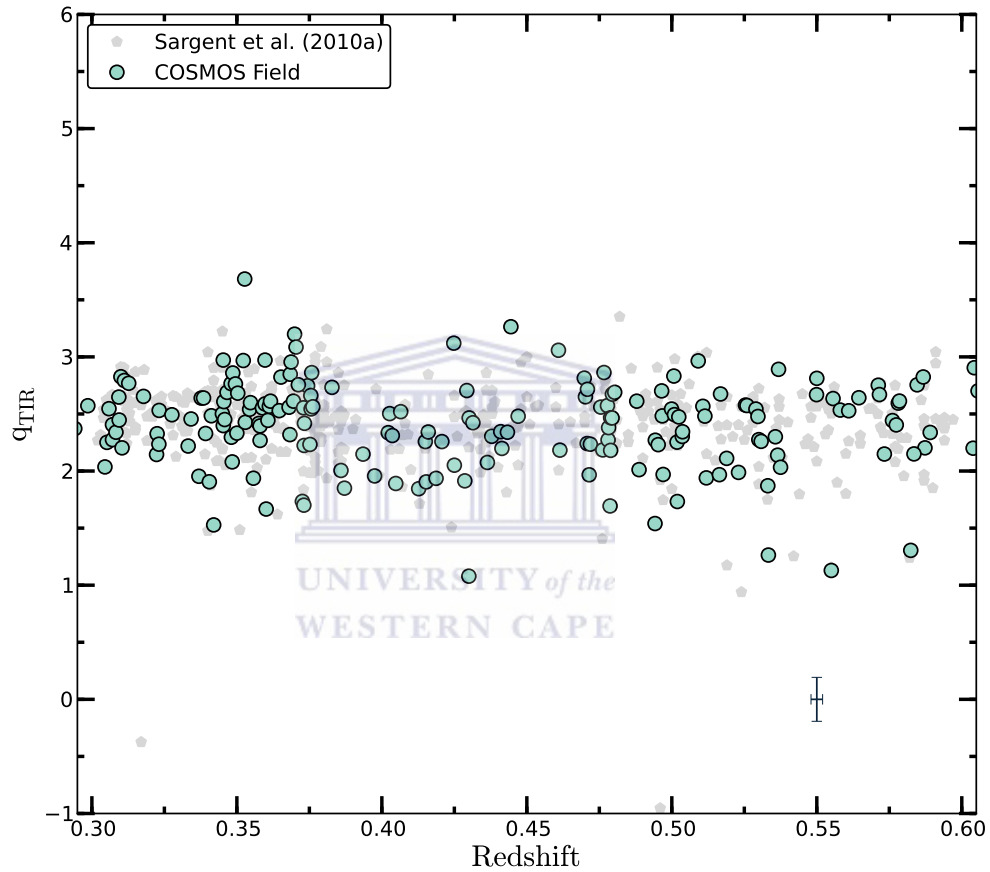
Figure 16: Plot of q_{TIR} as a function of redshift. Comparison of our measured q_{TIR} for the field galaxies in the VLA-COSMOS deep project with S-COSMOS GO3 catalogue and the published q_{TIR} from COSMOS catalogue (Sargent et al. 2010a, see also the lower panel of their Figure 17) where here q_{TIR} restricted only to $0.3 < z < 0.6$. The error bars correspond to average 1σ errors.
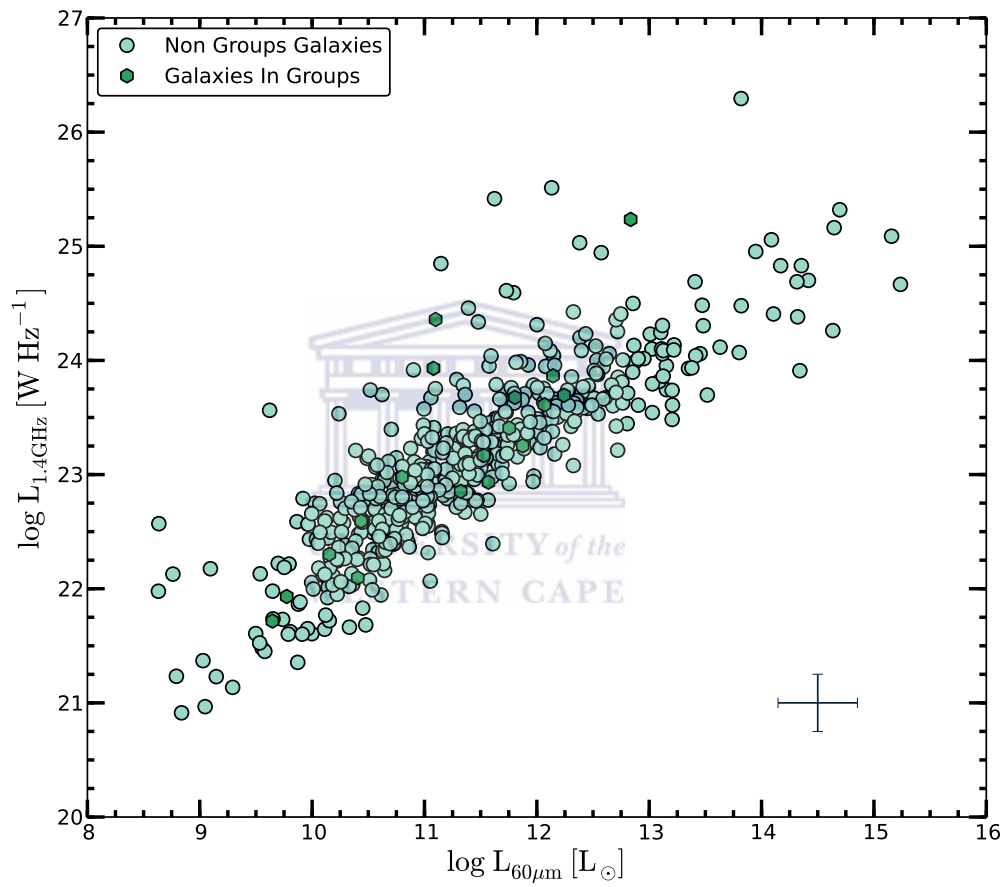
Figure 17: The 20 cm radio continuum luminosity ($L_{1.4GHz}$) against the far-IR luminosity ($L_{60\mu m}$) for the field galaxies in the VLA-COSMOS deep project and the S-COSMOS GO3 catalogue. The error bars correspond to average 1σ errors.

the two luminosities for field star-forming galaxies (Yun et al. 2001; Bell 2003).

7.5.3 The q_{FIR}-values as a function of Galaxy Environment
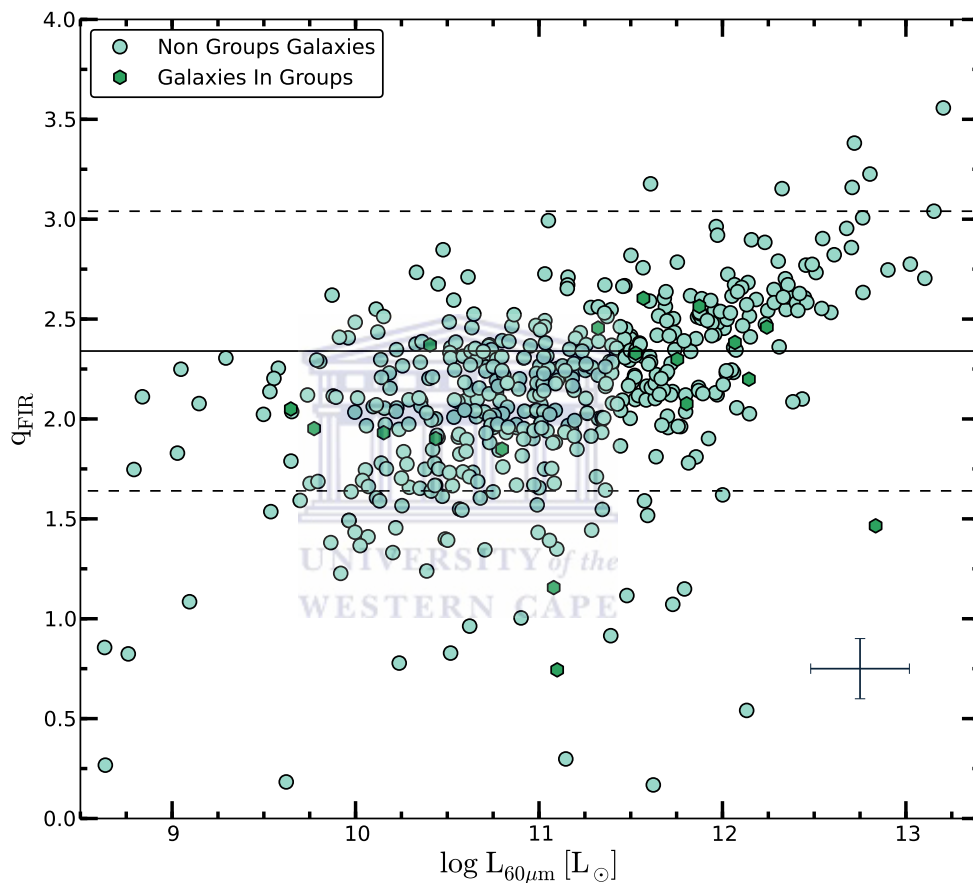
Figure 18: The logarithmic of the far-IR luminosity to 1.4 GHz radio continuum luminosity ratio (q_{FIR}) versus the IR luminosity ($L_{60\mu m}$) for the field galaxies in the VLA-COSMOS deep project and the S-COSMOS GO3 catalogue. The error bars correspond to average 1σ errors.

In Figure 18, we show the far-IR luminosity (L_{FIR}) to radio luminosity ($L_{1.4\mathrm{GHz}}$) ratio (q_{FIR}) against $L_{60\mu m}$. The boundaries delineating between IR- ($q_{\mathrm{FIR}} \geq 3.04$) and radio-excess ($q_{\mathrm{FIR}} \leq 1.64$) are adopted from Yun et al. (2001). As discussed in Sargent et al.

(2010a), the scatter in q_{FIR} at higher redshift (from z $\sim$ 1.4) is found to significantly increase, thus we applied a cut off in redshift for Figure 18 and use $0 < z < 1$ (resulting in total number of sources in the sample to 492) for a robust analysis of q_{FIR} and for a consistency to the COSMOS analysis in the literature.

7.6 Discussion

The mean q_{FIR} for the galaxy groups is q_{FIR} = 2.04$\pm$0.5, while q_{FIR} = 2.15$\pm$0.45 for non-group sources. This mean q_{FIR} value for groups is comparable with the low redshift clusters (q_{FIR} = 2.07$\pm$0.74) (Reddy and Yun 2004) as well.

We find that the fraction of IR and radio-excess for the non-groups member galaxies is 1$\pm$0.5% (6 of 474) and 10$\pm$1.5% (50 of 474), respectively. Galaxies in groups do not show any IR-excess, while the radio-excess is found to be 16$\pm$10% (3 of 18). This fraction is higher than that found in the field, but the small sample size means that it is not significantly different. When we run a Monte Carlo simulation by selecting 18 sources randomly from the full field sample, we find that 30% of the time the same number of excess sources is selected as in our group sample. Further observations will be required to confirm if the fraction of radio excess sources is indeed higher in groups.

We investigate the properties of q_{FIR} of galaxies in groups by splitting our sample from the galaxy groups into blue cloud (BC) and red sequence (RS) galaxies. Blue objects were defined as sources having $B - I < 2.5$ mag and we found that the 4 of 18 are RS and 14 of 18 are BC. Out of the radio-excess sources in groups, 1 of 3 is RS galaxy and 2 of 3 are BC galaxies. The group size of these radio-excess sources comprises of two or three spectroscopic group members.

A number of AGN-like sources are expected in the COSMOS field catalogue. Therefore, one caveat is that we do not have information on the fraction of sources with AGN activity in the catalogue. Given this constraint, we cannot infer the presence of an AGN in the field source, though the galaxies in groups are spectroscopically confirmed thus

bone fide (Knobel et al. 2012).

We find that $16\pm10\%$ (3 of 18) of the galaxies in groups are radio-excess sources with one RS galaxy. When combined with our results from massive clusters showing up to a fraction of $35\pm17\%$ radio-excess sources, we may be seeing hints that the number of radio-excess sources depends on the environment of the galaxies, similar to the morphology-density relationship seen within clusters by Dressler (1980); Dressler et al. (1997) and its extension into group regime (Postman and Geller 1984). We suggest that this shared properties is expected since galaxy clusters are built at least partially from galaxy groups, therefore what occurs in cluster environment depends at least partially on galaxy groups.

It is also possible for mechanisms such as stripping, strangulation, and mergers to occur in groups prior to infall onto clusters – known as "pre-processing" (e.g. Fujita 2004). Pre-processing quenches group members and field galaxies which have yet to fall into the cluster. In fact, it has been suggested that galaxy pre-processing occurs in groups which are later accreted into massive clusters Zabludoff and Mulchaey (1998); McGee et al. (2009). It has also been found that pre-processing is even more effective in compact groups compared to loose groups (Coenda et al. 2012). If the massive groups were infalling into the richest clusters, we conversely speculate that the extreme properties of the far-IR-radio relationship we observed in massive galaxy clusters may be the result of some pre-processing of galaxies in groups before infalling into the cluster (e.g. Zabludoff and Mulchaey 1998; McGee et al. 2009).

The pre-processing in groups has also been found to significantly contribute to the observed SFR-density relationship (e.g. von der Linden et al. 2010). Interestingly, it has been shown that both cluster environment (Poggianti et al. 2006, 2008) and group environment (Poggianti et al. 2006) can effectively reduce star-formation activity within galaxies. These imply the existence of SFR-density relationship in groups, thus supporting the proposed extension of the excess of radio sources into group regime. However, due to the small size of our group sample, a quantification of the correlation requires further works such as studies of larger sample and wider redshift.

7.7   Conclusion

In this Chapter, we have studied the properties of the far-IR-radio relationship for the COSMOS field galaxies both in group and in non-group members. We find a lower percentage of radio-excess sources in groups as compared to clusters. Our results are summarised as follows:

(i) We find that the distribution of the measured q_{TIR} is in good agreement with other measurements in the COSMOS field by Sargent et al. (2010a), implying that the methods used are consistent with each other.

(ii) Consequently, our results confirm that the measured far-IR-radio relationship for group and non-group member galaxies in the COSMOS field holds as well.

(iii) Despite the small sample size and large percentage error, we find that galaxies in groups possibly have a higher fraction of radio-excess sources $16\pm10\%$ (3 of 18) when compared with the non-group galaxies $10\pm1.5\%$ (50 of 474). If confirmed with additional observations, this extends the observation of radio excess sources to the group regime.

Chapter 8

Conclusions and Future Work

8.1   Overview

The present work is devoted to the enhancement of our current understanding of the far-IR-radio correlation of cluster galaxies for an intermediate redshift cluster sample and to some extent to sample of groups of galaxies. We have explored deep VLA and Spitzer observations to study a representative sample of galaxy clusters and galaxy groups.

In the local Universe, it is known that galaxies in groups and clusters which inhabit dense environments have properties substantially different from galaxies in low density or field environments. Here we have used three samples that span different environments. The samples used include cluster galaxies, field galaxies, and group galaxies which are all classified based on spectroscopic and photometric information.

This final Chapter is structured as follows. In Section 8.2 we first recap the observations, samples, and data analysis then we summarise our findings. In Section 8.3, we conclude by reviewing our main results. In Section 8.4, we present some future work. In Section 8.5, we include a list of scientific acknowledgment.

8.2 Summary

In this work, we have compared the properties of the far-IR-radio correlation of cluster galaxies in an intermediate redshift cluster sample to their low redshift cluster galaxies counterparts as well as galaxies in groups. We have investigated the link between the synchrotron emission traced by the radio continuum observations at 1.4 GHz and the thermal dust emission traced by the far-infrared data.

The far-IR-radio correlation for these clusters allowed us to better understand the star formation and cosmic-ray production in massive cluster at intermediate redshift. In addition, we found that the far-IR-radio relationship can be used to evaluate the main radiation mechanisms that produced proportional emissions and with radio-excess in clusters at low and intermediate redshift.

The results in this thesis can be summarised as follows: Chapter 1 has covered a general overview of the evolution of cluster galaxies and multi-wavelength technique and analysis that are needed for this work. Chapter 2 has provided a literature review of the far-IR-radio correlation. In particular it has covered an overview of the early work, theoretical models, prediction and observations for the relation for field galaxies. It has also provided a thorough overview of far-IR-radio correlation for low redshift galaxy clusters. Chapter 3 has given the details of the spectroscopic redshifts for each cluster and described our selection of the cluster and galaxy samples. Chapter 4 has introduced the specifications of the VLA continuum observations, data reductions, and data analysis. Chapter 5 has summarised the IR data followed by the details of the photometry and data analysis as well as the method for measuring IR luminosities of galaxies.

- Chapter 6 has presented and discussed our findings on the far-IR-radio relationship for a sample of distant galaxy cluster.

- Chapter 7 has presented and discussed our findings on the radio and infrared properties of galaxy groups in the COSMOS field.

8.3 Conclusions

In this thesis, we have studied the properties of the far-IR-radio correlation of cluster galaxies at intermediate redshifts, by comparing the relationship of these galaxies to the local clusters, and by giving particular focus on the interactions of intermediate-redshift galaxies with their environment, and also by looking at the extent to which galaxy type and groups environment the relationship may explain the radio-excess in cluster galaxies. We reported that the cluster galaxies have lower values of q_{FIR} which is an indicative of radio-excess. Furthermore, we also find a lower percentage of radio-excess sources in groups as compared to clusters.

Chapter 6 has presented and discussed our findings on the far-IR-radio relationship in the massive galaxy clusters. We find that the far-IR-radio relationship for distant cluster populations (q_{FIR} = 1.72±0.63) is in agreement with those measured in the low redshift clusters (q_{FIR} = 2.07±0.74), and indicates evidence of a cluster enhancement of radio-excess sources at this earlier epoch as well. We find two excess populations among the blue star forming galaxies and the four RS galaxies with radio-excess are likely to be obscured AGN if they are similar to the low redshift sample. We find that the cluster galaxies (q_{FIR} = 1.72±0.63) and the field galaxies (q_{FIR} = 1.58±0.71) at intermediate redshifts appear to have similar q_{FIR} values and scatter. However, further analysis is required to confirm the observed scatter in q_{FIR} for field galaxies due to higher probability of elevated AGN activities in the field. In agreement with other findings in the low redshift cluster galaxies (Miller and Owen 2001; Reddy and Yun 2004), our results suggest that cluster environmental effects can also be equally important at this earlier epoch, implying that the physical mechanism responsible for the far-IR-radio relationship in clusters is related to the ICM – with limited role played by the galaxy-galaxy interactions and mergers.

Chapter 7 has presented and discussed our findings on the radio and infrared properties of galaxies in the COSMOS group. We find that the distribution of the measured q_{TIR} is in good agreement with other measurements in the COSMOS field by Sargent et al. (2010a), implying that the methods used are consistent with each other. Consequently,

our results confirm that the measured far-IR-radio relationship for group and non-group member galaxies in the COSMOS field holds as well. Despite the small sample size and large percentage error, we find that galaxies in groups possibly have a higher fraction of radio-excess sources $16\pm10\%$ (3 of 18) when compared with the non-group galaxies $10\pm1.5\%$ (50 of 474), and if confirmed with additional observations, this extends the relationship to the group regime.

8.4   Future Work

Although the results presented in Chapter 6 and Chapter 7 give a clear indication that distant cluster galaxies do show radio-excess and to some extent in the group regime, it would be useful to quantify this result with a study of a larger sample of cluster and group members to better constrain the statistical results. In the future, it will be possible to measure the far-IR-radio relationship for distant cluster galaxies more accurately from the upcoming wider and deeper surveys such as MeerKAT and the Square Kilometre Array (SKA) will provide.

The present work has clearly indicated the importance of multi-wavelength observations in the studies of galaxies in clusters and groups. We are privileged to be working at a time when so many new telescopes and instruments are being commissioned plus those that will be coming online soon, which have the potential to provide answers many of the questions risen from this work.

Future multi-wavelength investigation of cluster galaxies will greatly benefit from the multi-wavelength surveys from the Southern African Large Telescope (SALT) spectroscopic information and when combined with the upcoming deep continuum surveys from the JVLA (e.g. Stripe 82 survey) and the MeerKAT/SKA (e.g. MeerKAT International Gigahertz Tiered Extragalactic Exploration or MIGHTEE survey), as they will provide an excellent resource for the identification of these galaxies.

In the near future, we will carry out star formation and AGN studies in massive galaxy

clusters at higher redshift. It aims to shed new light on the star formation properties of cluster galaxies and their evolution as function of redshift. It also intends to look for systematic evolution in the far-IR-radio relationship in a such distant and extreme environment.

8.5 Scientific Acknowledgements

In this section, we would like to include several scientific acknowledgements.

Bibliography

Abadi, M.G., Moore, B. and Bower, R.G. Ram pressure stripping of spiral galaxies in clusters. *MNRAS*, 308:947–954, October 1999.

Abell, G.O. The Distribution of Rich Clusters of Galaxies. *ApJS*, 3:211, May 1958.

Abell, G.O., Corwin, Jr., H.G. and Olowin, R.P. A catalog of rich clusters of galaxies. *ApJS*, 70:1–138, May 1989.

Abraham, R.G., Yee, H.K.C., Ellingson, E. et al. The CNOC Cluster Redshift Survey Catalogs. V. MS 1224.7+2007 and MS 1512.4+3647. *ApJS*, 116:231, June 1998.

Aitken, D.K., Roche, P.F., Allen, M.C. et al. A high-excitation optically obscured H II region in the nucleus of NGC 5253. *MNRAS*, 199:31P–35P, May 1982.

Andersen, V. and Owen, F.N. The far-infrared-radio relation in cluster spiral galaxies. *AJ*, 109:1582–1591, April 1995.

Antonucci, R. Unified models for active galactic nuclei and quasars. *ARA&A*, 31:473–521, 1993.

Appleton, P.N., Fadda, D.T., Marleau, F.R. et al. The Far- and Mid-Infrared/Radio Correlations in the Spitzer Extragalactic First Look Survey. *ApJS*, 154:147–150, September 2004.

Bahcall, N.A. X-ray clusters of galaxies - Correlation of X-ray luminosity with galactic content. *ApJL*, 218:L93–L95, December 1977.

Baldry, I.K., Glazebrook, K., Brinkmann, J. et al. Quantifying the Bimodal Color-Magnitude Distribution of Galaxies. *ApJ*, 600:681–694, January 2004.

Balogh, M.L., Navarro, J.F. and Morris, S.L. The Origin of Star Formation Gradients in Rich Galaxy Clusters. *ApJ*, 540:113–121, September 2000.

Balogh, M.L., Baldry, I.K., Nichol, R. et al. The Bimodal Galaxy Color Distribution: Dependence on Luminosity and Environment. *ApJL*, 615:L101–L104, November 2004.

Barger, A.J., Aragon-Salamanca, A., Ellis, R.S. et al. The life-cycle of star formation in distant clusters. *MNRAS*, 279:1–24, March 1996.

Beck, R. and Golla, G. Far-infrared and radio continuum emission of nearby galaxies. *A&A*, 191:L9–L12, February 1988.

Begelman, M.C., Blandford, R.D. and Rees, M.J. Theory of extragalactic radio sources. *Reviews of Modern Physics*, 56:255–351, April 1984.

Beichman, C.A. The IRAS view of the Galaxy and the solar system. *ARA&A*, 25:521–563, 1987.

Bekki, K. Unequal-Mass Galaxy Mergers and the Creation of Cluster S0 Galaxies. *ApJL*, 502:L133, August 1998.

Bekki, K., Couch, W.J. and Shioya, Y. Tidal Truncation of Gas Replenishment and Global Suppression of Galactic Star Formation in Distant Clusters. *PASJ*, 53:395–400, June 2001.

Bekki, K., Couch, W.J. and Shioya, Y. Passive Spiral Formation from Halo Gas Starvation: Gradual Transformation into S0s. *ApJ*, 577:651–657, October 2002.

Bell, E.F. Estimating Star Formation Rates from Infrared and Radio Luminosities: The Origin of the Radio-Infrared Correlation. *ApJ*, 586:794–813, April 2003.

Bell, E.F., Wolf, C., Meisenheimer, K. et al. Nearly 5000 Distant Early-Type Galaxies in COMBO-17: A Red Sequence and Its Evolution since z~1. *ApJ*, 608:752–767, June 2004.

Berkhuijsen, E.M., Nieten, C. and Haas, M. Radio-FIR correlations in M31. In Berkhuijsen, E.M., Beck, R. and Walterbos, R.A.M., editors, *Proceedings 232. WE-Heraeus Seminar*, pages 187–190, December 2000.

Best, P.N., van Dokkum, P.G., Franx, M. et al. μJy radio sources in the cluster MS1054-03. *MNRAS*, 330:17–34, February 2002.

Beswick, R.J., Muxlow, T.W.B., Thrall, H. et al. An evolution of the infrared-radio correlation at very low flux densities? *MNRAS*, 385:1143–1154, April 2008.

Bicay, M.D. and Helou, G. The 60 micron to 20 centimeter infrared-to-radio ratio within spiral galaxies. *ApJ*, 362:59–73, October 1990.

Bondi, M., Ciliegi, P., Schinnerer, E. et al. The VLA-COSMOS Survey. III. Further Catalog Analysis and the Radio Source Counts. *ApJ*, 681:1129–1135, July 2008.

Boselli, A. and Gavazzi, G. Environmental Effects on Late-Type Galaxies in Nearby Clusters. *PASP*, 118:517–559, April 2006.

Bourne, N., Dunne, L., Ivison, R.J. et al. Evolution of the far-infrared-radio correlation and infrared spectral energy distributions of massive galaxies over z= 0-2. *MNRAS*, 410:1155–1173, January 2011.

Boyle, B.J., Cornwell, T.J., Middelberg, E. et al. Extending the infrared radio correlation. *MNRAS*, 376:1182–1188, April 2007.

Bressan, A., Silva, L. and Granato, G.L. Far infrared and radio emission in dusty starburst galaxies. *A&A*, 392:377–391, September 2002.

Briel, U.G., Henry, J.P. and Boehringer, H. Observation of the Coma cluster of galaxies with ROSAT during the all-sky survey. *A&A*, 259:L31–L34, June 1992.

Bureau, M. and Carignan, C. Environment, Ram Pressure, and Shell Formation in Holmberg II. *AJ*, 123:1316–1333, March 2002.

Butcher, H. and Oemler, Jr., A. The evolution of galaxies in clusters. I - ISIT photometry of C1 0024+1654 and 3C 295. *ApJ*, 219:18–30, January 1978.

Butcher, H. and Oemler, Jr., A. The evolution of galaxies in clusters. V - A study of populations since Z approximately equal to 0.5. *ApJ*, 285:426–438, October 1984.

Byrd, G. and Valtonen, M. Tidal generation of active spirals and S0 galaxies by rich clusters. *ApJ*, 350:89–94, February 1990.

Calzetti, D., Wu, S.Y., Hong, S. et al. The Calibration of Monochromatic Far-Infrared Star Formation Rate Indicators. *ApJ*, 714:1256–1279, May 2010.

Chapman, S.C., Blain, A.W., Smail, I. et al. A Redshift Survey of the Submillimeter Galaxy Population. *ApJ*, 622:772–796, April 2005.

Chi, X. and Wolfendale, A.W. Implications of the correlation between radio and far-infrared emission for spiral galaxies. *MNRAS*, 245:101–107, July 1990.

Choudhuri, A.R. *Astrophysics for Physicists*. Cambridge University Press, 2010., March 2010.

Coenda, V., Muriel, H. and Martínez, H.J. Comparing galaxy populations in compact and loose groups of galaxies. *A&A*, 543:A119, July 2012.

Condon, J.J. Cosmological evolution of radio sources. *ApJ*, 287:461–474, December 1984.

Condon, J.J. Radio emission from normal galaxies. *ARA&A*, 30:575–611, 1992.

Condon, J.J., Condon, M.A., Gisler, G. et al. Strong radio sources in bright spiral galaxies. II - Rapid star formation and galaxy-galaxy interactions. *ApJ*, 252:102–124, January 1982.

Condon, J.J., Anderson, M.L. and Helou, G. Correlations between the far-infrared, radio, and blue luminosities of spiral galaxies. *ApJ*, 376:95–103, July 1991.

Conti, P.S. Wolf-Rayet galaxies - an introduction and a catalog. *ApJ*, 377:115–125, August 1991.

Couch, W.J., Ellis, R.S., Sharples, R.M. et al. Morphological studies of the galaxy populations in distant 'Butcher-Oemler' clusters with HST. 1: AC 114 AT Z = 0.31 and Abell 370 at Z = 0.37. *ApJ*, 430:121–138, July 1994.

Cox, M.J., Eales, S.A.E., Alexander, P. et al. The correlation between far-infrared and non-thermal radio emission at 151 MHz for galaxies - Observations and modelling. *MNRAS*, 235:1227–1243, December 1988.

Crawford, S.M., Bershady, M.A., Glenn, A.D. et al. Luminous Compact Blue Galaxies in Intermediate-Redshift Galaxy Clusters: A Significant but Extreme Butcher-Oemler Population. *ApJL*, 636:L13–L16, January 2006.

Crawford, S.M., Bershady, M.A. and Hoessel, J.G. The Red-Sequence Luminosity Function in Massive Intermediate-Redshift Galaxy Clusters. *ApJ*, 690:1158–1180, January 2009.

Crawford, S.M., Wirth, G.D., Bershady, M.A. et al. Spectroscopy of Luminous Compact Blue Galaxies in Distant Clusters. I. Spectroscopic Data. *ApJ*, 741:98, November 2011.

Crawford, S.M., Wirth, G.D. and Bershady, M.A. Spatial and Kinematic Distributions of Transition Populations in Intermediate Redshift Galaxy Clusters. *ApJ*, 786:30, May 2014.

Dale, D.A. and Helou, G. The Infrared Spectral Energy Distribution of Normal Star-forming Galaxies: Calibration at Far-Infrared and Submillimeter Wavelengths. *ApJ*, 576:159–168, September 2002.

Dale, D.A., Helou, G., Contursi, A. et al. The Infrared Spectral Energy Distribution of Normal Star-forming Galaxies. *ApJ*, 549:215–227, March 2001.

Devereux, N.A. and Eales, S.A. A reevaluation of the infrared-radio correlation for spiral galaxies. *ApJ*, 340:708–712, May 1989.

Diaferio, A., Kauffmann, G., Balogh, M.L. et al. The spatial and kinematic distributions of cluster galaxies in a ΛCDM universe: comparison with observations. *MNRAS*, 323: 999–1015, May 2001.

Donahue, M. Temperature and Metallicity of a Massive X-Ray Cluster at Redshift 0.5. *ApJ*, 468:79, September 1996.

Dressel, L.L. Powerful warm infrared sources in early-type galaxies. *ApJL*, 329:L69–L73, June 1988.

Dressler, A. Galaxy morphology in rich clusters - Implications for the formation and evolution of galaxies. *ApJ*, 236:351–365, March 1980.

Dressler, A., Oemler, Jr., A., Couch, W.J. et al. Evolution since Z = 0.5 of the Morphology-Density Relation for Clusters of Galaxies. *ApJ*, 490:577, December 1997.

Dressler, A., Smail, I., Poggianti, B.M. et al. A Spectroscopic Catalog of 10 Distant Rich Clusters of Galaxies. *ApJS*, 122:51–80, May 1999.

Drory, N., Bundy, K., Leauthaud, A. et al. The Bimodal Galaxy Stellar Mass Function in the COSMOS Survey to z ~ 1: A Steep Faint End and a New Galaxy Dichotomy. *ApJ*, 707:1595–1609, December 2009.

Eke, V.R., Baugh, C.M., Cole, S. et al. Galaxy groups in the 2dFGRS: the group-finding algorithm and the 2PIGG catalogue. *MNRAS*, 348:866–878, March 2004.

Elbaz, D., Dickinson, M., Hwang, H.S. et al. GOODS-Herschel: an infrared main sequence for star-forming galaxies. *A&A*, 533:A119, September 2011.

Ellis, R.S., Smail, I., Dressler, A. et al. The Homogeneity of Spheroidal Populations in Distant Clusters. *ApJ*, 483:582, July 1997.

Faber, S.M., Willmer, C.N.A., Wolf, C. et al. Galaxy Luminosity Functions to z˜1 from DEEP2 and COMBO-17: Implications for Red Galaxy Formation. *ApJ*, 665:265–294, August 2007.

Fadda, D., Girardi, M., Giuricin, G. et al. The Observational Distribution of Internal Velocity Dispersions in Nearby Galaxy Clusters. *ApJ*, 473:670, December 1996.

Fasano, G., Poggianti, B.M., Couch, W.J. et al. The Evolution of the Galactic Morphological Types in Clusters. *ApJ*, 542:673–683, October 2000.

Fazio, G.G., Hora, J.L., Allen, L.E. et al. The Infrared Array Camera (IRAC) for the Spitzer Space Telescope. *ApJS*, 154:10–17, September 2004.

Fitt, A.J., Alexander, P. and Cox, M.J. A two-temperature model for the infrared and radio emission from late-type galaxies. *MNRAS*, 233:907–921, August 1988.

Frayer, D.T., Fadda, D., Yan, L. et al. Spitzer 70 and 160 μm Observations of the Extragalactic First Look Survey. *AJ*, 131:250–260, January 2006.

Fujita, Y. Quantitative Estimates of Environmental Effects on the Star Formation Rate of Disk Galaxies in Clusters of Galaxies. *ApJ*, 509:587–594, December 1998.

Fujita, Y. Ram-Pressure Stripping of Galaxies in High-Redshift Clusters and the Influence of Intracluster Medium Heating. *ApJ*, 550:612–621, April 2001.

Fujita, Y. Pre-Processing of Galaxies before Entering a Cluster. *PASJ*, 56:29–43, February 2004.

Fujita, Y. and Nagashima, M. Effects of Ram Pressure from the Intracluster Medium on the Star Formation Rate of Disk Galaxies in Clusters of Galaxies. *ApJ*, 516:619–625, May 1999.

Galametz, M., Kennicutt, R.C., Calzetti, D. et al. Calibration of the total infrared luminosity of nearby galaxies from Spitzer and Herschel bands. *MNRAS*, 431:1956–1986, May 2013.

Garn, T., Green, D.A., Riley, J.M. et al. The relationship between star formation rate and radio synchrotron luminosity at 0 < z < 2. *MNRAS*, 397:1101–1112, August 2009.

Garrett, M.A. The FIR/Radio correlation of high redshift galaxies in the region of the HDF-N. *A&A*, 384:L19–L22, March 2002.

Gavazzi, G. and Boselli, A. On the local radio luminosity function of galaxies. II. Environmental dependences among late-type galaxies. *A&A*, 343:93–99, March 1999.

Gerke, B.F., Newman, J.A., Davis, M. et al. The DEEP2 Galaxy Redshift Survey: First Results on Galaxy Groups. *ApJ*, 625:6–22, May 2005.

Gilmour, R., Best, P. and Almaini, O. The distribution of active galactic nuclei in a large sample of galaxy clusters. *MNRAS*, 392:1509–1531, February 2009.

Gioia, I.M. and Luppino, G.A. The EMSS catalog of X-ray-selected clusters of galaxies. 1: an atlas of CCD images of 41 distant clusters. *ApJS*, 94:583–614, October 1994.

Gioia, I.M., Maccacaro, T., Schild, R.E. et al. The Einstein Observatory Extended Medium-Sensitivity Survey. I - X-ray data and analysis. *ApJS*, 72:567–619, March 1990.

Greisen, E.W. AIPS, the VLA, and the VLBA. *Information Handling in Astronomy - Historical Vistas*, 285:109, March 2003.

Gruppioni, C., Pozzi, F., Zamorani, G. et al. The radio-mid-infrared correlation and the contribution of 15-μm galaxies to the 1.4-GHz source counts. *MNRAS*, 341:L1–L6, May 2003.

Gunn, J.E. and Gott, III, J.R. On the Infall of Matter Into Clusters of Galaxies and Some Effects on Their Evolution. *ApJ*, 176:1, August 1972.

Harwit, M. and Pacini, F. Infrared galaxies - Evolutionary stages of massive star formation. *ApJL*, 200:L127–L129, September 1975.

Haynes, M.P. and Giovanelli, R. The pattern of H I deficiency in the Virgo cluster. *ApJ*, 306:466–482, July 1986.

Helou, G. The IRAS colors of normal galaxies. *ApJL*, 311:L33–L36, December 1986.

Helou, G. The relation between infrared and radio emission in spiral galaxies. In Duric, N. and Crane, P.C., editors, *The Interpretation of Modern Synthesis Observations of Spiral Galaxies*, volume 18 of *Astronomical Society of the Pacific Conference Series*, pages 125–133, 1991.

Helou, G. and Bicay, M.D. A physical model of the infrared-to-radio correlation in galaxies. *ApJ*, 415:93–100, September 1993.

Helou, G., Soifer, B.T. and Rowan-Robinson, M. Thermal infrared and nonthermal radio - Remarkable correlation in disks of galaxies. *ApJL*, 298:L7–L11, November 1985.

Helou, G., Khan, I.R., Malek, L. et al. IRAS observations of galaxies in the Virgo cluster area. *ApJS*, 68:151–172, October 1988.

Henriksen, M. and Byrd, G. Tidal Triggering of Star Formation by the Galaxy Cluster Potential. *ApJ*, 459:82, March 1996.

Hill, G.J. and Lilly, S.J. A change in the cluster environments of radio galaxies with cosmic epoch. *ApJ*, 367:1–18, January 1991.

Hippelein, H., Haas, M., Tuffs, R.J. et al. The spiral galaxy M 33 mapped in the FIR by ISOPHOT. A spatially resolved study of the warm and cold dust. *A&A*, 407:137–146, August 2003.

Hjellming, R.M. and Bignell, R.C. Radio astronomy with the very large array. *Science*, 216:1279–1285, June 1982.

Hoernes, P., Berkhuijsen, E.M. and Xu, C. Radio-FIR correlations within M 31. *A&A*, 334:57–70, June 1998.

Horner, D.J., Perlman, E.S., Ebeling, H. et al. The WARPS Survey. VII. The WARPS-II Cluster Catalog. *ApJS*, 176:374–413, June 2008.

Houck, J.R., Roellig, T.L., van Cleve, J. et al. The Infrared Spectrograph (IRS) on the Spitzer Space Telescope. *ApJS*, 154:18–24, September 2004.

Hubble, E.P. Extragalactic nebulae. *ApJ*, 64:321–369, December 1926.

Hubble, E.P. *Realm of the Nebulae*. Yale University Press, 1936, 1936.

Hughes, A., Wong, T., Ekers, R. et al. A multiresolution analysis of the radio-FIR correlation in the Large Magellanic Cloud. *MNRAS*, 370:363–379, July 2006.

Hughes, J.P. and Birkinshaw, M. A Measurement of the Hubble Constant from the X-Ray Properties and the Sunyaev-Zeldovich Effect of CL 0016+16. *ApJ*, 501:1, July 1998.

Hummel, E. The radio continuum-far infrared correlation and magnetic fields in SBC galaxies. *A&A*, 160:L4–L6, May 1986.

Hummel, E., Davies, R.D., Pedlar, A. et al. The radio continuum, far-infrared and optical emission from SBC galaxies and their relation to star formation. *A&A*, 199:91–104, June 1988.

Ibar, E., Cirasuolo, M., Ivison, R. et al. Exploring the infrared/radio correlation at high redshift. *MNRAS*, 386:953–962, May 2008.

Icke, V. Distant encounters between disk galaxies and the origin of S 0 spirals. *A&A*, 144:115–123, March 1985.

Irwin, J.A., Stil, J.M. and Bridges, T.J. SCUBA observations of NGC 1275. *MNRAS*, 328:359–369, December 2001.

Ivison, R.J., Alexander, D.M., Biggs, A.D. et al. BLAST: the far-infrared/radio correlation in distant galaxies. *MNRAS*, 402:245–258, February 2010a.

Ivison, R.J., Magnelli, B., Ibar, E. et al. The far-infrared/radio correlation as probed by Herschel. *A&A*, 518:L31, July 2010b.

Jarvis, M.J. and Rawlings, S. The accretion history of the universe with the SKA. *NewAR*, 48:1173–1185, December 2004.

Jarvis, M.J., Smith, D.J.B., Bonfield, D.G. et al. Herschel-ATLAS: the far-infrared-radio correlation at z<0.5. *MNRAS*, 409:92–101, November 2010.

Kessler, M.F., Steinz, J.A., Anderegg, M.E. et al. The Infrared Space Observatory (ISO) mission. *A&A*, 315:L27–L31, November 1996.

Klein, U., Wielebinski, R. and Thuan, T.X. Radio continuum observations of blue compact dwarf galaxies. *A&A*, 141:241–247, December 1984.

Knobel, C., Lilly, S.J., Iovino, A. et al. An Optical Group Catalog to z = 1 from the zCOSMOS 10 k Sample. *ApJ*, 697:1842–1860, June 2009.

Knobel, C., Lilly, S.J., Iovino, A. et al. The zCOSMOS 20k Group Catalog. *ApJ*, 753: 121, July 2012.

Koo, D.C. Multicolor photometry of the red cluster 0016+16 at Z = 0.54. *ApJL*, 251: L75–L79, December 1981.

Kormendy, J. and Richstone, D. Inward Bound—The Search For Supermassive Black Holes In Galactic Nuclei. *ARA&A*, 33:581, 1995.

Kovács, A., Chapman, S.C., Dowell, C.D. et al. SHARC-2 350 μm Observations of Distant Submillimeter-selected Galaxies. *ApJ*, 650:592–603, October 2006.

Lacki, B.C., Thompson, T.A. and Quataert, E. The Physics of the Far-infrared-Radio Correlation. I. Calorimetry, Conspiracy, and Implications. *ApJ*, 717:1–28, July 2010.

Lah, P., Pracy, M.B., Chengalur, J.N. et al. The HI gas content of galaxies around Abell 370, a galaxy cluster at z = 0.37. *MNRAS*, 399:1447–1470, November 2009.

Lake, G., Katz, N. and Moore, B. The Formation of Quasars in Low-Luminosity Hosts via Galaxy Harassment. *ApJ*, 495:152, March 1998.

Larson, R.B., Tinsley, B.M. and Caldwell, C.N. The evolution of disk galaxies and the origin of S0 galaxies. *ApJ*, 237:692–707, May 1980.

Lavery, R.J. and Henry, J.P. Evidence for galaxy-galaxy interactions as an active agent of the 'Butcher-Oemler' effect at a redshift of 0.2. *ApJ*, 330:596–600, July 1988.

Le Floc'h, E., Aussel, H., Ilbert, O. et al. Deep Spitzer 24 μm COSMOS Imaging. I. The Evolution of Luminous Dusty Galaxies — Confronting the Models. *ApJ*, 703: 222–239, September 2009.

Ledlow, M.J. and Owen, F.N. A 20 CM VLA Survey of Abell clusters of galaxies. 4: The radio sample and cluster properties. *AJ*, 109:853–873, March 1995.

Lilly, S.J., Le Fèvre, O., Renzini, A. et al. zCOSMOS: A Large VLT/VIMOS Redshift Survey Covering 0 ¡ z ¡ 3 in the COSMOS Field. *ApJS*, 172:70–85, September 2007.

Lilly, S.J., Le Brun, V., Maier, C. et al. The zCOSMOS 10k-Bright Spectroscopic Sample. *ApJS*, 184:218–229, October 2009.

Lisenfeld, U., Voelk, H.J. and Xu, C. A quantitative model of the FIR/radio correlation for normal late-type galaxies. *A&A*, 306:677, February 1996.

Lonsdale Persson, C.J. and Helou, G. On the origin of the 40-120 micron emission of galaxy disks A comparison with H-alpha fluxes. *ApJ*, 314:513–524, March 1987.

Lopes, P.A.A., de Carvalho, R.R., Gal, R.R. et al. The Northern Sky Optical Cluster Survey. IV. An Intermediate-Redshift Galaxy Cluster Catalog and the Comparison of Two Detection Algorithms. *AJ*, 128:1017–1045, September 2004.

Lotz, J.M., Martin, C.L. and Ferguson, H.C. The Star-forming Dwarf Galaxy Populations of Two z ˜ 0.4 Clusters: MS 1512.4+3647 and A851. *ApJ*, 596:143–158, October 2003.

Lubin, L.M., Postman, M., Oke, J.B. et al. A Study of Nine High-Redshift Clusters of Galaxies. III. Hubble Space Telescope Morphology of Clusters 0023+0423 and 1604+4304. *AJ*, 116:584–622, August 1998.

Lutz, D., Poglitsch, A., Altieri, B. et al. PACS Evolutionary Probe (PEP) - A Herschel key program. *A&A*, 532:A90, August 2011.

Magnelli, B., Popesso, P., Berta, S. et al. The deepest Herschel-PACS far-infrared survey: number counts and infrared luminosity functions from combined PEP/GOODS-H observations. *A&A*, 553:A132, May 2013.

Makino, J. and Hut, P. Merger Rate of Equal-Mass Spherical Galaxies. *ApJ*, 481:83, May 1997.

Makovoz, D. and Marleau, F.R. Point-Source Extraction with MOPEX. *PASP*, 117: 1113–1128, October 2005.

Mamon, G.A. Are cluster ellipticals the products of mergers? *ApJL*, 401:L3–L6, December 1992.

Mao, M.Y., Huynh, M.T., Norris, R.P. et al. No Evidence for Evolution in the Far-infrared-Radio Correlation out to z ˜ 2 in the Extended Chandra Deep Field South. *ApJ*, 731:79, April 2011.

Marinoni, C., Davis, M., Newman, J.A. et al. Three-dimensional Identification and Reconstruction of Galaxy Systems within Flux-limited Redshift Surveys. *ApJ*, 580:122–143, November 2002.

Marsh, K.A. and Helou, G. The spatial variation of the infrared-to-radio ratio in spiral galaxies. *ApJ*, 445:599–606, June 1995.

Martini, P., Sivakoff, G.R. and Mulchaey, J.S. The Evolution of Active Galactic Nuclei in Clusters of Galaxies to Redshift 1.3. *ApJ*, 701:66–85, August 2009.

McGee, S.L., Balogh, M.L., Bower, R.G. et al. The accretion of galaxies into groups and clusters. *MNRAS*, 400:937–950, December 2009.

Messias, H., Afonso, J., Hopkins, A. et al. A Multi-wavelength Approach to the Properties of Extremely Red Galaxy Populations. I. Contribution to the Star Formation Rate Density and Active Galactic Nucleus Content. *ApJ*, 719:790–802, August 2010.

Mihos, C. Interactions and Mergers of Cluster Galaxies. *ArXiv Astrophysics e-prints*, May 2003.

Miller, N.A. and Owen, F.N. The Far-Infrared-Radio Correlation in Nearby Abell Clusters. *AJ*, 121:1903–1914, April 2001.

Molikawa, K., Hattori, M., Kneib, J.P. et al. The giant luminous arc statistics. II. Spherical lens models based on ROSAT HRI data. *A&A*, 351:413–432, November 1999.

Moore, B., Katz, N., Lake, G. et al. Galaxy harassment and the evolution of clusters of galaxies. *Nature*, 379:613–616, February 1996.

Moore, B., Lake, G. and Katz, N. Morphological Transformation from Galaxy Harassment. *ApJ*, 495:139, March 1998.

Moore, B., Lake, G., Quinn, T. et al. On the survival and destruction of spiral galaxies in clusters. *MNRAS*, 304:465–474, April 1999.

Moorwood, A.F.M. Starburst Galaxies. *SSR*, 77:303–366, August 1996.

Moran, S.M., Ellis, R.S., Treu, T. et al. A Wide-Field Survey of Two z˜0.5 Galaxy Clusters: Identifying the Physical Processes Responsible for the Observed Transformation of Spirals into S0s. *ApJ*, 671:1503–1522, December 2007.

Morrison, G.E., Owen, F.N., Ledlow, M.J. et al. Radio-selected Galaxies in Very Rich Clusters at z = 0.25. I. Multiwavelength Observations and Data Reduction Techniques. *ApJS*, 146:267–298, June 2003.

Morrison, G.E., Owen, F.N., Dickinson, M. et al. Very Large Array 1.4 GHz Observations of the GOODS-North Field: Data Reduction and Analysis. *ApJS*, 188:178–186, May 2010.

Moss, C. and Whittle, M. An H-alpha survey of cluster spirals - Comparison of star formation in clusters and the field. *ApJL*, 407:L17–L20, April 1993.

Mullis, C.R., McNamara, B.R., Quintana, H. et al. The 160 Square Degree ROSAT Survey: The Revised Catalog of 201 Clusters with Spectroscopic Redshifts. *ApJ*, 594: 154–171, September 2003.

Murphy, E.J. The Far-Infrared-Radio Correlation at High Redshifts: Physical Considerations and Prospects for the Square Kilometer Array. *ApJ*, 706:482–496, November 2009.

Murphy, E.J., Braun, R., Helou, G. et al. An Initial Look at the Far-Infrared-Radio Correlation within Nearby Star-forming Galaxies Using the Spitzer Space Telescope. *ApJ*, 638:157–175, February 2006.

Murphy, E.J., Chary, R.R., Alexander, D.M. et al. Balancing the Energy Budget Between Star Formation and Active Galactic Nuclei in High-Redshift Infrared Luminous Galaxies. *ApJ*, 698:1380–1397, June 2009a.

Murphy, E.J., Kenney, J.D.P., Helou, G. et al. Environmental Effects in Clusters: Modified Far-Infrared-Radio Relations within Virgo Cluster Galaxies. *ApJ*, 694:1435–1451, April 2009b.

Murphy, E.J., Chary, R.R., Dickinson, M. et al. An Accounting of the Dust-obscured Star Formation and Accretion Histories Over the Last ˜11 Billion Years. *ApJ*, 732:126, May 2011.

Murphy, E.J., Stierwalt, S., Armus, L. et al. Radio and Mid-infrared Properties of Compact Starbursts: Distancing Themselves from the Main Sequence. *ApJ*, 768:2, May 2013.

Naab, T. and Burkert, A. Statistical Properties of Collisionless Equal- and Unequal-Mass Merger Remnants of Disk Galaxies. *ApJ*, 597:893–906, November 2003.

Neugebauer, G., Habing, H.J., van Duinen, R. et al. The Infrared Astronomical Satellite (IRAS) mission. *ApJL*, 278:L1–L6, March 1984.

Niklas, S. and Beck, R. A new approach to the radio-far infrared correlation for non-calorimeter galaxies. *A&A*, 320:54–64, April 1997.

Norris, R.P., Afonso, J., Appleton, P.N. et al. Deep ATLAS Radio Observations of the Chandra Deep Field-South/Spitzer Wide-Area Infrared Extragalactic Field. *AJ*, 132: 2409–2423, December 2006.

Oliva, E., Origlia, L., Kotilainen, J.K. et al. Red supergiants as starburst tracers in galactic nuclei. *A&A*, 301:55, September 1995.

Oliver, S.J., Bock, J., Altieri, B. et al. The Herschel Multi-tiered Extragalactic Survey: HerMES. *MNRAS*, 424:1614–1635, August 2012.

Owen, F.N. and Morrison, G.E. The Deep Swire Field. I. 20 cm Continuum Radio Observations: A Crowded Sky. *AJ*, 136:1889–1900, November 2008.

Paladino, R., Murgia, M., Helfer, T.T. et al. Thermal and non-thermal components of the interstellar medium at sub-kiloparsec scales in galaxies. *A&A*, 456:847–859, September 2006.

Pierini, D., Popescu, C.C., Tuffs, R.J. et al. The far-infrared/radio correlation in the ISO era. The warm and cold far-infrared/radio correlations. *A&A*, 409:907–916, October 2003.

Piffaretti, R., Arnaud, M., Pratt, G.W. et al. The MCXC: a meta-catalogue of x-ray detected clusters of galaxies. *A&A*, 534:A109, October 2011.

Pilbratt, G.L., Riedinger, J.R., Passvogel, T. et al. Herschel Space Observatory. An ESA facility for far-infrared and submillimetre astronomy. *A&A*, 518:L1, July 2010.

Pimbblet, K.A. At the Vigintennial of the Butcher-Oemler Effect. *PASA*, 20:294–299, 2003.

Pimbblet, K.A., Smail, I., Kodama, T. et al. The Las Campanas/AAT Rich Cluster Survey - II. The environmental dependence of galaxy colours in clusters at z˜0.1. *MNRAS*, 331: 333–350, March 2002.

Poggianti, B. Evolution of galaxies in clusters. In Dettmar, R., Klein, U. and Salucci, P., editors, *Baryons in Dark Matter Halos*, December 2004.

Poggianti, B.M., von der Linden, A., De Lucia, G. et al. The Evolution of the Star Formation Activity in Galaxies and Its Dependence on Environment. *ApJ*, 642:188– 215, May 2006.

Poggianti, B.M., Desai, V., Finn, R. et al. The Relation between Star Formation, Morphology, and Local Density in High-Redshift Clusters and Groups. *ApJ*, 684:888–904, September 2008.

Postman, M. and Geller, M.J. The morphology-density relation - The group connection. *ApJ*, 281:95–99, June 1984.

Postman, M., Franx, M., Cross, N.J.G. et al. The Morphology-Density Relation in z ˜ 1 Clusters. *ApJ*, 623:721–741, April 2005.

Price, R. and Duric, N. New results on the radio-far-infrared relation for galaxies. *ApJ*, 401:81–86, December 1992.

Quilis, V., Moore, B. and Bower, R. Gone with the Wind: The Origin of S0 Galaxies in Clusters. *Science*, 288:1617–1620, June 2000.

Rakos, K.D. and Schombert, J.M. Color evolution from Z = 0 to Z = 1. *ApJ*, 439:47–59, January 1995.

Reddy, N.A. and Yun, M.S. Radio and Far-Infrared Emission as Tracers of Star Formation and Active Galactic Nuclei in Nearby Cluster Galaxies. *ApJ*, 600:695–715, January 2004.

Rengarajan, T.N., Karnik, A.D. and Iyengar, K.V.K. Far-infrared and radio continuum properties of spiral galaxies in clusters. *MNRAS*, 290:1–6, September 1997.

Rickard, L.J. and Harvey, P.M. Far-infrared observations of galactic nuclei. *AJ*, 89: 1520–1530, October 1984.

Rieke, G.H. and Low, F.J. Infrared Photometry of Extragalactic Sources. *ApJL*, 176:L95, September 1972.

Rieke, G.H., Young, E.T., Engelbracht, C.W. et al. The Multiband Imaging Photometer for Spitzer (MIPS). *ApJS*, 154:25–29, September 2004.

Rieke, G.H., Alonso-Herrero, A., Weiner, B.J. et al. Determining Star Formation Rates for Infrared Galaxies. *ApJ*, 692:556–573, February 2009.

Rybicki, G.B. and Lightman, A.P. *Radiative processes in astrophysics*. WILEY-VCH, 1979.

Sadler, E.M., McIntyre, V.J., Jackson, C.A. et al. Radio Sources in the 2dF Galaxy Redshift Survey I. Radio Source Populations*. *PASA*, 16:247–256, December 1999.

Saintonge, A., Tran, K.V.H. and Holden, B.P. Spitzer/MIPS 24 μm Observations of Galaxy Clusters: An Increasing Fraction of Obscured Star-forming Members from z = 0.02 to z = 0.83. *ApJL*, 685:L113–L116, October 2008.

Sajina, A., Yan, L., Lutz, D. et al. Spitzer Mid-Infrared Spectroscopy of Infrared Luminous Galaxies at z $\sim$ 2. III. Far-IR to Radio Properties and Optical Spectral Diagnostics. *ApJ*, 683:659–682, August 2008.

Sanders, D.B. and Mirabel, I.F. Luminous Infrared Galaxies. *ARA&A*, 34:749, 1996.

Sanders, D.B., Mazzarella, J.M., Kim, D.C. et al. The IRAS Revised Bright Galaxy Sample. *AJ*, 126:1607–1664, October 2003.

Sanders, D.B., Salvato, M., Aussel, H. et al. S-COSMOS: The Spitzer Legacy Survey of the Hubble Space Telescope ACS 2 deg^2 COSMOS Field I: Survey Strategy and First Analysis. *ApJS*, 172:86–98, September 2007.

Sargent, M.T., Schinnerer, E., Murphy, E. et al. The VLA-COSMOS Perspective on the Infrared-Radio Relation. I. New Constraints on Selection Biases and the Non-Evolution of the Infrared/Radio Properties of Star-Forming and Active Galactic Nucleus Galaxies at Intermediate and High Redshift. *ApJS*, 186:341–377, February 2010a.

Sargent, M.T., Schinnerer, E., Murphy, E. et al. No Evolution in the IR-Radio Relation for IR-luminous Galaxies at z < 2 in the COSMOS Field. *ApJL*, 714:L190–L195, May 2010b.

Schinnerer, E., Carilli, C.L., Scoville, N.Z. et al. The VLA-COSMOS Survey. I. Radio Identifications from the Pilot Project. *AJ*, 128:1974–1989, November 2004.

Schinnerer, E., Smolčić, V., Carilli, C.L. et al. The VLA-COSMOS Survey. II. Source Catalog of the Large Project. *ApJS*, 172:46–69, September 2007.

Schinnerer, E., Sargent, M.T., Bondi, M. et al. The VLA-COSMOS Survey. IV. Deep Data and Joint Catalog. *ApJS*, 188:384–404, June 2010.

Scodeggio, M. and Gavazzi, G. 21 centimeter study of spiral galaxies in clusters. III - Neutral gas content, star formation, and radio continuum properties. *ApJ*, 409:110–125, May 1993.

Scoville, N. and Young, J.S. The molecular gas distribution in M51. *ApJ*, 265:148, February 1983.

Scoville, N., Aussel, H., Brusa, M. et al. The Cosmic Evolution Survey (COSMOS): Overview. *ApJS*, 172:1–8, September 2007.

Seymour, N., Huynh, M., Dwelly, T. et al. Investigating the far-IR/radio correlation of star-forming Galaxies to z = 3. *MNRAS*, 398:1573–1581, September 2009.

Smail, I., Ivison, R.J. and Blain, A.W. A Deep Sub-millimeter Survey of Lensing Clusters: A New Window on Galaxy Formation and Evolution. *ApJL*, 490:L5, November 1997.

Smail, I., Edge, A.C., Ellis, R.S. et al. A statistical analysis of the galaxy populations of distant luminous X-ray clusters. *MNRAS*, 293:124, January 1998.

Smith, A.J., Wang, L., Oliver, S.J. et al. HerMES: point source catalogues from deep Herschel-SPIRE observations. *MNRAS*, 419:377–389, January 2012.

Smith, G.P., Treu, T., Ellis, R.S. et al. Evolution since z = 1 of the Morphology-Density Relation for Galaxies. *ApJ*, 620:78–87, February 2005.

Soifer, B.T., Neugebauer, G. and Houck, J.R. The IRAS view of the extragalactic sky. *ARA&A*, 25:187–230, 1987.

Sopp, H.M. and Alexander, P. A composite plot of far-infrared versus radio luminosity, and the origin of far-infrared luminosity in quasars. *MNRAS*, 251:14P–16P, July 1991.

Stern, D., Eisenhardt, P., Gorjian, V. et al. Mid-Infrared Selection of Active Galaxies. *ApJ*, 631:163–168, September 2005.

Stetson, P.B. DAOPHOT - A computer program for crowded-field stellar photometry. *PASP*, 99:191–222, March 1987.

Stocke, J.T., Morris, S.L., Gioia, I.M. et al. The Einstein Observatory Extended Medium-Sensitivity Survey. II - The optical identifications. *ApJS*, 76:813–874, July 1991.

Strateva, I., Ivezić, Ž., Knapp, G.R. et al. Color Separation of Galaxy Types in the Sloan Digital Sky Survey Imaging Data. *AJ*, 122:1861–1874, October 2001.

Struble, M.F. and Rood, H.J. A Compilation of Redshifts and Velocity Dispersions for ACO Clusters. *ApJS*, 125:35–71, November 1999.

Tabatabaei, F.S., Beck, R., Krause, M. et al. A multi-scale study of infrared and radio emission from Scd galaxy M 33. *A&A*, 466:509–519, May 2007a.

Tabatabaei, F.S., Beck, R., Krügel, E. et al. High-resolution radio continuum survey of M 33. II. Thermal and nonthermal emission. *A&A*, 475:133–143, November 2007b.

Toomre, A. and Toomre, J. Galactic Bridges and Tails. *ApJ*, 178:623–666, December 1972.

Trump, J.R., Impey, C.D., McCarthy, P.J. et al. Magellan Spectroscopy of AGN Candidates in the COSMOS Field. *ApJS*, 172:383–395, September 2007.

Urry, C.M. and Padovani, P. Unified Schemes for Radio-Loud Active Galactic Nuclei. *PASP*, 107:803, September 1995.

Valluri, M. Compressive tidal heating of a disk galaxy in a rich cluster. *ApJ*, 408:57–70, May 1993.

van der Kruit, P.C. Observations of core sources in Seyfert and normal galaxies with the Westerbork synthesis radio telescope at 1415 MHz. *A&A*, 15:110–122, November 1971.

van der Kruit, P.C. High-resolution Radio Continuum Observations of Bright Spiral Galaxies at 1415 MHz: A General Discussion. *A&A*, 29:263, December 1973.

Voelk, H.J. The correlation between radio and far-infrared emission for disk galaxies - A calorimeter theory. *A&A*, 218:67–70, July 1989.

Voges, W., Aschenbach, B., Boller, T. et al. ROSAT All-Sky Survey Bright Source Catalogue. *IAU Circ.*, 6420:2, June 1996.

Voges, W., Aschenbach, B., Boller, T. et al. The ROSAT all-sky survey bright source catalogue. *A&A*, 349:389–405, September 1999.

Vollmer, B. NGC 4654: Gravitational interaction or ram pressure stripping? *A&A*, 398: 525–539, February 2003.

von der Linden, A., Wild, V., Kauffmann, G. et al. Star formation and AGN activity in SDSS cluster galaxies. *MNRAS*, 404:1231–1246, May 2010.

Werner, M.W., Roellig, T.L., Low, F.J. et al. The Spitzer Space Telescope Mission. *ApJS*, 154:1–9, September 2004.

White, D.A. and Fabian, A.C. Einstein Observatory evidence for the widespread baryon overdensity in clusters of galaxies. *MNRAS*, 273:72–84, March 1995.

Windhorst, R.A., Miley, G.K., Owen, F.N. et al. Sub-millijansky 1.4 GHz source counts and multicolor studies of weak radio galaxy populations. *ApJ*, 289:494–513, February 1985.

Wold, I.G.B., Owen, F.N., Wang, W.H. et al. Very Large Array 1.4 GHz Catalogs of the A370 and A2390 Cluster Fields. *ApJS*, 202:2, September 2012.

Wrobel, J.M. and Heeschen, D.S. Radio-continuum sources in nearby and bright E/S0 galaxies - Active nuclei versus star formation. *AJ*, 101:148–169, January 1991.

Wunderlich, E. and Klein, U. A further study of the radio-far-infrared relation in galaxies. II - The ubiquity of the correlation. *A&A*, 206:47–52, November 1988.

Wunderlich, E., Wielebinski, R. and Klein, U. A further study of the relation of the radio-far-infrared in galaxies. I - Observations and data processing. *A&AS*, 69:487–504, June 1987.

Xu, C. Heating of the cool dust in spiral galaxies and the far-infrared/radio correlation. *ApJL*, 365:L47–L50, December 1990.

Yee, H.K.C., Ellingson, E. and Carlberg, R.G. The CNOC Cluster Redshift Survey Catalogs. I. Observational Strategy and Data Reduction Techniques. *ApJS*, 102:269, February 1996.

Young, L.M., Bendo, G.J. and Lucero, D.M. Mid- to Far-Infrared Emission and Star Formation in Early-Type Galaxies. *AJ*, 137:3053–3070, February 2009.

Younger, J.D., Omont, A., Fiolet, N. et al. A millimetre survey of starburst dominated ultraluminous infrared galaxies at z ∼ 2. *MNRAS*, 394:1685–1694, April 2009.

Yun, M.S., Reddy, N.A. and Condon, J.J. Radio Properties of Infrared-selected Galaxies in the IRAS 2 Jy Sample. *ApJ*, 554:803–822, June 2001.

Zabludoff, A.I. and Mulchaey, J.S. The Properties of Poor Groups of Galaxies. I. Spectroscopic Survey and Results. *ApJ*, 496:39, March 1998.